

U N I K A S S E L  
V E R S I T Ä T

---

Automatisation of a  
chirped-pulse Fourier transform  
millimeter-wave spectrometer  
and its application

FB 10 - Faculty of Mathematics and Natural Sciences

Laboratory Astrophysics

Thesis

submitted for the attainment of the degree

Master of Science

by

Andreas Körner

September 2021

---

First examiner: Prof. Dr. Thomas Giesen

Second examiner: Prof. Dr. Arno Ehresmann



# Contents

<b>Abstract</b>	<b>IV</b>
<b>Acknowledgements</b>	<b>V</b>
<b>Statutory Declaration / Eigenständigkeitserklärung</b>	<b>VII</b>
<b>1. Introduction</b>	<b>1</b>
<b>2. Theory of Molecular Spectroscopy</b>	<b>3</b>
2.1. Molecular Rotational Spectroscopy . . . . .	3
2.1.1. Rigid Rotor . . . . .	3
2.1.2. Diatomic and Linear Molecules . . . . .	5
2.1.3. Selection Rules . . . . .	6
2.1.4. Light Matter Interaction . . . . .	8
2.1.5. Spectra of Diatomic and Linear Molecules . . . . .	9
2.1.6. Centrifugal Force . . . . .	10
2.1.7. Influence of Vibrational and Electronic States on the Ro- tational Constants . . . . .	11
2.1.8. Vibrational angular momentum . . . . .	13
2.1.9. Line Intensities . . . . .	13
2.1.10. Describing Extended Molecules . . . . .	15
2.1.11. Symmetric Tops . . . . .	15
2.1.12. Asymmetric Tops . . . . .	20
2.1.13. Internal rotation . . . . .	22
2.2. Line Shapes and Broadening . . . . .	22
2.2.1. Lorentzian Line Shape . . . . .	23
2.2.2. Pressure Broadening . . . . .	24
2.2.3. Doppler Effect . . . . .	25

<b>3. Automatisation of a CPFTmmW spectrometer</b>	<b>28</b>
3.1. Experimental Setup . . . . .	28
3.1.1. Control Devices . . . . .	29
3.1.2. Generation Arm . . . . .	29
3.1.2.1. Arbitrary Waveform Generator . . . . .	29
3.1.2.2. Amplifier Multiplier Chain . . . . .	30
3.1.3. Receiver Arm . . . . .	30
3.1.4. Interaction Volume . . . . .	32
3.1.5. Vacuum Chamber . . . . .	33
3.1.6. Setup of SuJeSTA . . . . .	34
3.1.6.1. Supersonic Jet Source . . . . .	34
3.1.6.2. Laser Ablation . . . . .	37
3.1.6.3. Multipass Reflection Cell . . . . .	37
3.2. LabView Programming . . . . .	38
3.2.1. Front Panel - Human User Interface . . . . .	39
3.2.1.1. General Settings . . . . .	40
3.2.1.2. Arbitrary Waveform Generator Settings . . . . .	40
3.2.1.3. Oscilloscope Settings . . . . .	41
3.2.1.4. Fast Fourier Transform and Window Function . . . . .	41
3.2.1.5. Measurement Feedback . . . . .	42
3.2.1.6. Saving Parameters . . . . .	42
3.2.1.7. Calibration . . . . .	43
3.2.2. Back Panel - Programming Code . . . . .	43
3.2.2.1. Device Settings . . . . .	44
3.2.2.2. Chirp Generation . . . . .	45
3.2.2.3. Iterative Acquisition of the Spectrum . . . . .	46
3.3. Averaging Measurements . . . . .	48
<b>4. Results and Discussion</b>	<b>51</b>
4.1. Gas Flow Experiments . . . . .	51
4.1.1. Methanol Spectrum in Gas Flow Experiments and General Spectral Properties . . . . .	52
4.1.2. Isotopologues of Acetonitrile . . . . .	55
4.1.3. Solid Samples . . . . .	58

4.2. Measurements Using SuJeSTA . . . . .	59
4.2.1. Jet Measurements . . . . .	59
4.2.2. Laser Ablation Measurements . . . . .	64
4.2.2.1. Bismuth Tribromide . . . . .	65
4.2.2.2. Titanium Species . . . . .	66
4.3. General Discussion . . . . .	67
<b>5. Conclusion and Outlook</b>	<b>70</b>
5.1. Conclusion . . . . .	70
5.2. Outlook . . . . .	71
<b>Bibliography</b>	<b>73</b>
<b>List of Figures</b>	<b>82</b>
<b>List of Tables</b>	<b>83</b>
<b>Appendix A. Used software and programs</b>	<b>84</b>
A.1. LabView . . . . .	84
A.2. Python . . . . .	84
A.3. PGopher . . . . .	85
<b>Appendix B. Setup Components</b>	<b>86</b>
<b>Appendix C. LabView Backpanel</b>	<b>89</b>
<b>Appendix D. List of Molecular Databases</b>	<b>90</b>
<b>Appendix E. Jet Experiments - Considered Lines</b>	<b>91</b>
<b>Units and constants</b>	<b>93</b>
<b>Abbreviations</b>	<b>94</b>

# Abstract

Identifying molecules in space to understand astrochemistry requires laboratory reference spectra. To obtain these, a chirped-pulse FOURIER transform (CPFT) spectrometer operating at millimetre waves (mmW) in the frequency range around 100 GHz was used. To facilitate the acquisition of spectra, the instrument and data processing has been automatised using LABVIEW™.

The automatised spectrometer was used in gas flow, supersonic jet and laser ablation experiments with various test molecules. In gas flow experiments, the properties of a spectrum of methanol ( $\text{CH}_3\text{OH}$ ) are analysed and the sensitivity for naturally abundant isotopologues of acetonitrile ( $\text{CH}_3\text{CN}$ ) is demonstrated. The temperature of molecules in supersonic jet experiments is estimated. In laser ablation experiments with bismuth tribromide ( $\text{BiBr}_3$ ) optical excitation of the jet correlated with line features in the mmW spectrum. However, further investigation and efforts are required to reliably combine laser ablation with the CPFTmmW spectrometer.

It can be concluded that the automatisation of the CPFTmmW spectrometer with LABVIEW™ was successful. High-quality spectra were recorded automatically, converted by fast FOURIER transformation, frequency calibrated, and subspectra were concatenated resulting in a broadband frequency domain mmW spectrum. This can then further be analysed by the techniques of rotational spectroscopy.

# Acknowledgements

Science cannot exist without discussion and collaboration. Neither can a scientist survive in a social vacuum. For having the best of both worlds, I have to thank a few people.

I want to thank PROF. DR. THOMAS GIESEN for hooking me up on the topic of molecular spectroscopy and its application for space research. He gave me the opportunity to do my internship and master thesis in his group. I am grateful for the trust, freedom and feedback helping me to find a way in this project. I also want to thank PROF. DR. ARNO EHRESMANN for his prompt willingness to accompany the project as second examiner.

A special thanks goes to DR. GUIDO FUCHS. He supervised the project primarily and always shared ideas, knowledge and experience that greatly benefited the work and gave it the general direction. I also do appreciate the discussions often revealing the truth behind an effect or an unforeseen hurdle, not to mention the support operations in the lab when the laser focus for SUJESTA had to be adjusted. The input was valuable guidance for me.

The most important person to thank here is M.SC. PASCAL STAHL. The spectrometer is in fact his PhD project, and I am honoured to put my fingers on it. Your introduction into the topic, the setup, the techniques, and the science behind it gave me a chance to understand what we are doing. At all times I could ask questions (usually the same ones multiple times) and rely on your help and support. My appreciation is not limited to the scientific input. I also very much enjoyed the exchange in our breaks and the informal talks. They helped to make the usual day in the lab pleasant. I really enjoyed working with you.

My thanks of course extend to the whole AG GIESEN. I very much enjoyed both the scientific discussions and the conversations in between. All of you gave me a warm welcome and a pleasant atmosphere. Especially I want to thank DR. ALEXANDER BREIER for his valuable insights regarding the laser ablation

and our detector JAMES. Important experience with SUJESTA was shared by M.Sc. BJÖRN WASSMUTH helping us to finally get the jet measurements going and giving a few suggestions for the analysis. I also appreciate the support of M.Sc. EILEEN DÖRING for some tricks, techniques, and hints on how things work in the lab and where to find them. Thanks also to B.Sc. JAN JAKOB for discussions on related scientific subjects and extensive support in handling JAMES. Many thanks also to LUISA BLUM for the collegial exchange and the shared organization of some of the group events. I also want to give credit to B.Sc. JOSHUA BALDEH for the informal talks and valuable off-topic discussions. My appreciation also goes to ANNETTE WESTERMANN for the administration around the science, because everything was already organised, when the need for it had barely risen.

Enormous gratitude is due to the people around me for granting me a life outside the university. In the past few years, I had wonderful moments and memorable moments with you, that helped to keep my physical and mental sanity. We enjoyed time together and shared great experiences. Through all this you bore my moods, even when it was foolish or frustrated. A special warm thanks to my flatmates M.Sc. JAN THIEME and B.Sc. KRISHNA ANANDA EKAPUTERA for going through this with me, basically any time any day, and for the evening in our home cinema or around the game board. I also want to thank the people motivating me to do sports in the last stages of my studies: B.A. LAURA LÖSLEIN, M.Sc. STEFAN UHLENKÜKEN and especially M.Sc. ARMINA MORTAZAVI. Without you, leaving my home office again would have been a physical challenge. I also want to thank my family. You raised me, put me on the path and always gave your feedback and support. And I am most happy to have you. Lots of love and kisses also to my girlfriend MARTHE. You are the one that cared the most, could understand my frustration and showed me where to find the light in the tunnel when it was dark. I thank you with all my heart.

# **Statutory Declaration / Eigenständigkeitserklärung**

Hereby I declare, that I have authored the present thesis independently and did not use any other than the declared sources/resources. I have explicitly marked all material, which is protected by intellectual property rights.

Hiermit bestätige ich, dass ich die vorliegende Arbeit selbständig verfasst und keine anderen als die angegebenen Hilfsmittel benutzt habe. Die Stellen der Arbeit, die dem Wortlaut oder dem Sinn nach anderen Werken (dazu zählen auch Internetquellen) entnommen sind, wurden unter Angabe der Quelle kenntlich gemacht.

Andreas Körner  
Kassel, September 6, 2021



# 1. Introduction

For millennia humanity has gazed upon the night sky, wondering what is to be found in those celestial spheres. Science has acquired a set of tools to investigate the matter, enabling us to unravel the fabric of the universe. One such tool is the Atacama Large Millimetre Array ALMA, a radio telescope interferometer providing extensive spectra in the need to be interpreted. To shed light on the origin of the signals, high-resolution spectroscopic experiments carried out at the same frequencies in the laboratory can be used as a supporting reference. This allows to identify molecules and evaluate their abundance in the investigated areas. With this approach millimetre and sub-millimetre investigations of molecular lines using radio telescopes have helped to shape the concept of the interstellar medium (ISM).<sup>1</sup>

Understanding a molecule means to determine its molecular parameters, which requires spectroscopic methods. Different parts of the spectrum usually obtain information on different properties, such as electronic, vibrational, or rotational states. Millimetre wave (mmW) and microwave spectra usually show features of rotational transitions and are therefore used for structure determination. Taking broadband spectra in these frequency regions with chirped pulse techniques became feasible due to recent advances in fast digital electronics broadband FOURIER transform spectroscopy.<sup>2</sup>

Chirp technology is a powerful tool because it provides fast acquisition of broadband spectra with high sensitivity and high frequency resolution in the regime of kHz.<sup>3</sup> This allows to get an overview of the molecular features in the region of investigation. Due to the fast acquisition many transitions can be investigated simultaneously and the sample consumption is often reduced in comparison to

---

<sup>1</sup>Ziurys, “Millimeter and Submillimeter Wave Spectroscopy and Astrophysical Applications”, 2011, p. 939.

<sup>2</sup>Shipman and Pate, “New Techniques in Microwave Spectroscopy”, 2011.

<sup>3</sup>Park and Field, “Perspective: The first ten years of broadband chirped pulse Fourier transform microwave spectroscopy”, 2016.

## 1. Introduction

standard step-scan techniques. The chirped pulse technique also allows to separately control bandwidth and pulse duration. Therefore, the frequency range of the excitation and the energy delivered to the sample become decoupled.<sup>4</sup>

The efficient acquisition of mostly rotational spectra allows to advance in different fields of spectroscopy.<sup>5</sup> For example special techniques such as supersonic expansion jets can be used to investigate gases at cold temperature with barely any collisions between the gas particles. This resembles the conditions found in the interstellar gas, which is cold and diffuse by terrestrial standards.<sup>6</sup> But not only thermodynamical conditions play an important role; also the synthesis of species of astrophysical interest is relevant in this context. In space, because of the low density, collisions seldomly occur and transient species may exist for comparably long time. To detect new interstellar molecules, it is desirable to combine the spectrometer with adequate production techniques required by these transient molecules.<sup>7</sup>

This work provides insight into the automatisisation of the chirped pulse FOURIER transform millimetre wave (CPFTmmW) spectrometer used at the Laboratory Astrophysics group located in KASSEL. The instrument is operated in different setups to investigate various molecules. Gas flow experiments with methanol and acetonitrile were conducted to demonstrate the spectrometer's capabilities and derive information on the sensitivity. In a next step, more elaborate molecule production techniques have been tested. One approach involved heating of a solid sample of glyceraldehyde (GA) to evaporate the material and investigate its molecules in the gas phase. In another setup supersonic expansion jets allowed to cool the molecular gas of propylene oxide (PO) far below the ambient temperature. Finally, laser ablation experiments using bismuth tribromide ( $\text{BiBr}_3$ ) and titanium were conducted in an effort to create transient molecules.

But first some insights are given into the principles and theory of rotational molecular spectroscopy that is thus introduced in the next chapter.

---

<sup>4</sup>G. G. Brown et al., "A broadband Fourier transform microwave spectrometer based on chirped pulse excitation", 2008.

<sup>5</sup>Shipman and Pate, "New Techniques in Microwave Spectroscopy", 2011.

<sup>6</sup>Ziurys, "Millimeter and Submillimeter Wave Spectroscopy and Astrophysical Applications", 2011, p. 939.

<sup>7</sup>Ziurys, "Millimeter and Submillimeter Wave Spectroscopy and Astrophysical Applications", 2011, p.946.

## 2. Theory of Molecular Spectroscopy

This chapter gives an overview on the physical principles and theory to facilitate the understanding of the work done in the frame of this project.

### 2.1. Molecular Rotational Spectroscopy

At first the basic principles of molecular rotational spectroscopy are outlined. This chapter is based on *Spectra of Atoms and Molecules* from P. BERNATH, especially chapter 6 *Rotational Spectroscopy*.<sup>8</sup>

Molecules are extended objects in space and therefore able to rotate. This rotational movement can be described by classical mechanics. To start, it will be described in the limit of the rigid rotor, before introducing centrifugal distortions. Considerations on the light-matter interaction will be outlined.

#### 2.1.1. Rigid Rotor<sup>9</sup>

A rigid body is an inelastic object. The origin of the coordinate system is placed to coincide with the centre of mass. The angular velocity  $\omega$  and the angular momentum  $L$  are vectors related by the moment of inertia  $\mathbf{I}$ . The latter can be represented by a symmetric  $3 \times 3$  matrix.

$$L = \mathbf{I}\omega \tag{1}$$

A molecule consists of multiple particles (identified by the subscript  $\alpha$ ) with mass  $m_\alpha$  located at fixed positions  $r_\alpha$  relative to the origin in a Cartesian coordinate

---

<sup>8</sup>Bernath, *Spectra of atoms and molecules*, 2005, p. 161 et sqq.

<sup>9</sup>Based on section 6.1 *Rotation of Rigid Bodies* from Bernath, *Spectra of atoms and molecules*, 2005, pp. 161 - 169.

## 2. Theory of Molecular Spectroscopy

system. To approximate the rigid body bond lengths are fixed and vibrations ignored. The molecule rotates with angular velocity  $\omega$ . The angular momentum can then be given as

$$\begin{aligned} L &= \sum_{\alpha} m_{\alpha} r_{\alpha} \times (\omega \times r_{\alpha}) \\ &= \sum_{\alpha} m_{\alpha} (\omega(x_{\alpha}^2 + y_{\alpha}^2 + z_{\alpha}^2) - r_{\alpha}(x_{\alpha}\omega_x + y_{\alpha}\omega_y + z_{\alpha}\omega_z)). \end{aligned} \quad (2)$$

The principal axis system (i.e., the moment of inertia tensor only has entries along the main diagonal and is 0 otherwise) can be assumed to produce

$$\begin{pmatrix} L_x \\ L_y \\ L_z \end{pmatrix} = \begin{pmatrix} I_x & 0 & 0 \\ 0 & I_y & 0 \\ 0 & 0 & I_z \end{pmatrix} \begin{pmatrix} \omega_x \\ \omega_y \\ \omega_z \end{pmatrix} \quad (3)$$

with three principal moments of inertia  $I_x, I_y, I_z$ . The rotational kinetic Energy  $E_k$  then takes the form

$$\begin{aligned} E_k &= \frac{1}{2}I_x\omega_x^2 + \frac{1}{2}I_y\omega_y^2 + \frac{1}{2}I_z\omega_z^2 \\ &= \frac{L_x^2}{2I_x} + \frac{L_y^2}{2I_y} + \frac{L_z^2}{2I_z} \end{aligned} \quad (4)$$

While the origin of the coordinate system rests in the centre of mass of the molecule, the direction of the axis is chosen by conventions. The  $z$ -axis always points along the highest order axis of rotational symmetry, while the  $x$ -axis points out of plane in case of a planar molecule. Furthermore, a scheme labelling axes as  $a, b$  and  $c$  based on the magnitude of inertia, can be chosen to ensure that the condition

$$I_A \leq I_B \leq I_C \quad (5)$$

holds. Based on the relations between the components of the moment of inertia along each axis, molecules can be classified into one of the following five categories:

- Linear molecules,  $I_A = 0; I_B = I_C$
- Spherical tops,  $I_A = I_B = I_C$
- Prolate symmetric tops,  $I_A < I_B = I_C$

## 2.1. Molecular Rotational Spectroscopy

- Oblate symmetric tops,  $I_A = I_B < I_C$
- Asymmetric tops,  $I_A < I_B < I_C$

The classification eases the analysis of the spectra.

### 2.1.2. Diatomic and Linear Molecules<sup>10</sup>

For simplicity the unsophisticated case of a diatomic or rigid linear molecule with no net orbital or spin angular momentum is investigated here.

When assuming atoms as point masses, in a linear molecule, such as a diatomic one, the moment of inertia tensor can be reduced to a scalar since

$$I_z = 0 \quad \text{and} \quad I_x = I_y = I.$$

The scalar nature enables to calculate the moment of inertia for diatomic molecules with the reduced mass constant  $\mu$ , composed of the masses  $m_1, m_2$  of the involved atoms, and the equilibrium distance between the nuclei  $r$ .

$$\begin{aligned} \mu &= \frac{m_1 m_2}{m_1 + m_2} \\ I &= \mu r^2 \end{aligned} \tag{6}$$

The rotational kinetic energy from equation (4) then becomes

$$\begin{aligned} E_k &= \frac{1}{2} I_x \omega_x^2 + \frac{1}{2} I_y \omega_y^2 \\ &= \frac{L_x^2}{2I} + \frac{L_y^2}{2I} = \frac{L^2}{2I}. \end{aligned} \tag{7}$$

$L = I\omega$  is then the total angular momentum of the diatomic or linear molecule exclusive of nuclear spin. The rotational Hamiltonian operator for a linear molecule in a field-free (isotropic) space can be given as

$$\hat{H} = \frac{\hat{J}^2}{2I} \tag{8}$$

---

<sup>10</sup>Based on section 6.2 *Diatomic and Linear Molecules* from Bernath, *Spectra of atoms and molecules*, 2005, pp. 169 - 181.

## 2. Theory of Molecular Spectroscopy

which can be solved using spherical harmonics ( $\Psi_{LM} = Y_{JM}$ ) due to its isotropy. The stationary SCHRÖDINGER equation for this case is

$$\begin{aligned}\frac{\hat{J}^2\Psi}{2I} &= E\Psi \\ &= \frac{J(J+1)\hbar^2\Psi}{2I} \\ &= BJ(J+1)\Psi.\end{aligned}\tag{9}$$

$J = 0, 1, 2, \dots$  is the rotational quantum number. The energy eigenvalue  $F(J)$  becomes

$$F(J) = BJ(J+1)\tag{10}$$

with the rotational constant  $B$ . This can be expressed with the reduced mass from equation (6).

$$\begin{aligned}B &= \frac{\hbar^2}{2I} \\ &= \frac{\hbar^2}{2\mu r^2}\end{aligned}\tag{11}$$

### 2.1.3. Selection Rules<sup>11</sup>

The transition dipole moment  $\mu$  describes the displacement of a centre of mass and the centre of charge within the molecule. It is a measure of the strength of interaction between the molecule and the electromagnetic field. It therefore dominates the formula for the intensity  $M$  (distinguished from the magnetic quantum number  $M$  by plain, non-italic font) of a pure rotational transition.

$$M = \int \Psi_{J'M'}\mu\Psi_{JM}d\tau\tag{12}$$

The wavefunction  $\Psi_{JM}$  for a linear molecule can be given with the help of spherical harmonics as:

$$\Psi_{JM} = Y_{JM}(\theta, \phi) = \Theta_{JM}(\theta)\frac{e^{iM\phi}}{\sqrt{2\pi}}\tag{13}$$

---

<sup>11</sup>Based on Bernath, *Spectra of atoms and molecules*, 2005, p. 171 - 173.

## 2.1. Molecular Rotational Spectroscopy

The electric dipole moment can only be oriented along the internuclear axis of the molecule in the laboratory axis system. With  $\hat{e}_n$  being the respective unit vector this results in

$$\begin{aligned}\mu &= \mu_x \hat{e}_1 + \mu_y \hat{e}_2 + \mu_z \hat{e}_3 \\ &= \mu_0 (\sin(\theta) \cos(\phi) \hat{e}_1 + \sin(\theta) \sin(\phi) \hat{e}_2 + \cos(\theta) \hat{e}_3).\end{aligned}\quad (14)$$

Rewriting equation (12) creates

$$\begin{aligned}M &= \frac{\mu_0}{2\pi} \left( \hat{e}_1 \int_0^{2\pi} \int_0^\pi \Theta_{J'M'} e^{-iM'\phi} \sin(\theta) \cos(\phi) \Theta_{JM} e^{iM\phi} \sin(\theta) d\theta d\phi \right. \\ &\quad + \hat{e}_2 \int_0^{2\pi} \int_0^\pi \Theta_{J'M'} e^{-iM'\phi} \sin(\theta) \sin(\phi) \Theta_{JM} e^{iM\phi} \sin(\theta) d\theta d\phi \\ &\quad \left. + \hat{e}_3 \int_0^{2\pi} \int_0^\pi \Theta_{J'M'} e^{-iM'\phi} \cos(\theta) \Theta_{JM} e^{iM\phi} \sin(\theta) d\theta d\phi \right).\end{aligned}\quad (15)$$

A recursion relationship for the associated LEGENDRE polynomials is employed by

$$\begin{aligned}(2l+1)zP_l^m(z) &= (l+m)P_{l-1}^m(z) + (l-m+1)P_{l+1}^m(z) \\ &\text{with } z = \cos\theta.\end{aligned}$$

Applying the equations

$$\begin{aligned}\cos\phi &= (e^{i\phi} + e^{-i\phi})/2 \\ \sin\phi &= (e^{i\phi} - e^{-i\phi})/2i \\ \Theta_{JM}(\theta) &= NP_l^m(\cos\theta)\end{aligned}$$

yields the following selection rules:

$$\Delta M = 0, \pm 1 \quad \text{and} \quad \Delta J = \pm 1.\quad (16)$$

Here,  $J$  is the angular momentum quantum number. The angular momentum  $\vec{J}$  has  $2J+1$  possible orientations. This is described by the magnetic quantum number  $M$ , which is the projection of  $\vec{J}$  onto  $Z$  in the laboratory frame.

## 2. Theory of Molecular Spectroscopy

The selection rules imply that transitions are only possible when they occur between two subsequent energy levels. They are furthermore only allowed if the permanent dipole moment is not zero ( $\mu_0 \neq 0$ ). Considering solely one-photon electric-dipole interactions, symmetric molecules may have no pure rotational transitions. However, molecules without permanent dipole moment can still interact with the electromagnetic field via magnetic-dipole interactions. Alternatively they exhibit a displacement from the centre of mass in relation to the centre of charge upon vibration, therefore inducing a dipole moment to allow for weak rotational transitions.

When  $\Delta J = +1$ , a transition is labelled to be in the *P*-Branch, while  $\Delta J = -1$  corresponds to the *R*-Branch. So far, no additional vibrational, orbital or spin angular momenta are considered. Such an additional angular momentum also allows *Q*-branch rotational transitions, i.e.,  $\Delta J = 0$ .

### 2.1.4. Light Matter Interaction<sup>12</sup>

Interaction between the electromagnetic field and the molecule mediated by the dipole moment can be understood as an energy transfer. *Absorption* is the process, when energy is transferred from the electromagnetic field to the rotation of the molecule, i.e., the resulting state of the molecule is energetically higher. Its reverse process is then labelled *emission*. By convention the process can be indicated by arrows between two states, with the energy of a state indicated by primes:  $J'$  corresponds to the upper state, while double primes  $J''$  indicate the lower state. Customarily upper states are written first. Therefore

$$\begin{aligned} J' \leftarrow J'' & \text{ corresponds to absorption, while} \\ J' \rightarrow J'' & \text{ is for emission.} \end{aligned} \tag{17}$$

The intensity of the lines is determined by the transition dipole moment (as will be discussed in chapter 2.1.9) and the population difference of the involved states, which can be calculated from statistical thermodynamics for the case of thermal

---

<sup>12</sup>Based on Bernath, *Spectra of atoms and molecules*, 2005, p. 172, 173.

## 2.1. Molecular Rotational Spectroscopy

equilibrium. The rotational partition function can be given as

$$q_r = \sum_f (2J + 1) e^{-BJ(J+1)/k_B T} \approx \frac{k_B T}{\sigma B} \quad (18)$$

with the symmetry number  $\sigma = 2$  for a symmetric or  $\sigma = 1$  for a nonsymmetric molecule,  $k_B$  the BOLTZMANN constant and  $T$  the temperature. For simplicity in this consideration only the ground vibrational and electronic states are populated at temperature  $T$ . From a total concentration  $N$  of all molecules, the concentration  $N_J$  of molecules in the rotational quantum number  $J$  becomes

$$N_J \approx N(2J + 1) \frac{e^{-BJ(J+1)/k_B T}}{k_B T / \sigma B}. \quad (19)$$

The population of a state therefore largely depends on the temperature.

### 2.1.5. Spectra of Diatomic and Linear Molecules<sup>13</sup>

Using the SCHROEDINGER equation (9) and the selection rules from equation (16) creates a set of states and possible transitions, which can be depicted in an energy diagram as shown in figure 2.1.1.

In a spectroscopic experiment (a part of) the electromagnetic spectrum is scanned. Either the absorption or the emission of the molecule is detected. For the former the energy values needed for the transitions appear “missing” or as dips compared to the reference spectrum, which is the (normalised) constant radiation background. In case of emission the transitions appear as peaks respectively.

A transition in accordance with the selection rule  $\Delta J = \pm 1$  results in frequencies

$$\begin{aligned} \nu_{J+1 \leftarrow J} &= F(J') - F(J'') \\ &= B(J + 1)(J + 2) - BJ(J + 1) \\ &= 2B(J + 1). \end{aligned} \quad (20)$$

From equation (20) and figure 2.1.1 a constant energy difference of  $2B$  can be derived. Lines in the respective absorption (or emission) spectrum therefore appear evenly separated by the energy value  $2B$ . An example of a hypothetical molecule in the approximation of the rigid rotor is shown in figure 2.1.2.

---

<sup>13</sup>Based on Bernath, *Spectra of atoms and molecules*, 2005, p. 172 - 174.

## 2. Theory of Molecular Spectroscopy

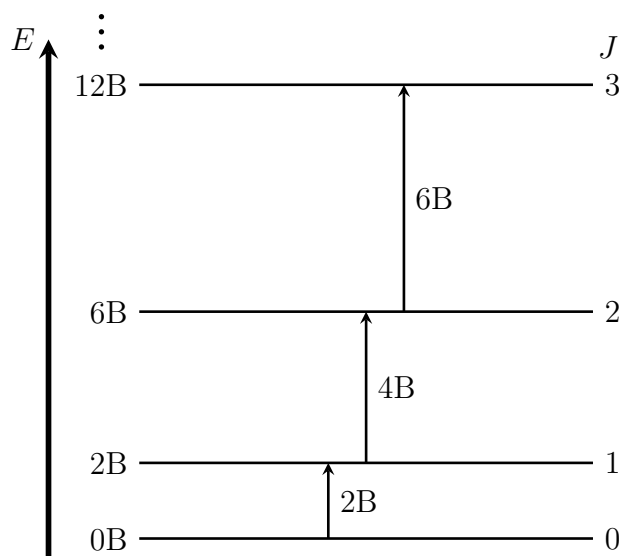


**Figure 2.1.1.:** Energy diagram showing the rotational transitions of a linear molecule. The differences between the energy states, i.e., the energy of the corresponding transition are increments of  $2B$ .<sup>14</sup>

### 2.1.6. Centrifugal Force<sup>15</sup>

When a molecule rotates, the particles are subject to centrifugal forces. The approximation of the rigid rotor is no longer valid: The bonds between the atoms distort to maintain an equilibrium between the centrifugal force and a restoring force depending on the bond strength. For diatomic or linear molecules this can be described by a TAYLOR series with an increasing amount of higher order distortion corrections

$$F(J) = BJ(J + 1) - D[J(J + 1)]^2 + H[J(J + 1)]^3 + L[J(J + 1)]^4 + \dots \quad (21)$$

The negative sign in the second term was chosen to make the centrifugal distortion constant  $D$  a positive number.  $L$  and  $H$  are higher order correction terms.

In the case of a diatomic molecule the centrifugal distortion increases the space

<sup>14</sup>Inspired by Bernath, *Spectra of atoms and molecules*, 2005, p. 173, figure 6.13.

<sup>15</sup>Based on *Centrifugal Distortion* from Bernath, *Spectra of atoms and molecules*, 2005, pp. 174 - 177.

## 2.1. Molecular Rotational Spectroscopy

between the nuclei. This in turn influences the effective rotational constant:

$$B_{eff} = B - DJ(J + 1). \quad (22)$$

When aborting the TAYLOR series from equation (21) after the second term, the equation (20) can be modified to comprise centrifugal distortion and becomes:

$$\begin{aligned} \nu_{J+1 \leftarrow J} &= F(J + 1) - F(J) \\ &= 2B(J + 1) - 4D(J + 1)^3 \\ &= 2 \left[ B - 2D(J + 1)^2 \right] (J + 1). \end{aligned} \quad (23)$$

The negative sign indicates that the centrifugal distortion term reduces the energy separation for the transition. The spacing between the lines will consequently always be smaller than  $2B$ . With increasing  $J$ , lines will therefore appear closer together. This effect is shown in figure 2.1.2 alongside the rotational spectrum of a hypothetical rigid rotor.

### 2.1.7. Influence of Vibrational and Electronic States on the Rotational Constants<sup>16</sup>

The rotational constant also depends on vibrational and electronic states: When a molecule vibrates, the positions of the nuclei can be described by the MORSE potential. This means, that nuclei in a higher excited vibrational state will spend more time at larger distances  $\langle r \rangle$  (angle brackets indicate time average). Increasing the vibrational quantum number  $v$  leads to an increase of  $\langle r \rangle$ , which creates in turn a decreasing rotational constant compared to the rotational constant at equilibrium  $B_e$  as

$$B_v = \frac{h^2}{8\pi^2\mu} \left\langle \frac{1}{r^2} \right\rangle. \quad (24)$$

Parametrisation yields the following set of equations for the rotational constant  $B$ , the centrifugal distortion coefficient  $D$  and the rotational energy level expressions  $F$  in dependence of the vibrational quantum number  $v$ . Dots indicate higher order

---

<sup>16</sup>Based on Bernath, *Spectra of atoms and molecules*, 2005, pp. 175 - 177.

## 2. Theory of Molecular Spectroscopy

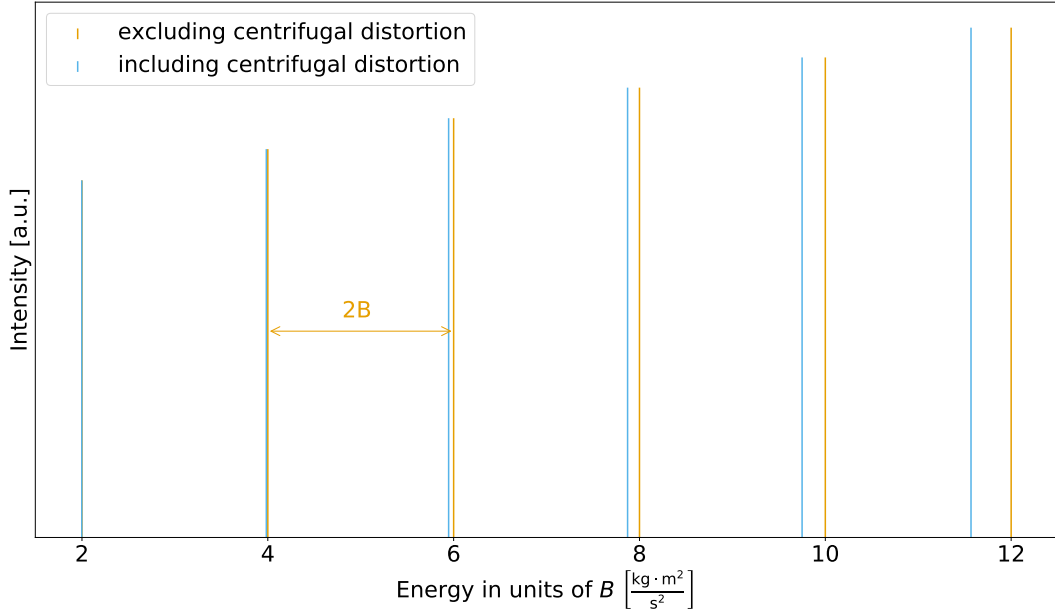


**Figure 2.1.2.:** Spectrum predicted for a hypothetical molecule with  $B = 1 \frac{\text{kg}\cdot\text{m}^2}{\text{s}^2}$  and  $D = 5 \cdot 10^{-4} \frac{\text{kg}\cdot\text{m}^2}{\text{s}^2}$ . Orange lines indicate prediction not considering centrifugal distortion while blue lines include centrifugal distortion effects. Lines for the rigid rotor are evenly spaced at  $2B$ , while according to equation (23) the deviation from the rigid rotor caused by centrifugal distortion increases for large  $J$  at higher frequencies. This Spectrum is based on hypothetical molecular parameters for a diatomic molecule.

terms, which are neglected in this consideration.

$$\begin{aligned}
 B_v &= B_e - \alpha_e \left(v + \frac{1}{2}\right) + \gamma_e \left(v + \frac{1}{2}\right)^2 + \dots \\
 D_v &= D_e + \beta_e \left(v + \frac{1}{2}\right) + \dots \\
 F_v(J) &= B_v(J + 1) - D_v(J(J + 1))^2 + \dots
 \end{aligned} \tag{25}$$

The expression for the transition frequency including the effects of centrifugal distortion and the influence of the vibration onto rotational constants then becomes:

$$\nu_{J+1 \leftarrow J} = 2B_v(J + 1) - 4D_v(J + 1)^3. \tag{26}$$

### 2.1.8. Vibrational angular momentum<sup>17</sup>

When looking classically at a linear molecule, vibrations of nuclei in  $x$ - and  $y$ -direction can be phased such that they execute circular motions about the  $z$ -axis. Thus, degenerate vibrations can contribute to the angular momentum.<sup>18</sup> These motions become quantised, so only multiples of  $\hbar$  can be realized. Therefore a contribution to the total angular momentum  $\hat{J}$  in a linear molecule is the vibrational angular momentum  $\hat{l}$ . It can be described by a new quantum number  $l$  and takes the magnitude of  $\pm|l|\hbar$ . The double degeneracy of  $l$  is associated with either clockwise or counterclockwise vibrational angular momentum. The rotational  $\hat{R}$  and vibrational  $\hat{l}$  angular momenta couple to give the total angular momentum

$$\hat{J} = \hat{R} + \hat{l}. \quad (27)$$

Hence, the total angular momentum  $J$  can only take values of or larger than  $|l|$ .

### 2.1.9. Line Intensities<sup>19</sup>

Estimating the intensity of a line is essential for spectroscopy. Only when relative intensities match between prediction and sample, a spectroscopist may assign lines properly.

The transition dipole moment from equation (12) for a transition between two quantum states  $|J'M'\rangle \leftrightarrow |J''M''\rangle$  with the dipole operator  $\mu$  is

$$M = \langle J'M' | \mu | J''M'' \rangle. \quad (28)$$

The integrals in equation (15) are evaluated separately. Considering suitable sets of selection rules, spherical harmonics and associated LEGENDRE polynomials

<sup>17</sup>Based on *Vibrational Angular Momentum* from Bernath, *Spectra of atoms and molecules*, 2005, pp. 177 - 181.

<sup>18</sup>See also Townes and Schawlow, *Microwave spectroscopy*, 2012, p.79-82.

<sup>19</sup>Based on *Line Intensities for Diatomic and Linear Molecules* from Bernath, *Spectra of atoms and molecules*, 2005, pp. 182 - 184.

## 2. Theory of Molecular Spectroscopy

leads the squared transition dipole moment magnitude to become

$$\begin{aligned} |M|_{J+1 \leftarrow J, M}^2 &= \mu_0^2 (J+1) \\ |M|_{J+1 \rightarrow J, M}^2 &= \mu_0^2 (J+1) \end{aligned} \quad (29)$$

for absorption and emission respectively. Including a lineshape function  $g(\nu - \nu_{10})$  the EINSTEIN  $A$  coefficient becomes

$$(A_{J+1 \rightarrow J})_\nu = \frac{16\pi^3 \nu^3 \mu_0^2 (J+1)}{3\epsilon_0 h c^3 (2J+3)} g(\nu - \nu_{10}) \quad (30)$$

The absorption cross section  $\sigma$  can be given as

$$\sigma_{J+1 \leftarrow J} = \frac{2\pi^2 \nu \mu_0^2 (J+1)}{3\epsilon_0 h c (2J+1)} g(\nu - \nu_{10}). \quad (31)$$

With the help of the absorption cross section, the absorption coefficient  $\alpha$  can be calculated with

$$\alpha = \sigma \left( N_0 - N_1 \frac{2J+1}{2J+3} \right). \quad (32)$$

For convenience  $N_0$  and  $N_1$  can be replaced with a total concentration  $N$ . Excluding vibrational or electrical degeneracy, a purely  $(2J+1)$ -fold rotational degeneracy of state  $J$  is assumed to give

$$N_0 = P_J N = \frac{N(2J+1)e^{-E_J/k_B T}}{q}. \quad (33)$$

Inserting the partition function  $q = q_{el} + q_{vib} + q_{rot}$  this yields

$$\alpha = \frac{2\pi^2 \nu \mu_0^2 (J+1) N e^{-E_J/k_B T}}{3\epsilon_0 h c q} \left( 1 - e^{-h\nu/k_B T} \right) g(\nu - \nu_{10}). \quad (34)$$

With this, BEER'S law including a stimulated emission correction can be given as

$$I = I_0 e^{-\sigma(N_0 - N_1 \frac{2J+1}{2J+3})l} = I_0 e^{-\alpha l}. \quad (35)$$

### 2.1.10. Describing Extended Molecules<sup>20</sup>

Molecules, that are neither diatomic nor linear can extend into all three space dimensions. The classical energy for the rigid rotor is then given by

$$E = \frac{J_a^2}{2I_A} + \frac{J_b^2}{2I_B} + \frac{J_c^2}{2I_C}, \quad (36)$$

which results in the rigid asymmetric Hamiltonian operator

$$\hat{H} = \frac{\hat{J}_a^2}{2I_A} + \frac{\hat{J}_b^2}{2I_B} + \frac{\hat{J}_c^2}{2I_C}. \quad (37)$$

This can now be used to obtain energy level expressions for any molecule in the boundaries of the rigid body approximation. Because symmetry eases the analysis, symmetric tops are investigated before analysing the more general case of asymmetric tops.

### 2.1.11. Symmetric Tops<sup>21</sup>

Symmetry facilitates the analysis of extended rotating bodies. Symmetric tops can be classified into two groups depending on the distribution of moments of inertia. Prolate tops with  $I_B = I_C$  and oblate tops with  $I_A = I_B$ . In the case of a rigid body the classical energy-level expression, equation (36), becomes

$$E_p = \frac{J_a^2}{2I_A} + \frac{J_b^2 + J_c^2}{2I_B} \quad (\text{prolate top}) \quad (38)$$

$$E_o = \frac{J_a^2 + J_b^2}{2I_B} + \frac{J_c^2}{2I_C} \quad (\text{oblate top}) \quad (39)$$

In the following only the prolate symmetric top will be considered, as the derivation is analogous to the oblate top by interchanging the labels  $a$  and  $c$ . With

$$J^2 = J_a^2 + J_b^2 + J_c^2 \quad \Leftrightarrow \quad J^2 - J_a^2 = J_b^2 + J_c^2$$

<sup>20</sup>Based on Bernath, *Spectra of atoms and molecules*, 2005, pp. 193 - 195.

<sup>21</sup>Based on section 6.4 *Symmetric Tops* from Bernath, *Spectra of atoms and molecules*, 2005, pp. 185 - 193.

## 2. Theory of Molecular Spectroscopy

equation (38) can be given as

$$E = \frac{1}{2I_B} J^2 + \left( \frac{1}{2I_A} \frac{1}{2I_B} \right) J_a^2, \quad (40)$$

which enables to give the quantum mechanical Hamiltonian operator to equation (40) as

$$\hat{H} = \frac{1}{2I_B} \hat{J}^2 + \left( \frac{1}{2I_A} \frac{1}{2I_B} \right) \hat{J}_a^2. \quad (41)$$

Two coordinate systems are used to describe rotation of molecules in space. The space-fixed laboratory system is indicated by capital letters for the directional axis:  $X, Y, Z$ ; the molecular coordinate system by lower case letters:  $x, y, z$  ( $a, b, c$ ). Both have the centre of mass of the molecule as their origin. Their orientation is described by EULER angles.  $\theta$  and  $\phi$  are the polar and azimuthal angles of the molecular  $z$ -axis in the space-fixed system.  $\chi$  corresponds to the internal orientation of the molecule in relation to the molecular  $z$ -axis. Space-fixed and molecular coordinate system relate via a transformation matrix  $\mathbf{S}$ .

$$\begin{pmatrix} x \\ y \\ z \end{pmatrix} = \begin{pmatrix} \Phi_{xX} & \Phi_{xY} & \Phi_{xZ} \\ \Phi_{yX} & \Phi_{yY} & \Phi_{yZ} \\ \Phi_{zX} & \Phi_{zY} & \Phi_{zZ} \end{pmatrix} \begin{pmatrix} X \\ Y \\ Z \end{pmatrix} = \mathbf{S} \begin{pmatrix} X \\ Y \\ Z \end{pmatrix} \quad (42)$$

$$\mathbf{S} = \begin{pmatrix} \cos \theta \cos \phi \cos \chi - \sin \phi \sin \chi & \cos \theta \sin \phi \cos \chi + \cos \phi \sin \chi & -\sin \theta \cos \chi \\ -\cos \theta \cos \phi \sin \chi - \sin \phi \sin \chi & -\cos \theta \sin \phi \sin \chi + \cos \phi \cos \chi & -\sin \theta \sin \chi \\ \sin \theta \cos \phi & \sin \theta \sin \phi & \cos \theta \end{pmatrix} \quad (43)$$

Angular momenta measured in the molecular frame can be expressed as

$$\hat{J}_x = \Phi_{xX} \hat{J}_X + \Phi_{xY} \hat{J}_Y + \Phi_{xZ} \hat{J}_Z \quad (44)$$

$$\hat{J}_y = \Phi_{yX} \hat{J}_X + \Phi_{yY} \hat{J}_Y + \Phi_{yZ} \hat{J}_Z \quad (45)$$

$$\hat{J}_z = \Phi_{zX} \hat{J}_X + \Phi_{zY} \hat{J}_Y + \Phi_{zZ} \hat{J}_Z. \quad (46)$$

## 2.1. Molecular Rotational Spectroscopy

Combining the above equations and the elements of the transformation matrix  $\mathbf{S}$ , yields the following expressions:

$$\hat{J}_x = -i\hbar \left( \frac{-\cos\chi}{\sin\theta} \frac{\partial}{\partial\phi} + \frac{\cos\chi \cos\theta}{\sin\theta} \frac{\partial}{\partial\chi} + \sin\chi \frac{\partial}{\partial\theta} \right) \quad (47)$$

$$\hat{J}_y = -i\hbar \left( \frac{\sin\chi}{\sin\theta} \frac{\partial}{\partial\phi} - \frac{\sin\chi \cos\theta}{\sin\theta} \frac{\partial}{\partial\chi} + \cos\chi \frac{\partial}{\partial\theta} \right) \quad (48)$$

$$\hat{J}_z = -i\hbar \frac{\partial}{\partial\chi} \quad (49)$$

Written in the laboratory frame this results in:

$$\hat{J}_x = -i\hbar \left( \frac{-\cos\phi \cos\theta}{\sin\theta} \frac{\partial}{\partial\phi} + \frac{\cos\phi}{\sin\theta} \frac{\partial}{\partial\chi} - \sin\phi \frac{\partial}{\partial\theta} \right) \quad (50)$$

$$\hat{J}_y = -i\hbar \left( \frac{\sin\phi \cos\theta}{\sin\theta} \frac{\partial}{\partial\phi} - \frac{\sin\phi}{\sin\theta} \frac{\partial}{\partial\chi} + \cos\phi \frac{\partial}{\partial\theta} \right) \quad (51)$$

$$\hat{J}_z = -i\hbar \frac{\partial}{\partial\chi} \quad (52)$$

With the symmetric top Hamiltonian operator from equation (41) a set of simultaneous eigenfunctions results from the commutation of  $\hat{J}^2$ ,  $\hat{J}_Z$  and  $\hat{J}_z$ .

$$\hat{H} |JKM\rangle = E |JKM\rangle \quad (53)$$

$$\hat{J}^2 |JKM\rangle = J(J+1)\hbar^2 |JKM\rangle \quad (54)$$

$$\hat{J}_Z |JKM\rangle = M_J \hbar |JKM\rangle \quad (55)$$

$$\hat{J}_z |JKM\rangle = K \hbar |JKM\rangle \quad (56)$$

When  $\hat{J}$  is projected along the molecular  $z$ -axis, the resulting vector is  $K\hbar$ .

Raising operators (indicated by a negative sign (-)) and lowering operators (positive sign (+)) can be defined as  $\hat{J}^+ = \hat{J}_x + i\hat{J}_y$  and  $\hat{J}^- = \hat{J}_x - i\hat{J}_y$ . The sign in the superscript designates the molecular frame, while a subscript represents the laboratory frame. Raising and lowering operators affect the symmetric top

## 2. Theory of Molecular Spectroscopy

eigenfunctions as following:

$$\hat{J}_+ = \hbar\sqrt{J(J+1) - M(M+1)} |JKM+1\rangle \quad (57)$$

$$\hat{J}_- = \hbar\sqrt{J(J+1) - M(M-1)} |JKM-1\rangle \quad (58)$$

$$\hat{J}^+ = \hbar\sqrt{J(J+1) - K(K-1)} |JK-1M\rangle \quad (59)$$

$$\hat{J}^- = \hbar\sqrt{J(J+1) - K(K+1)} |JK+1M\rangle \quad (60)$$

With the symmetric top Hamiltonian operator, equation (41), the SCHRÖDINGER equation can be solved using the symmetric top wavefunction.

$$\begin{aligned} \hat{H}\psi_{JKM} &= \left( \frac{1}{2I_B} \hat{J}^2 + \left( \frac{1}{2I_A} \frac{1}{2I_B} \right) \hat{J}_a^2 \right) |JKM\rangle \\ &= \left( \frac{\hbar^2}{2I_B} J(J+1) + \left( \frac{\hbar^2}{2I_A} \frac{\hbar^2}{2I_B} \right) K^2 \right) |JKM\rangle \quad (\text{prolate top}) \end{aligned} \quad (61)$$

$$\begin{aligned} \hat{H}\psi_{JKM} &= \left( \frac{1}{2I_B} \hat{J}^2 + \left( \frac{1}{2I_C} \frac{1}{2I_B} \right) \hat{J}_c^2 \right) |JKM\rangle \\ &= \left( \frac{\hbar^2}{2I_B} J(J+1) + \left( \frac{\hbar^2}{2I_C} \frac{\hbar^2}{2I_B} \right) K^2 \right) |JKM\rangle \quad (\text{oblate top}) \end{aligned} \quad (62)$$

This leads to the energy expressions:

$$E_{JK_a} = BJ(J+1) + (A-B)K_a^2 \quad (\text{prolate top}) \quad (63)$$

$$E_{JK_c} = BJ(J+1) + (C-B)K_c^2 \quad (\text{oblate top}) \quad (64)$$

with the rotational constants

$$A = \frac{\hbar^2}{2I_A}, \quad B = \frac{\hbar^2}{2I_B}, \quad C = \frac{\hbar^2}{2I_C}. \quad (65)$$

$M$  does not appear in the formulae for the energy-level expression. The  $2J+1$  degeneracy therefore remains. With  $2J+1$  possible values for  $K$  the degeneracy is lifted, but states in  $\pm K$  still have the same energy due to the square. The twofold degeneracy can be understood as the equal amount of energy in clockwise and counterclockwise rotation.

Applying selection rules allows to determine spectra. The selection rules are

$$\Delta J = \pm 1, \quad \Delta M = 0, \pm 1 \quad \text{and} \quad \Delta K = 0. \quad (66)$$

## 2.1. Molecular Rotational Spectroscopy

In consequence, all transitions are confined to a respective  $K$ -ladder. This is indicated by grey arrows in figure 2.1.3.

$$\nu_{J+1,K \leftarrow J,K} = 2B(J+1) \quad (67)$$

Including the centrifugal distortion effects the energy levels can be described as

$$F(J, K) = BJ(J+1) - D_J(J(J+1))^2 + (A-B)K^2 - D_K K^4 - D_{JK}J(J+1)K^2 \quad (68)$$

with the centrifugal distortion constants  $D_J$ ,  $D_K$ , and  $D_{JK}$ . The transition frequencies can be calculated with

$$\begin{aligned} \nu_{J+1,K \leftarrow J,K} &= F(J+1, K) - F(J, K) \\ &= 2B(J+1) - 4D_J(J+1)^3 - 2D_{JK}(J+1)K^2 \end{aligned} \quad (69)$$

The corresponding energy-level diagram for a prolate and an oblate symmetric top molecule and their allowed electric dipole transitions is shown in figure 2.1.3. Note that the shift in the energy levels with increasing  $K$  is caused by the centrifugal distortion.

The line intensity can be estimated with the dipole moment  $\mu_0$  and the selection rules  $\Delta J = \pm 1$ ,  $\Delta K = 0$  with the expressions:

$$S_{J+1,K \leftarrow J,K} = \mu_0^2 \frac{(J+1)^2 - K^2}{J+1} \quad \text{and} \quad S_{J-1,K \leftarrow J,K} = \mu_0^2 \frac{J^2 - K^2}{J}. \quad (70)$$

These factors are further complicated by various effects including nuclear spin statistics and are usually given as HÖNL-LONDON factors in tabularly form, e.g. table 9.4 in BERNATHS *Spectra of atoms and molecules*<sup>22</sup>.

<sup>22</sup>Bernath, *Spectra of atoms and molecules*, 2005, p. 335.

<sup>23</sup>Inspired by Bernath, *Spectra of atoms and molecules*, 2005, p. 191, figures 6.29 and 6.30.

## 2. Theory of Molecular Spectroscopy

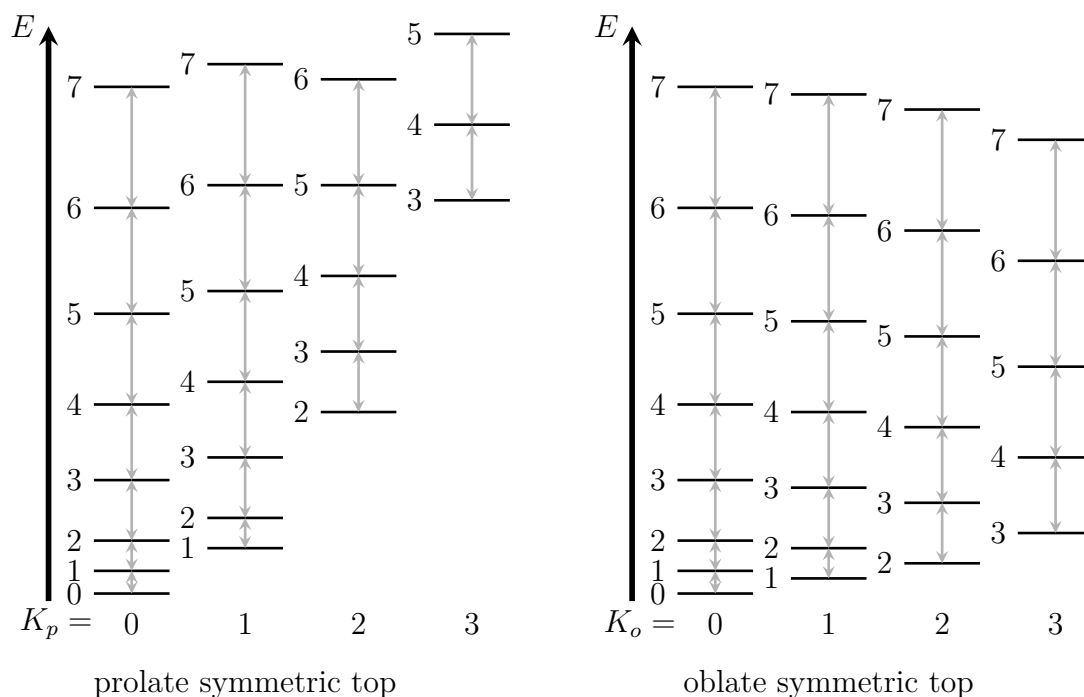


**Figure 2.1.3.:** Energy diagram showing the rotational transitions of prolate and oblate symmetric top molecules. Allowed electric dipole transitions are indicated by grey arrows. The numbers to the left of the energy levels indicate the rotational quantum number  $J$ .<sup>23</sup>

### 2.1.12. Asymmetric Tops<sup>24</sup>

For asymmetric tops, because  $I_A \neq I_B \neq I_C$ , symmetry does not ease the analysis. Numerical solving is needed as general analytical solutions are not available. But the results from the symmetric top can be used, because the asymmetric top can be viewed as the blend between the limits of an oblate and a prolate symmetric top. That property is quantified by RAY's asymmetry parameter  $\kappa$ .

$$\kappa = \frac{2B - A - C}{A - C} \quad (71)$$

$\kappa = -1$  represents a prolate symmetric top and  $\kappa = +1$  an oblate symmetric top. In figure 2.1.4 the energy levels for both extremes and their blend in the form of the asymmetric top is shown. This allows to label the individual energy states, depending on the good quantum number  $J$  and the labels  $K_a$  and  $K_c$ . The latter

<sup>24</sup>Based on section 6.5 *Asymmetric Tops* from Bernath, *Spectra of atoms and molecules*, 2005, pp. 193 - 198.

## 2.1. Molecular Rotational Spectroscopy

qualify as good quantum numbers in the prolate or oblate symmetric top limits and enable labelling a specific energy level for the asymmetric top.

In an approximation, the wavefunction of an asymmetric top is given by<sup>26</sup>

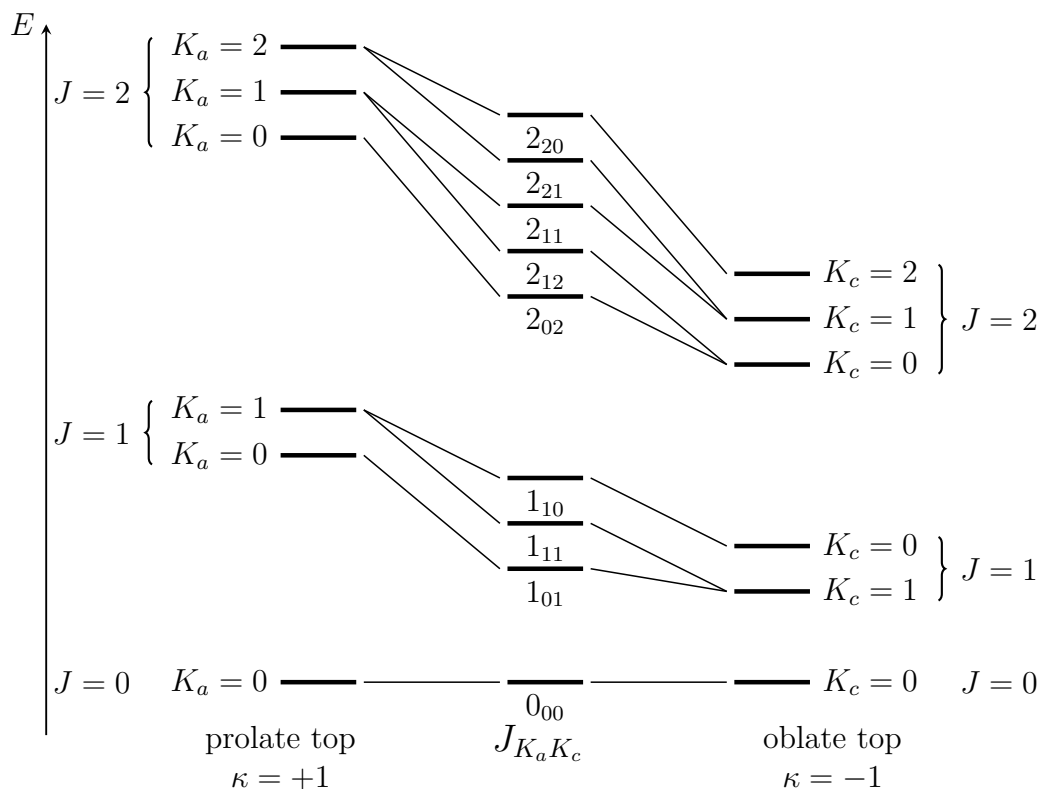


**Figure 2.1.4.:** Correlation diagram for labelling asymmetric top energy levels. Levels are not to scale. Lines connecting the energy levels are hypothetical distortions of the molecule.<sup>25</sup>

$$\Psi_{JK_a K_c M} = \sum_K a_{JK} \Psi_{JKM} \quad (72)$$

with the wavefunction  $\Psi_{JK}$  of an prolate or oblate symmetric top (depending on what describes the molecule the best) and a numerical parameter  $a_{JK}$ , describing the probability of rotation with angular momenta  $J$  and  $K$ .

Selection rules can be derived from symmetry and parity considerations as done in Townes and Schawlow, *Microwave spectroscopy*, 2012, pp. 18 - 24. The selection

<sup>25</sup>Inspired by Bernath, *Spectra of atoms and molecules*, 2005, p. 195, figure 6.33.

<sup>26</sup>Townes and Schawlow, *Microwave spectroscopy*, 2012, p. 95, 96.

## 2. Theory of Molecular Spectroscopy

rules are<sup>27</sup>

$$\Delta J = 0, \pm 1 \quad \text{and} \quad \Delta M = 0, \pm 1. \quad (73)$$

The asymmetric top allows three types of transitions depending on the direction of nonvanishing dipole transition moments  $\mu_a$ ,  $\mu_b$  or  $\mu_c$ . The selection rules for each type are depicted in table 2.1. For low symmetry molecules transitions of all three types can occur together.<sup>28</sup>

**Table 2.1.:** Selection rules for  $a$ ,  $b$  and  $c$  type asymmetric tops. In brackets weak allowed transitions are shown.

Type of transition	$\Delta K_a$	$\Delta K_c$
$a$ ( $\mu_a \neq 0$ )	0 ( $\pm 2, \pm 4, \dots$ )	$\pm 1$ ( $\pm 3, \pm 5, \dots$ )
$b$ ( $\mu_b \neq 0$ )	$\pm 1$ ( $\pm 3, \pm 5, \dots$ )	$\pm 1$ ( $\pm 3, \pm 5, \dots$ )
$c$ ( $\mu_c \neq 0$ )	$\pm 1$ ( $\pm 3, \pm 5, \dots$ )	0 ( $\pm 2, \pm 4, \dots$ )

### 2.1.13. Internal rotation

The structure of some molecules allows interactions between subgroups enabling movements called internal rotations. As the system can tunnel between the states, tunnel-splitting of states is observed. Therefore, hindered internal rotation or torsion significantly increase the complexity of the rotational spectrum as additional energy levels are generated and density of states can be high, due to generation of avoided crossings and mixing between ground and low lying excited torsional states.<sup>29</sup> Internal rotation is therefore only mentioned here for completeness.

## 2.2. Line Shapes and Broadening

Features in a spectrum created by interaction of radiation with matter are called lines. In the following sections a selection of effects are discussed, which influence the shape of these lines. The whole section is based on Bernath, *Spectra of atoms and molecules*, 2005, pp. 21 - 34.

<sup>27</sup>Bernath, *Spectra of atoms and molecules*, 2005, p. 195.

<sup>28</sup>Bernath, *Spectra of atoms and molecules*, 2005, p. 196, 197.

<sup>29</sup>Ziurys, "Millimeter and Submillimeter Wave Spectroscopy and Astrophysical Applications", 2011, p. 949.

### 2.2.1. Lorentzian Line Shape<sup>30</sup>

Assuming instantaneous emission, the lines would have the shape of a DIRAC delta function  $\delta(\nu - \nu_{10})$ . Due to the finite lifetime of an excited state, this line gets naturally broadened.

Given a two level system to be excited into a superposition, e.g. by interaction with electromagnetic radiation, the dipole moment  $M$  of the system oscillates with the BOHR angular frequency  $\omega_{10}$  as  $M(t) = 2a\mu_{10} \cos(\omega_{10}t)$ , with a real number  $a$  to represent the amplitude, the pulsance  $\omega$  and time  $t$ . When the population of the excited state decays, the amplitude of this oscillation is damped by an enveloping exponential function with the parameter  $\gamma$ .

$$M(t) = M_0 e^{-\gamma t/2} \cos(\omega_{10}t) \quad (74)$$

This time-domain consideration can be analysed with help of FOURIER transformations.

$$F(\omega) = \int_{-\infty}^{\infty} f(t) e^{-i\omega t} dt \quad (75)$$

The inverse FOURIER transform can be given as

$$f(t) = \frac{1}{2\pi} \int_{-\infty}^{\infty} F(\omega) e^{i\omega t} d\omega, \quad (76)$$

which implies that the sum or integral over plane waves  $e^{i\omega t}$  with amplitude  $F(\omega)$  produces any arbitrary waveform  $f(t)$ .

For a decay beginning at  $t = 0$  and approximating the non-resonant term to be negligible, the FOURIER transform of the time dependent part of equation (74) becomes

$$\begin{aligned} F(\omega) &= \int_{-\infty}^{\infty} e^{-\gamma t/2} \cos(\omega_{10}t) e^{-i\omega t} dt \\ &\approx \frac{1}{2} \frac{1}{\gamma/2 + i(\omega - \omega_{10})}. \end{aligned} \quad (77)$$

---

<sup>30</sup>Based on the subsections *Lineshape Functions* and *Natural Lifetime Broadening* from Bernath, *Spectra of atoms and molecules*, 2005, pp. 21 - 27.

## 2. Theory of Molecular Spectroscopy

Semiclassically, radiation of power of an oscillating dipole moment occurs at a rate proportional to  $|\mu_{10}|^2$ . The lineshape function therefore becomes an unnormalized LORENTZIAN.

$$|F(\omega)|^2 = \frac{1}{4} \frac{1}{(\gamma/2)^2 + (\omega - \omega_{10})^2} \quad (78)$$

With the requirement for normalization  $\int_{-\infty}^{\infty} g(\omega - \omega_{10}) d\omega = 1$  equation (78) is transformed into a normalized LORENTZIAN of finite width.

$$g(\omega - \omega_0) = \frac{\gamma}{(\gamma/2)^2 + (\omega - \omega_{10})^2}. \quad (79)$$

The parameter  $\gamma$  can be interpreted as the full width at half maximum (FWHM) of the line feature, as  $\gamma = \frac{1}{\tau_{sp}}$  (index *sp* represents spontaneous).

### 2.2.2. Pressure Broadening<sup>31</sup>

Pressure broadening depends on the intermolecular potential of the involved colliding particles. It therefore is an elaborate topic, that shall not be discussed in detail here. Instead, only a simplified model explains the general concept.

The pressure  $p$  inside a closed volume is a measure for frequency at which particles collide, as its reciprocal is proportional to the average time  $T$  between two collisions.

$$p \propto \frac{1}{T} \quad (80)$$

Collisions between particles can alter or interrupt the oscillation of the dipole moment discussed above. The oscillation cosine is then broken into several pieces with an average length  $T$ . Applying a FOURIER transformation results in a LORENTZIAN with a width given by

$$\begin{aligned} \Delta\nu_{1/2} &= \frac{1}{\pi T}, \\ &= bp \end{aligned} \quad (81)$$

---

<sup>31</sup>Based on subsection *Pressure Broadening* from Bernath, *Spectra of atoms and molecules*, 2005, pp. 27, 28.

with the pressure broadening coefficient  $b$ . Pressure broadening is a homogeneous broadening, as all molecules within the sample volume experience the same pressure (the same amount of collisions) and hence have identical lineshape functions.

### 2.2.3. Doppler Effect<sup>32</sup>

The influence of the DOPPLER effect causes lines to appear shifted in frequency, depending on the molecules' relative velocity towards or away from the radiation. Many particles with a MAXWELL-BOLTZMANN distribution of velocity components contribute to a broadening of the originally homogeneously broadened line as can be seen in figure 2.2.1.

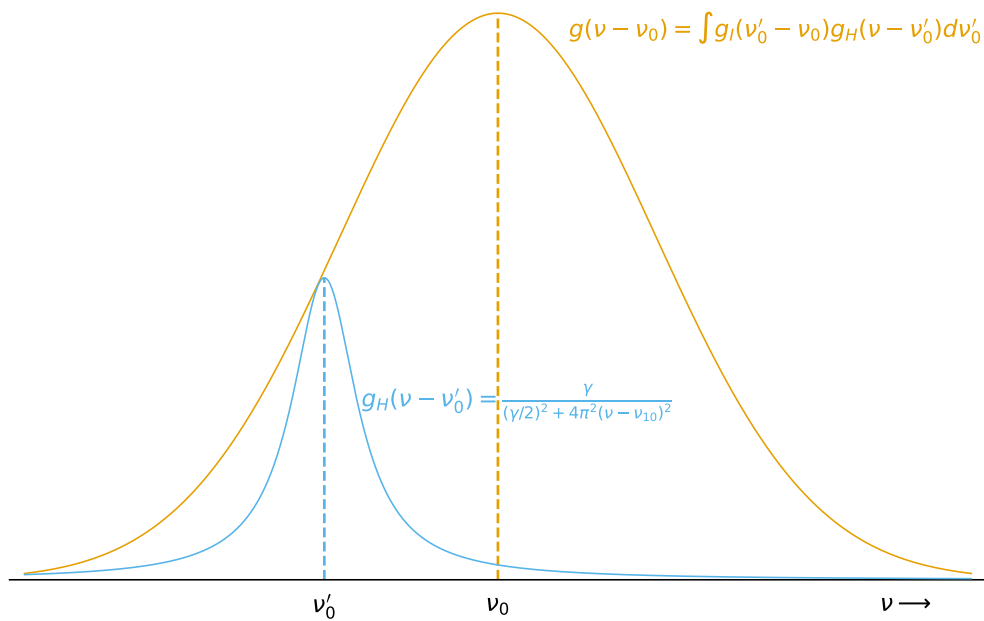


**Figure 2.2.1.:** The emission of a molecule with a certain velocity component results in a homogeneous LORENTZIAN lineshape (blue). Molecules of multiple velocity components in the gas then convolve with an inhomogeneous GAUSSIAN lineshape to a VOIGT profile (orange). This is due to the DOPPLER effect and therefore called DOPPLER broadening.<sup>33</sup>

<sup>32</sup>Based on subsection *DOPPLER broadening* from Bernath, *Spectra of atoms and molecules*, 2005, pp. 28 - 31.

<sup>33</sup>Inspired by Bernath, *Spectra of atoms and molecules*, 2005, p. 29. Figure reproduced with *Python*.

## 2. Theory of Molecular Spectroscopy

Therefore, DOPPLER broadening is the result of a convolution of homogeneously broadened lines  $g_H$  discussed in the previous chapters with an inhomogeneous function  $g_I$ . The total lineshape function is described by the expression

$$g(\nu - \nu_0) = \int_{-\infty}^{\infty} g_I(\nu'_0 - \nu_0)g_H(\nu - \nu'_0)d\nu'_0. \quad (82)$$

As  $g_H$  is commonly a LORENTZIAN while  $g_I$  is composed of a GAUSSIAN function, the convolution is referred to as a VOIGT profile. The resulting lineshape can be thought of as a superposition of LORENTZIAN responses due to each velocity group of a GAUSSIAN velocity distribution.<sup>34</sup> As the result is an inhomogeneous lineshape again, DOPPLER broadening is considered an inhomogeneous broadening effect.

The electromagnetic wave vector in the particle-fixed coordinate system gets elongated or compressed due to the movement of the particle. The movement creates either a blue shift, i.e., an increase of frequency in the case of a movement towards the detector; or a red shift, i.e., a decrease of frequency in case of a movement away from the detector. Considering a wave vector component  $k$  of electromagnetic radiation parallel to the velocity component  $v$  of the moving particle, the frequency shift can be expressed as

$$\nu' = \nu \left( 1 - \frac{vk}{c|k|} \right), \quad (83)$$

neglecting relativistic second order effects. This causes spectra of particles at different velocities to differ slightly in frequency position. The distribution of velocity components in a gaseous system at equilibrium with no net flux is given by the MAXWELL-BOLTZMANN distribution function

$$p_v dv = \left( \frac{m}{2\pi k_B T} \right)^{\frac{1}{2}} e^{-mv^2/2k_B T} dv \quad (84)$$

with particle mass  $m$ , the BOLTZMANN constant  $k_B$  and temperature  $T$ . By taking the differential of equation (83)  $d\nu = (c/\nu_0)d\nu'_0$  is obtained. This inserted to equation (84) results in the normalized inhomogeneous lineshape function for

---

<sup>34</sup>Grabow, "Fourier Transform Microwave Spectroscopy Measurement and Instrumentation", 2011.

## 2.2. Line Shapes and Broadening

DOPPLER broadening.

$$g_D(\nu - \nu_0) = \frac{1}{\nu_0} \left( \frac{mc^2}{2\pi k_B T} e^{-mc^2(\nu - \nu_0)^2 / 2k_B T \nu_0^2} \right) \quad (85)$$

The FWHM  $\Delta\nu_D$  is accordingly

$$\Delta\nu = 2\nu_0 \sqrt{\frac{2k_B T \ln(2)}{mc^2}}. \quad (86)$$

DOPPLER broadening can usually be neglected when considering low frequencies. In a reasonable approximation considering the "antiresonant" term, lines can be described with the VAN VLECK-WEISSKOPF function in good agreement with experimental observations of rotational transitions in the microwave spectral region:<sup>35</sup>

$$g(\nu - \nu_{10}) = \frac{\nu}{\pi\nu_{10}} \left( \frac{\Delta\nu/2}{(\Delta\nu/2)^2 + (\nu - \nu_{10})^2} + \frac{\Delta\nu/2}{(\Delta\nu/2)^2 + (\nu + \nu_{10})^2} \right) \quad (87)$$

---

<sup>35</sup>Bernath, *Spectra of atoms and molecules*, 2005, p. 184.

# 3. Automatisations of a CPFTmmW spectrometer

This chapter provides an overview on the used devices and their interaction creating a chirped pulse FOURIER transform spectrometer operating in the millimetre wave regime. The automatisations is the main part of this work. To facilitate the understanding of the functionality the spectrometer and its parts are presented in short. More details can be found in the PhD thesis of PASCAL STAHL<sup>36</sup>. Emphasis is then put on the aspect of automatisations of the measurement process using a LABVIEW™ program.

## 3.1. Experimental Setup

This section introduces the components. It gives insight to the setup automatisated and used in the frame of this work. Although various arrangements were realised, the general configuration of the spectrometer was the same. A schematic overview of the spectrometer setup is shown in figure 3.1.1.

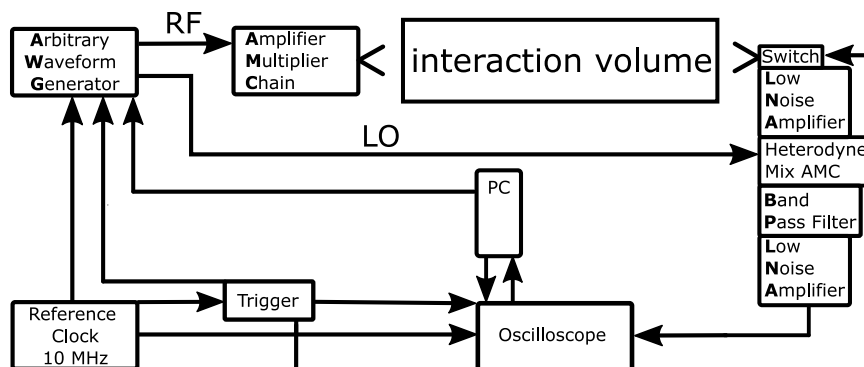


Figure 3.1.1.: Schematic setup of the spectrometer.

<sup>36</sup>Stahl, “PhD thesis: in preparation; Title pending”, 2022.

The spectrometer is composed of four main parts:

- The *generation arm* is responsible for the emission of the excitation pulse (chirp).
- The *interaction volume* produces or holds sample molecules and therefore allows for light-matter interactions.
- The *receiver arm* detects the signal emitted by the sample molecules in the interaction volume.
- The *control devices* are the human interface devices and provide the infrastructure for controlling and synchronising the setup as well as data handling and storage.

An overview on the specific devices and their specifications is given in Appendix B *Setup Components*.

#### 3.1.1. Control Devices

The control devices consist of a personal computer (PC) as the main human interaction interface; a trigger box (9520 DIGITAL DELAY PULSE GENERATOR from QUANTUM COMPOSERS INC.) to set devices into action with the proper timing, also subject to human interaction; and a 10 MHz Rubidium reference clock (STREAMLINE 501-04609A from WENZEL ASSOCIATES INC.) to achieve high precision phase stable synchronisation of the setup. The PC runs a LABVIEW™ program for measurement automatisisation. More details can be found in section 3.2 *LabView Programming*.

#### 3.1.2. Generation Arm

The generation arm is placed in front of the interaction volume and handles the generation of the excitation pulse. It consists of the arbitrary waveform generator (AWG) and the amplifier multiplier chain (AMC) with an attached horn antenna.

##### 3.1.2.1. Arbitrary Waveform Generator

The AWG is able to convert received input data to sample an analogue signal of arbitrary waveforms via digital-to-analog-converters (DACs). The setup uses the

### 3. Automatisation of a CPFTmmW spectrometer

KEYSIGHT M8190A. The AWG produces output in two channels with a peak-to-peak power between 200 and 2000 mV. The maximum sampling rate is 12 GHz.<sup>37</sup> According to the NYQUIST-SHANNON<sup>38</sup> theorem, signals up to a frequency of 6 GHz can be generated. The signal of one channel is used for the excitation pulse generation (chirp); the other one is used for signal retrieval by heterodyne mixing in the receiver arm.

#### 3.1.2.2. Amplifier Multiplier Chain

The AMC is able to further up-convert the frequency and simultaneously amplify the signal amplitude to the desired output power. It is equipped with a WR10.0 horn antenna to emit the radiation as an electro-magnetic (EM) wave into the interaction volume. In the frame of this work, two different AMCs were used. Their properties and abilities are shortly outlined here.

#### Standard AMC

The AMC467 from VIRGINIA DIODES was used mainly for testing of the setup. It is specified to operate in the range 75 - 110 GHz.<sup>39</sup>

#### High Power AMC

The AMC672 from VIRGINIA DIODES is referred to as the High Power AMC (HPAMC), due to its ability to emit radiation with a peak power of 1 W. It is specified to operate in the range of 100 - 110 GHz<sup>40</sup>, but was used up to 112.5 GHz. As long as not stated otherwise, the HPAMC was used.

### 3.1.3. Receiver Arm

The receiver arm deals with the reception of the molecular emission signal. This is referred to as the free induction decay (FID). The receiver arm is placed behind

---

<sup>37</sup>Keysight Technologies, *M8190A Arbitrary Waveform Generator: 12 GSa/s Arbitrary Waveform Generator: Data Sheet*, 2021.

<sup>38</sup>See National Instruments Corp., *Erfassen von Analogsignalen: Bandbreite, Nyquist-Abtasttheorem und Alias-Effekt*, 2019;

for original publications see Shannon, "Communication in the Presence of Noise", 1949 and Nyquist, "Certain topics in telegraph transmission theory", 2002

<sup>39</sup>Virginia Diodes, Inc., *WR8.0AMC-I Specifications: Data Sheet*.

<sup>40</sup>Virginia Diodes, Inc., *AMC672 105 GHz: User Guide*.

### 3.1. Experimental Setup

the sample interaction volume and consists of a WR10.0 horn antenna, a switch, low noise amplifiers (LNA), a heterodyne mixAMC, a bandpass filter and the oscilloscope.

The horn antenna collects and guides the radiation towards the detector. The switch blocks the strong radiation from the excitation chirp to protect the sensitive detector electronics. It opens as soon as this has passed to allow for the molecular emission signal to propagate.

The LNAs enhance the signal for easier detectability. The heterodyne mixAMC allows to convert frequencies to a detectable range, while harmonics of this process need to be filtered out by a bandpass filter. This process is described in the following.

#### Heterodyne Mixing

The FID signal emitted by the molecules is about 100 GHz in the experiments in the frame of this work. This is too fast for most electronics to detect. Heterodyne mixing can be used to shift the frequency of the molecular signal to a detectable range. The principle of heterodyne mixing is therefore explained here on basis of “Technische Grundlagen der Radioastronomie”<sup>41</sup>.

Upon mixing, two frequencies are superimposed. This can happen in any device with a non-linear current-voltage characteristic. Small modulations  $\delta U$  around a constant bias voltage  $U_0$  can be described by a TAYLOR series:

$$I(U_0 + \delta U) = I(U_0) + \frac{dI}{dU}\delta U + \frac{1}{2}\frac{d^2I}{dU^2}(\delta U)^2 + \frac{1}{6}\frac{d^3I}{dU^3}(\delta U)^3 + \dots \quad (88)$$

which can be equivalently written as

$$I(U_0 + \delta U) = k_0 + k_1\delta U + k_2\delta U^2 + k_3\delta U^3 + \dots \quad (89)$$

For mixing, the quadratic term is important. The modulation  $\delta U$  is caused by the signal frequency  $f_S = \frac{\omega_S}{2\pi}$  and the frequency of the local oscillator  $f_{LO} = \frac{\omega_{LO}}{2\pi}$ :

$$\delta U = A \sin(\omega_{LO}t) + B \sin(\omega_S t) \quad (90)$$

---

<sup>41</sup>Hachenberg and Vowinkel, *Technische Grundlagen der Radioastronomie*, 1982, p. 167, 168.

### 3. Automatisation of a CPFTmmW spectrometer

The trigonometric identity<sup>42</sup>  $\sin \theta_1 \cdot \sin \theta_2 = \frac{1}{2} \cos(\theta_1 - \theta_2) - \frac{1}{2} \cos(\theta_1 + \theta_2)$  can be used to insert equation (90) into (89) to produce:

$$\begin{aligned}
 I = & k_0 + \overbrace{k_1(A \sin(\omega_{LO}t) + B \sin(\omega_S t))}^{\text{original frequencies}} + \overbrace{k_2 \left( \frac{A^2}{2} + \frac{B^2}{2} \right)}^{\text{rectified current}} \\
 & - k_2 \left( \frac{A^2}{2} \cos(2\omega_{LO}t) + \frac{B^2}{2} \cos(2\omega_S t) \right) \quad \rightarrow \text{higher harmonicals} \\
 & + \underbrace{k_2(AB \cos[(\omega_{LO} - \omega_S)t])}_{\text{difference frequency}} - \underbrace{k_2(AB \cos[(\omega_{LO} + \omega_S)t])}_{\text{sum frequency}} + \dots \quad (91)
 \end{aligned}$$

The main contributions, apart from the original frequencies, lie at two positions with the frequencies  $|f_{LO} \pm f_S|$ . With a bandpass filter the lower ( $|f_{LO} - f_S|$ ) frequency can then be selected to yield a signal that is detectable by the oscilloscope, which acquires a single or multiple instances of the FID signal. This is then either stored as a dataset to be used later for data processing on a PC or processed onboard to display a FOURIER transformed spectrum directly.

#### 3.1.4. Interaction Volume

The interaction volume provides space for molecules of interest to interact with radiation. Usually it is a vacuum chamber designed to enable (transient) molecules to exist or be created locally and to allow for interaction with the excitation pulse as well as collimation of the molecular signal.

Adjusting the pressure inside a vacuum chamber correctly is crucial for a successful emission measurement. Two physical effects have to be balanced. When the pressure is high, intermolecular collisions will result in pressure broadening of the molecular lines as stated in section 2.2.2 *Pressure Broadening*. For an even higher pressure the collisions will destroy any coherence due to the fast relaxation processes. The signal of the molecules of interest will then eventually vanish. When the pressure is too low on the other hand, too few molecules may be available in the sample volume for an effective light-matter interaction. The signal then may become too weak to detect. A balance has to be found between these extrema. Therefore adjusting the pressure properly is already a delicate task assuming

<sup>42</sup>See Bronstein et al., *Teubner-Taschenbuch der Mathematik*, 2009, p. 61.

### 3.1. Experimental Setup

that only the desired species is present in the sample volume. However, vacuum systems are prone to a number of sources of undesired molecules. These can be caused by leakage, as every part of the system may allow molecules from the environment to diffuse into the chamber, or evaporation of residual gases stuck on the wall after opening the system, or due to contamination with sample molecules from previous measurements. It is crucial to reduce the risk of leakage, working cleanly especially when exposing the interior of the chamber to the atmosphere and thoroughly pump residual gases from previous measurements. However, contamination cannot always be fully avoided.

The pressure therefore is a delicate parameter in gas flow experiments, but even more so in jet-spectroscopy measurements, as it may compromise the stability of the jet formation. When the pressure varies during the acquisition, different parts of the spectrum may be taken at different conditions in the interaction volume. Therefore, they are not comparable as line-widths or intensities may be altered. It is therefore the aim of the experimenter to keep constant pressure settings during the whole measurement.

In the frame of this work two distinctively different interaction volumes were used. The first is a simple vacuum chamber (or gas flow cell) designed to hold in-stock molecules evaporating from either a liquid or solid source. The second is a chamber holding a laser ablation source for direct creation of molecules from solid samples and nozzle gases. The latter will be referred to by the acronym **SUJESTA** (**S**upersonic **J**et **S**pectrometer for **T**erahertz **A**pplications). Both systems will be discussed in the following sections.

#### 3.1.5. Vacuum Chamber

A vacuum chamber was constructed from a 1.36 m long pipe vacuum piece connected to a T-piece on one side and a double-cross on the other side. The sides of these pieces opposite to the connection to the pipe were closed with polytetrafluorethylene pipe windows to allow propagation of radiation. The T-piece allowed to attach a turbo-molecular pump preceded by a rotary vane pump to enable evacuation of the cell. A manometer was placed at the connection between turbo and rotary pump. The double-cross section was closed with a blind flange on two sides and contained a viewing glass on top for visual support of the measurement. The flange mounted at the bottom hosted the molecular sources. A valve allowed

### 3. Automatisation of a CPFTmmW spectrometer

to let in gases of interest by evaporating from a liquid source in a flask through a needle valve. Additionally, a heatable stainless steel crucible holder containing a low round zirconia crucible (product *LR52Z* from ALMATH CRUCIBLES LTD) was mounted to the flange. This allowed to heat up solid samples placed into the crucible to  $\approx 620$  K and eventually evaporate them. The system therefore enabled gas phase spectroscopy of a broad range of materials initially in the solid or liquid phase.

However, the system is limited to stable molecules in laboratory conditions. They are mostly well investigated. Transient molecules or exotic conditions need to be created artificially, which was done in SUJESTA.

#### 3.1.6. Setup of SuJeSTA

SUJESTA is an experimental set up, combining a vacuum chamber as the interaction volume with a molecular source and a multipass reflection cell. The molecular source allows to measure supersonically expanding jets and furthermore allows to combine these with laser ablation of solid samples to create transient molecules. The aspects of SUJESTA will be outlined in this section.<sup>43</sup>

##### 3.1.6.1. Supersonic Jet Source<sup>44</sup>

Supersonic jets are able to produce cold gas samples using the cooling effect of adiabatic expansion. Rotational spectroscopy benefits from this due to the strong temperature dependence of the transition intensity in the microwave region.<sup>45</sup>

A jet can be created from the expansion of a high-pressure gas inlet to the low-pressure ambient background of the continuously pumped vacuum chamber. The expansion becomes supersonic, when the relation of the pressure at the nozzle  $p_0$  to the vacuum chamber background  $p_b$  becomes larger than  $G = \left(\frac{\gamma+1}{2}\right)^{\frac{\gamma}{\gamma-1}}$  with the isentropic exponent of the used gas  $\gamma$ . In the supersonic case, the exit pressure becomes independent from  $p_b$  and is instead proportional to  $\frac{p_0}{G}$ . The expansion then occurs isentropically. Upon expansion, different regions can be observed. In

---

<sup>43</sup>For further information see Breier, “High-Resolution Microwave Spectroscopy of Radioactive Molecules: Mass-independent studies fo AlF, AlH, AlO, AlS, TiO and FeO”, 2019  
for the multireflection cell: Waßmuth, “Entwicklung einer THz-Multireflexionsoptik und hochauflösende Rotationsspektroskopie von Eisenmonoxid”, 2021

<sup>44</sup>Based on Scoles et al., *Atomic and Molecular Beam Methods*, 1992, pp. 14 - 32 and 54 - 63.

<sup>45</sup>Shipman and Pate, “New Techniques in Microwave Spectroscopy”, 2011.

### 3.1. Experimental Setup

the so-called freezing region, the transition from continuum flow to molecular flow occurs. Properties are “frozen” at this point due to the lack of intramolecular collisions. The area considered to contain molecules in the collision-free molecular flow only is called the “zone of silence”. It is framed by shock-waves: thin non-isentropic regions, where molecules suddenly meet boundary conditions when interacting with background gases. The zones of a typical jet are shown in figure 3.1.2.

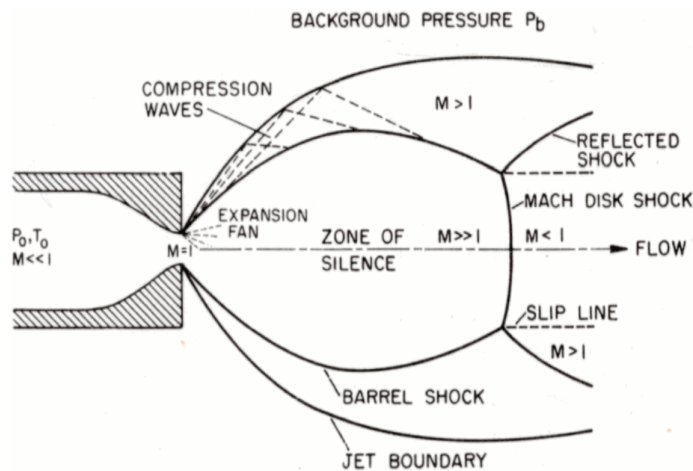


**Figure 3.1.2.:** Continuum free-jet expansion and labels of the typically characteristic zones.<sup>46</sup>

The zone of silence is the ideal environment to observe a FID. Due to the lack of collisions, non-emissive relaxation mechanisms are strongly suppressed in the zone of silence. The drastically decreased collision rate also reduces the linewidth originating from pressure broadening (see section 2.2.2 *Pressure Broadening*). In addition, this also creates a pleasant environment for transient species (see section 3.1.6.2 *Laser Ablation*), where chemical reactions are suppressed, providing a lifetime long enough for spectroscopic investigation. It is therefore desirable to solely probe the zone of silence with the excitation beam.

The isentropic expansion also allows to rapidly cool the expanding gas to a temperature  $T$ , while accelerating it to a one-dimensional terminal flow velocity  $v_\infty$ . For an ideal gas with constant molar heat capacity in continuous flow these values

<sup>46</sup>Scoles et al., *Atomic and Molecular Beam Methods*, 1992, p. 15, Figure 2.1.

### 3. Automatisation of a CPFTmmW spectrometer

become:

$$T = \frac{T_0}{1 + \frac{\gamma-1}{2}M^2} \quad (92)$$

$$\text{with } M = A \left( \frac{x - x_0}{d} \right)^{\gamma-1} - \frac{\frac{1}{2} \frac{\gamma+1}{\gamma-1}}{A \left( \frac{x-x_0}{d} \right)^{\gamma-1}}, \quad (93)$$

$$v_\infty = \sqrt{\frac{2R}{W} \frac{\gamma}{\gamma-1} T_0}, \quad (94)$$

with the initial gas temperature  $T_0$  (usually  $T_0 \approx 298$  K), the cross-sectioned area  $A$  of the nozzle, the distance along the centreline  $x$ , the source position  $x_0$ , the diameter of the source exit  $d$  and the average molecular weight  $W$ . The MACH number  $M = \bar{v}/v_{sound}$  is the relation of the mean ensemble speed  $\bar{v}$  to the speed of sound  $v_{sound}$ . Equation (93) is best suited for positions far away from the source nozzle,  $\left(\frac{x}{d}\right) > \left(\frac{x}{d}\right)_{min} \approx 10$ , i.e., usually 10 times the nozzle diameter.

Instead of continuous flow, also pulsed gas nozzles can be used, creating a discrete molecular beam with spatial length  $\Delta x$  and temporal length  $\Delta t$ . The average background pressure when using a pulsed jet  $p_{bp}$  (index *bp* for background pulsed) depends on the source pressure  $p_{sp}$  (index *sp* for source pulsed), the nozzle conductance (volume flow rate)  $c_p$  and the pumping speed  $z$  as  $p_{bp} = f p_{sp} \frac{c_p}{z}$ . The duty factor is given by  $f = \rho \Delta t$  with the pulse repetition rate  $\rho$ . As in real applications the flow intensity is usually not an ideal square function and rather time dependent on conductance and gas flow dynamics, the pulse duration  $\Delta t$  is approximated by the FWHM of the actual width. For real applications therefore usually  $f_{real} < f$ .

In pulsed jets the MACH disk centre is usually further away from the nozzle compared to continuous flow experiments. Shocks caused by compression of the background gas are created in pulsed beam systems mainly by reflections from the vacuum chamber walls. Before this happens, the gas first has to traverse the chamber. This poses fewer requirements on pumping speeds. Another advantage is that a specific gas source can be provided for longer due to reduced gas throughput rates. This allows to maintain stable measurement conditions for extended periods of time.

However, non-continuum flow of pulsed jet systems is more complicated. The opening nozzle acts as a biased oscillator, which makes the valve subject to re-

opening. Secondary maxima of the gas flow are usually observed. In addition, the valve as a mechanical structure is subject to wear so gas flow dynamics may change over long measurement intervals.

#### 3.1.6.2. Laser Ablation

Laser ablation is a technique to create sample molecules in the gas phase by evaporating a solid sample. This is done with a pulsed Nd:YAG-laser operating at 30 Hz and a wavelength of 355 nm. The molecular cloud is forced into the interaction volume by actuating a nozzle, which releases a pulse of carrier gas. This can further react with the evaporated source material and creates a supersonic jet (see section 3.1.6.1 *Supersonic Jet Source*), which allows for investigations under low temperature conditions.

The creation of the desired molecules requires a set of proper conditions, i.e., timing of laser ablation and nozzle actuation, laser intensity, gas mixture and source pressure, background pressure, and length of the reaction channel. When chosen and set up correctly, this creates the right chemical environment for the desired molecules to form. The proper adjustment of these parameters is, however, a delicate task.

#### 3.1.6.3. Multipass Reflection Cell

Another key element to SUJESTA is a multipass reflection cell, which is used to probe the sample volume perpendicularly to the jet. Two sphere-planar mirrors provide an elongated beam path through the interaction volume by reflecting both, the excitation pulse and the molecular signal back and forth several times. By adjustment of the mirror position the number of cycles in the cell can be varied. In the frame of this work 60 reflections were chosen, creating a total beam path of 30 m. The increased beam length provides additional interaction volume and therefore a higher intensity in the measured signal. When performing jet spectroscopy measurements the alignment can be chosen to allow for a maximum of passes in the jets zone of silence (see section 3.1.6.1 *Supersonic Jet Source*).

### 3.2. LabView Programming

LabView™ was used to enable synchronous communication between certain hardware components described above while enabling the user to set up, control and read-out the measurement. After initialization the system works mostly autonomously, easing the otherwise laborious procedure of taking a broadband spectrum. The key aspects and main functionalities of the software are outlined here. A schematic overview is given in figure 3.2.1. General remarks on the software package LabView™ can be found in Appendix A *Used software and programs*.

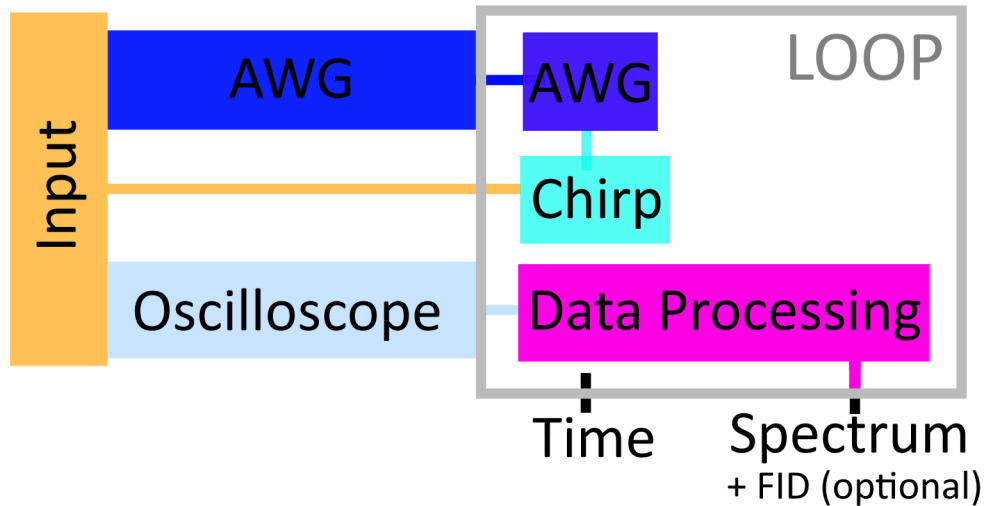


**Figure 3.2.1.:** Schematic function of the LABVIEW™ program. Input parameters entered by the user are read in and converted (orange). They are passed to the spectrometer devices, the AWG (blue) and the oscilloscope (light blue), to prepare their status for the measurement. The spectrum is divided into segments of a given bandwidth. In a loop (grey), the chirp (cyan) for each segment is iteratively calculated, passed to the AWG its the output is activated. The oscilloscope then acquires multiple FIDs. When the entered number of acquisitions is reached, the oscilloscope sends the averaged time domain signal to the PC, where the data is processed (pink). The FOURIER transformed signal is saved. The raw averaged FID signal can be saved optionally. In each loop, the remaining measurement time is estimated.

### 3.2.1. Front Panel - Human User Interface

The front panel serves as the human user interface. Input values can be entered here to adjust properties of the measurement. For most parameters standard values are predefined, which may remain constant for most measurements. However, most values are adjustable. This is useful to set up special measurement conditions or to test the experiment after modifications. Figure 3.2.2 shows the front panel superimposed with an assignment of each subpanel to its function.

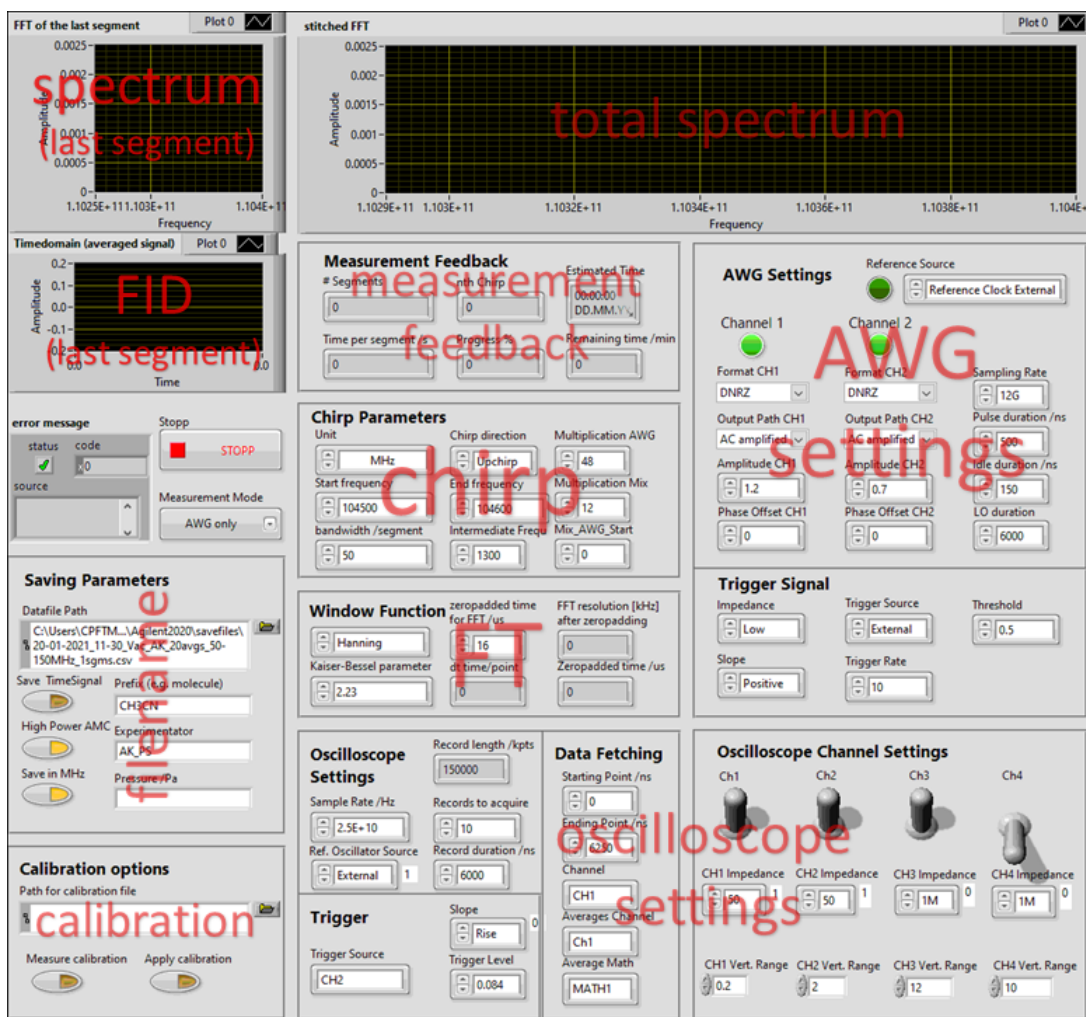


Figure 3.2.2.: Frontpanel of the automatised LABVIEW™ program used to take broadband spectra. The screenshot is superimposed with an assignment of each subpanel to its function.

In the following, the areas on the front panel for each device, their respective parameters and the feedback to the user are presented.

### 3. *Automatisation of a CPFTmmW spectrometer*

#### **3.2.1.1. General Settings**

General parameters for the spectrum are set in this subpanel. The borders of the spectrum to be taken are defined by the start and the end frequency. The spectral width of each individual chirp is given by the bandwidth per segment. The intermediate frequency (IF) is used in the heterodyne mixing process performed by the mix-AMC. For convenience the unit of all frequencies can be adjusted in a drop-down menu, with MHz being the predefined unit. As the frequency produced by the AWG for both, heterodyne mixing and excitation pulse, is increased by frequency multiplier devices, the multiplication factor of the multiplication chain for each path has to be entered. The output frequency of the AWG is calculated from this so the desired frequency is achieved at the end of the multiplication chain. The shape and parameters of the chirp are mainly defined by the AWG.

#### **3.2.1.2. Arbitrary Waveform Generator Settings**

For the AWG important parameters to be set are the sampling rate, pulse duration and amplitude of the signal. These define the properties of the chirp and the local oscillator (LO) signal used for the heterodyne mixing of the molecule signal. A drop-down menu allows to select either increasing (up-chirp) or decreasing (down-chirp) frequency sweeps. The trigger rate defines the frequency at which individual chirps are produced by the AWG.

The generation of the signal for the heterodyne mixing in the receiver arm is delayed in respect to the excitation pulse chirp by a value called "idle duration". The signal has a length defined by the parameter "pulse duration". These parameters allow to shift the output of the signal to be mixed in the region, where the detection of the FID is expected.

The other controls of the AWG are designed to mimic the functionalities of the manufacturer-provided control software accompanying the KEYSIGHT M8190A. Standard parameters allow for the generation of chirps with linear increase or decrease in frequency and detection of molecular signals with the given setup. Boolean lights and numeric outputs are displayed to provide the user with confirmation on access and functionality of the device and sanity checks.

### 3.2.1.3. Oscilloscope Settings

The oscilloscope has a multitude of parameters to adjust. This includes activation and assignment of individual channels to the corresponding signal as well as the respective adjustment of the vertical range (which also influences amplitude resolution), input impedance and bandwidth for each channel. Also, definition of acquisition type, reference oscillator source, sampling rate and record duration for a single chirp is necessary. Feedback on the record length is given as a sanity check. Additionally a “math mode” is activated and defined on the acquisition channel, allowing for on-board averaging (integration) of multiple single shot measurements. This is faster and more data efficient compared to later calculations on a PC. The number of averages taken can be set from 1 (single-shot measurement) to  $2.1475 \cdot 10^9$ . The effect of averaging is discussed in section 3.3 *Averaging Measurements*. Data-fetching of the averaged signal from the corresponding channel can be tailored by defining the starting and ending point. The former is usually chosen to ignore remnants or reflections of the excitation chirp pulse. The latter is adjusted to include the relevant part of the molecular FID signal while decreasing the amount of unnecessary information or noise after the signal has decayed. Finally a trigger needs to be defined to start the data acquisition with the right timing. This is done by adjusting the trigger source channel, its coupling, position, threshold level and whether it is activated on a rising or falling slope.

### 3.2.1.4. Fast Fourier Transform and Window Function

A further adjustment can be made on the post-measurement data processing. The time-domain data (FID signal) fetched from the oscilloscope is converted to a frequency domain signal by a (fast) FOURIER transform ((F)FT). In this conversion a window-function is commonly applied. The user may choose from a variety of window functions such as HAMMING, HANNING, BLACKMAN-HARRIS or KAISER-BESSEL. For the latter the adjustable parameter  $\beta$ , which influences the width of the function, can be specified. The standard parameter is a HANNING window function. Alternatively, the absence of a window function (a.k.a. a rectangular window, i.e., weighting all measurement points equally) can be chosen.

In this context also a desired signal time can be specified. When it is longer

### 3. *Automatisation of a CPFTmmW spectrometer*

than the data obtained from the oscilloscope during the measurement, it will be elongated by a process called “zero-padding”. This process appends zeros to the measurement data until the desired signal time is reached. It does not add information, but artificially increases the resolution of the spectrum. As more datapoints in the time domain spectrum become available to be processed by the FFT, also the frequency spectrum obtains more points, hence the higher resolution.

#### **3.2.1.5. Measurement Feedback**

After initiation, several output subpanels provide the user with feedback on the ongoing measurement. This is refreshed for each segment after the number of averages is reached and the data is fetched from the oscilloscope. Displayed to the user is the time domain signal (FID) from the previously completed segment, the respective FFT and the combined FFT of the spectrum as far as it is already taken. The real-time feedback provides the user with the ability to judge the quality of the ongoing measurement and intervene if necessary.

From the specified limits of the spectrum to be taken and the bandwidth of the individual chirp the needed number of segments is calculated and displayed. At the end of the acquisition for each segment, the user is provided with feedback on the progress of the measurement. This information includes the amount of time needed for the acquisition of the respective segment, which largely depends on the number of averages to be taken and the trigger frequency. A termination time is estimated by extrapolating onto the number of remaining segments.

#### **3.2.1.6. Saving Parameters**

For saving the spectrum after acquisition, several parameters can be supplied. This includes the destination to a storage folder. The filename is constructed from several parameters, which allow to identify individual measurements reliably and provide a consistent naming schematic. These parameters include

- date and time of the measurement
- a prefix entered by the user; may include information on probed molecule or special circumstances of the measurement
- the name or acronym of the experimenter as entered by the user

- the number of acquisitions of each segment for averaging
- the start and end frequency
- the number of segments
- the duration of the chirp in nanoseconds
- the pressure in the interaction volume as entered by the user
- information on whether the high-power AMC is used.

The FFT performed by the programme is saved. Storage of the time domain signal is deactivated by default, because it is costly in terms of available disk space, but is available optionally. The saving is done automatically after the measurement of each segment is complete. If the measurement is aborted the frequency domain spectrum will be stored as far as taken except for the segment that is in the process of being averaged. The same applies to the time domain FID signal, if it was chosen to be saved. This is because the interruption of the measurement causes the termination of the loop. The data is therefore neither fetched from the oscilloscope nor processed.

#### 3.2.1.7. Calibration

In the calibration panel the user has the option to perform or apply a calibration measurement to extract the background from the measurement. Without any sample in the vacuum chamber the signal obtained originates from background noise only. Averages over the bandwidth of a chirp provide a baseline to be subtracted from measurements with the same chirp settings. This corrects the baseline and facilitates the comparison between different frequency ranges of the spectrum. However, line intensities proved to be orders of magnitude larger than any baseline calibration, so this was omitted for all spectra shown in this work. If a calibration measurement is done or needs to be applied, the path of the corresponding calibration file to be saved or to be read can be specified in this panel.

#### 3.2.2. Back Panel - Programming Code

The back panel serves as the graphical “program code”. The programme takes values entered on the front panel, calculates new parameters if necessary and

### 3. *Automatisation of a CPFTmmW spectrometer*

passes them to the respective devices to prepare the measurement. When a measurement of a segment is complete (i.e., the number of averages to be taken is reached) data is collected from the oscilloscope, the progress is displayed and automatically the measurement of the next segment in the spectrum is prepared. An overview of the back panel with an assignment on the function of each part is shown in Appendix C *LabView Backpanel*. The main features of the program are outlined in more detail hereafter.

#### 3.2.2.1. **Device Settings**

When the program is started by clicking “Run” in the LABVIEW™ toolbar, it will attempt to establish a connection with the respective devices, i.e., the AWG and the oscilloscope. Further, the parameters entered on the front panel will be passed to the instruments. Some are modified computationally; e.g. each frequency will be multiplied with the selected prefactor to resemble a plain number in Hz and is adjusted to the specified multiplication factors of the AMCs before being passed to the AWG. Further values are calculated from the parameters set on the front panel, such as the number of segments or the sample count (number of datapoints in a single chirp). For the communication with the devices the manufacturer provided LABVIEW™ code libraries were used (i.e., AGILENT M8190.LVLIB for the AWG and TEKTRONIX MSO5X SERIES.LVLIB for the oscilloscope). When either connection with a device is not possible or invalid values were attempted to be set, an error message will be displayed interrupting the procedure.

#### **AWG**

Each channel on the AWG is activated and set up with a value for the sampling rate and a specification of the source reference clock. To trigger the data acquisition and the switch, the marker output is attempted to be set in the program. Unfortunately, the manufacturer provided module library does not support this setting on the used AWG model. Instead, the signal of the trigger box is used for this task.

The AWG uses an array of numbers resembling the waveform to be produced as input. The math behind calculating the chirp in this format is described in section 3.2.2.2 *Chirp Generation*. The array is required to have a length of a

multiple of 64, which is ensured by a process called granularity check. Granularity describes, that the sample count (number of datapoints in a single chirp) is matched to this requirement. If the total sample count (duration of pulse, idle and local oscillator in nanoseconds) is not a multiple of 64, the duration will be increased to fulfil the requirement of being divisible without remainder. The additional datapoints are set to zero.

### Oscilloscope

After a connection to the oscilloscope is established, certain parameters need to be set. These values include:

- source reference clock
- trigger properties (trigger threshold level, rising/falling slope)
- the channel averaging is performed on
- the number of records to be acquired for averaging
- activation of automatised horizontal positioning
- channels to activate; for each one:
  - impedance
  - bandwidth
  - vertical range

Once the devices are set, they are waiting for numerical input, which is produced inside a loop. This is further explained in section 3.2.2.3 *Iterative Acquisition of the Spectrum*.

#### 3.2.2.2. Chirp Generation

A chirped pulse is used to excite the molecules in the interaction volume. Chirping means that the momentary frequency is dependent on time, as it is swept over a given range in the duration of the pulse. In general, the electric component of

### 3. Automatisation of a CPFTmmW spectrometer

the EM wave of a linear chirp has the form<sup>47</sup>

$$E(t) = E_{max} \cdot \sin \left( 2\pi \int_{t_s}^{t_e} f(\tau) d\tau \right) \quad |f(\tau) = f_s + \alpha t$$

$$E(t) = E_{max} \cdot \sin \left( 2\pi \left( f_s + \frac{\alpha}{2} t \right) t \right), \quad (95)$$

with a maximum amplitude  $E_{max}$ , time  $t$  with the indices  $s$  for start and  $e$  for end, the start frequency  $f_s$  and the chirp constant  $\alpha$ . For  $\alpha > 0 \frac{1}{s^2}$ , the chirp is referred to as an up-chirp, while for  $\alpha < 0 \frac{1}{s^2}$  refers to a down-chirp. A visualisation is given in figure 3.2.3.

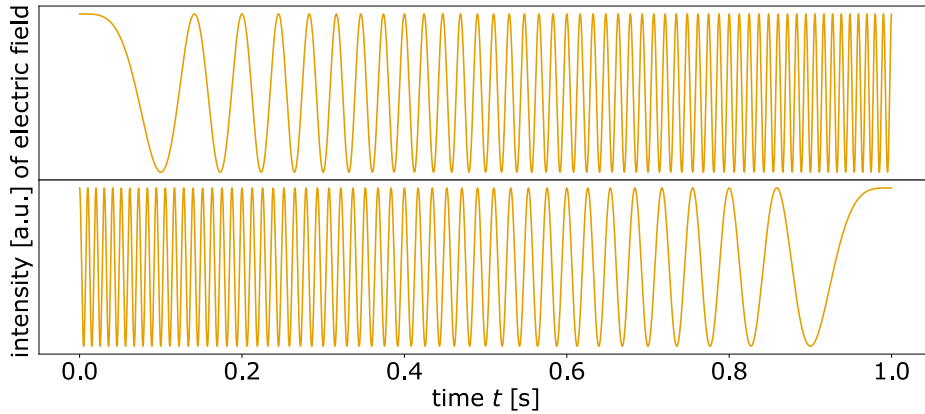


**Figure 3.2.3.:** Visualisation of chirped pulses with a length of 1 s. Shown is only the electric field component. The top graph shows an up-chirp starting at  $f_s = 0$  Hz with  $\alpha = 100 \frac{1}{s^2}$ . The bottom graph depicts a down-chirp starting at  $f_s = 100$  Hz with  $\alpha = -100 \frac{1}{s^2}$ .

#### 3.2.2.3. Iterative Acquisition of the Spectrum

As a single chirp usually only probes a small part of a broader spectrum of interest, multiple chirps are needed to sample a significant part of a molecular spectrum. One such chirp with certain frequency limits is referred to as a segment. When the devices are properly set, a loop sequentially calculates waveforms of the chirp for the AWG, activates its output, lets the desired number of averages

<sup>47</sup> This formula is the real part of the complex function  $E(t) = E_{max} \cdot e^{i(f_0 t + 0.5 \alpha t^2)}$  given by equations (1) and (2) in G. G. Brown et al., “A broadband Fourier transform microwave spectrometer based on chirped pulse excitation”, 2008. The imaginary part can be interpreted as the magnetic field. For visualisation of the chirp, only the electric field is regarded.

of the FID signal be acquired on the oscilloscope, fetches the data of the segment, processes it in a FT and pieces together the spectrum. This process is explained in more detail in the following.

#### Chirp Generation

Before a new waveform is sent to the AWG, the channel's waveform generation is aborted and its memory is cleared. Then a new wavefunction can be passed to the AWG. For each of the two channels, one wavefunction is generated using equation (95). One channel produces the output as the local oscillator for the heterodyne mixing. It represents a sine wave, which is effectively a chirp with  $\alpha = 0 \frac{1}{s^2}$ , covering a bandwidth of zero. The other wavefunction is the excitation pulse (chirp) itself. The parameters

- phase offset (defined on the front panel)
- bandwidth (chirp bandwidth; defined on the front panel)
- sweep rate  $\alpha$  (calculated as chirp bandwidth times the sampling rate divided by sample count after granularity check;  $\alpha = BW \cdot \frac{SR}{SC}$ )
- start frequency (given by the iteration through the spectrum)

are used to produce the values of the chirps wave function in an array. This array is passed to the AWG as the waveform. After activation it produces it repetitively at the given trigger rate provided by the pulse box.

#### Data processing

The oscilloscope averages the set amounts of individual FID signals. Once enough acquisitions are reached, the data is fetched from the oscilloscope and processed. The FID is weighted with a specified window function from the built-in method NI\_AALPRO.LVLIB and is displayed on the front panel. To artificially enhance the signal resolution, the data array is zeropadded to the desired length (see section 3.2.1.4 *Fast Fourier Transform and Window Function*). The signal is then processed by the built-in method NI\_MAPRO.LVLIB:FFT SPECTRUM (REAL-IM).VI (as described in section 3.2.1.4 *Fast Fourier Transform and Window Function*) to produce the FFT. The absolute value of the FOURIER transformed spectrum is used for further analysis. The relevant part of the spectrum, i.e., the frequency range that has been probed with the excitation chirp, is extracted. This is then displayed on the front panel. If multiple chirps have yet

### 3. Automatisation of a CPFTmmW spectrometer

been obtained, a stitched spectrum is shown as well. The raw FID data is saved only, if this is specified by the user.

#### Iteration

For each segment, new wavefunctions are calculated and passed to the AWG. The data acquisition on the oscilloscope is restarted. Within a loop function the segments are scanned through in succession until the whole desired spectrum is taken. For an up-chirp the starting frequency of the first segment is the lowest frequency in the whole broadband spectrum, while its end frequency is the start frequency plus the bandwidth of the chirp. The end frequency of a segment is the start frequency of the subsequent one. For a down-chirp the start frequency of the chirp is the upper and the end frequency is the lower limit of the segment respectively. For both, up and down chirps, the spectrum is taken starting with the segment with the lowest frequency, iterating to higher frequencies.

The whole spectrum of the frequency domain signal is then stored with clear identifiers, some of them provided by the user, coded into the filename as described in section 3.2.1.6 *Saving Parameters*. The optional storage of the time-domain spectrum (FID) is done sequentially in a separate file. It is deactivated by default due to the rather intensive memory demands. To recalculate a FOURIER transformed spectrum with any particular window function from this, a PYTHON script *FID\_to\_FFT.ipynb* is provided.

## 3.3. Averaging Measurements

As gas phase spectroscopy deals with comparably weak signals, a single measurement (or ‘shot’) will be prone to a rather high level of noise. To increase the signal to noise ratio (SNR) averaging of multiple shots can be used. This reduces the influence of random events or “white noise”. Taking  $n$  averages increases the SNR by  $\sqrt{n}$ .<sup>48</sup> In the case of FT spectrometry this means, that multiple instances of FIDs will be averaged. More averages mean that the white noise components will be “averaged out”, i.e., the amplitude of these components will tend towards zero, while the actual FID or molecular signal stays prominent. This facilitates the post-measurement processing of the data, as especially weak lines are more

---

<sup>48</sup>Tkachenko, *Optical spectroscopy: Methods and instrumentations*, 2006, p. 142.

easily identifiable in a spectrum with a good SNR compared to a spectrum with noisy background.

Averaging is therefore beneficial for spectroscopy. It also poses new challenges to overcome: As the FID signal is averaged directly, phase stability is critical for the electrical setup devices, while sample stability in the course of the measurement is a crucial requirement for the vacuum system and the molecular source.

#### **Phase Stability**

Phase stability is a problem that appears between individual shots. Phase jitter of the trigger may lead to a mismatch or shift between the time domain signal of separate shots, which are to be averaged. Lines in the FT-frequency domain will then appear much weaker or disappear entirely as their signal pattern is averaged out. The phase-stable triggering of data acquisition by the oscilloscope is provided by the AWG signal used for the heterodyne mixing. It is split off before the frequency multiplication and the first rising (or falling) slope triggers the acquisition. The phase is prevented from drifting by locking all devices to a 10 MHz rubidium-disciplined crystal oscillator reference clock. A high-quality phase stability enables to harness the benefits of multiple shot averaging.

#### **Sample Stability**

Sample stability is problematic, when averaging occurs over time periods in the order of minutes or hours. The challenge is to provide stable conditions of the sample for the measurement to be successful. If not taken care of, parameters may be prone to change, such as temperature, pressure or even chemical composition of the sample itself. The situation differs for gas flow measurements, where molecules are introduced to the interaction chamber directly and jet-spectroscopy measurements, where molecules are freshly produced.

In the case of gas flow measurements, temperature can usually be assumed as rather constant with ambient temperature (usually  $\approx 298$  K), because the sample molecules are in thermal equilibrium with the wall of the vacuum system. The chemical composition of molecules should be considered, as chemical reactions may deteriorate the purity of the original sample. However, the molecules investigated in gas flow experiments in the frame of this work are stable under standard conditions and barely provide opportunities to interact with residual

### 3. *Automatisation of a CPFTmmW spectrometer*

gases. However, keeping a constant pressure is both crucial but also a delicate task as described in section 3.1.4 *Interaction Volume*. Evaporation of residual gases can influence the pressure severely, which affects the intensity of line features. Therefore, the turbomolecular pump was used to pump out residual gases each time the sample molecule was changed. Under measurement conditions a stable pressure was achieved by the use of a needle valve (type EVN116 from PFEIFFER VACUUM AG), which was adjusted to provide a constant pressure in equilibrium with the rotary vane backing vacuum pump.

Jet-spectroscopy measurements provide further challenges to stabilize the parameters. Temperature; background and nozzle pressure; pulse rate, width and shape; and molecular composition influence each other in a complex manner as outlined in section 3.1.6.1 *Supersonic Jet Source*. This complicates the stabilisation and therefore, the averaging of the signal. For laser jet ablation spectroscopy even more parameters need to be considered, as the timing of the laser pulse becomes influential. In this case also the measurement is limited by the depletion of the source material.

In any case, the number of averages therefore has to be adjusted accordingly, so that conditions can be kept approximately constant in the timeframe needed to take a full spectrum.

#### **Systematic Errors**

Not all components of noise are independent or “white” noise. Some contributions are systematic, such as harmonical modes of certain frequencies, and can therefore not be eradicated by increasing the number of averages. Systematic errors provide an additional challenge to eliminate.

## 4. Results and Discussion

The target of this work is the automatization of a chirped pulse FOURIER transform millimetre wave spectrometer, which is described in section 3.1 *Experimental Setup* with LABVIEW™. The programming is extensively explained in section 3.2 *LabView Programming*. This chapter focuses on the investigation of molecules and the analysis of the obtained spectra.

Features and properties of the taken spectra are elaborated in section 4.1 *Gas Flow Experiments*. Experiments including the use of jets and laser ablation are described in section 4.2 *Measurements Using SuJeSTA*. Introductory words to each experiment are accompanied by an overview on the investigated molecules. The structure is presented, and an introduction is given to its chemical and spectroscopic properties, earthly existence in addition to astrochemical abundance as far as known. Information on the source of predictions used for each molecule is summarised in Appendix D *List of Molecular Databases*. Concluding remarks are given in section 4.3 *General Discussion*.

### 4.1. Gas Flow Experiments

Gas flow experiments were conducted using a vacuum flow chamber as described in section 3.1.5 *Vacuum Chamber*. The obtained spectra are presented along with predictions from molecular databases<sup>49</sup> plotted mirror-inverted along the frequency axis for better comparability. If necessary, special features of the spectra are highlighted. This section also analyses exemplarily properties of the acquired spectra such as line width, line position and signal to noise ratio (SNR).

---

<sup>49</sup>See Endres, Schlemmer, Schilke, et al., “The Cologne Database for Molecular Spectroscopy, CDMS, in the Virtual Atomic and Molecular Data Centre, VAMDC”, 2016 and Pickett et al., “Submillimeter, millimeter, and microwave spectral line catalog”, 1998. Detailed information on each database entry and the origin of the data is given in appendix D *List of Molecular Databases*

#### 4. Results and Discussion

The SNR in this work is defined as the peak maximum height or intensity  $I_{signal}$  of a line feature as obtained from a LORENTZIAN least squares fit divided by the average noise  $I_{noise}$  (baseline height) in an area far away (usually  $> 3 \times \text{FWHM}$ ) from the signals.

$$SNR = I_{signal}/I_{noise} \quad (96)$$

##### 4.1.1. Methanol Spectrum in Gas Flow Experiments and General Spectral Properties

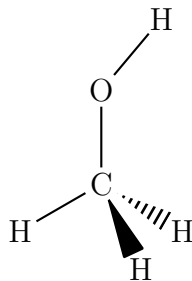


Figure 4.1.1.: Chemical structure of methanol.

Methanol is the simplest alcohol consisting of a methyl group ( $\text{CH}_3$ ) with a hydroxyl group (OH) substitute as shown in figure 4.1.1. Due to its simple structure it is the most abundant organic gas in earth’s atmosphere after methane.<sup>50</sup> Astrochemically methanol has been identified as ice in protoplanetary discs and is deemed a key component for more complex chemistry and therefore the support of carbon-based life.<sup>51</sup>

When rotation is concerned, the methyl group can be considered a near-prolate<sup>52</sup> symmetric top. The methyl group can rotate in relation to the hydroxyl group. This internal rotation is hindered by the periodic potential due to the interaction of the hydrogen atoms. The entire molecule can be viewed in the approximation of the rigid rotor or as a hindered rotor.

<sup>50</sup>Jacob, “Global budget of methanol: Constraints from atmospheric observations”, 2005.

<sup>51</sup>See Walsh and Hook, *First Detection of Methyl Alcohol in a Planet-forming Disc*, 2016. and Zasowski et al., “SPITZER infrared spectrograph observations of Class I/II objects in Taurus: Composition and thermal history of the circumstellar ices”, 2009

<sup>52</sup>Nummelin et al., “A Three-Position Spectral Line Survey of Sagittarius B2 between 218 and 263 GHz. II. Data Analysis”, 2000.

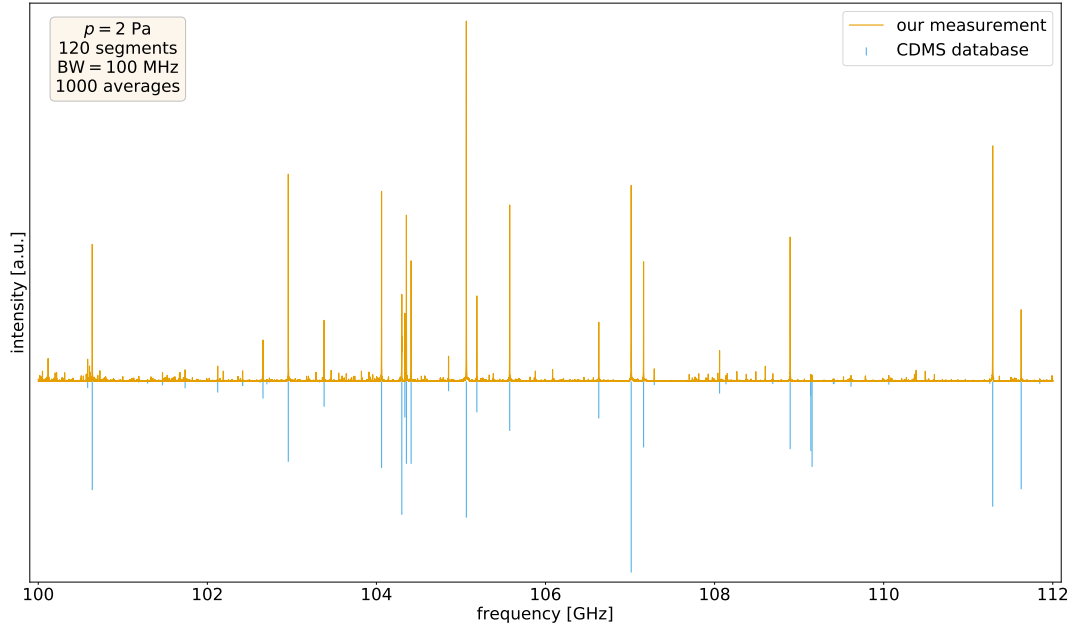


**Figure 4.1.2.:** Overview spectrum of methanol measured in a gas flow cell with a prediction from the CDMS-database.<sup>53</sup>

Figure 4.1.2 shows the obtained methanol spectrum. The main features match the prediction from the COLOGNE DATABASE FOR MOLECULAR SPECTROSCOPY (CDMS) database. Some disturbing signals are observable. They may originate from vibrationally excited states, but some of them can be credited to remnants of propylene oxide, which has previously been probed in the gas flow cell. For a more detailed analysis the spectrum is zoomed at the area from 107.15 GHz to 107.17 GHz shown in figure 4.1.3.

The line feature is fitted to a LORENTZIAN profile, given in equation (79), depicted by the green line. The feature properties stated in the figure are calculated from the fit parameters as  $FWHM = \gamma$ , the line position ( $\omega_0$ ) and SNR as given in equation (96). Additionally, the line width was estimated by taking the width of the line at half its peak value (black dotted lines) resulting in a width of 707 kHz. This is in good agreement with the fit value of 786.7 kHz obtained from the LORENTZIAN fit. The source of the deviation is due to the usage of a KAISER-BESSEL window function, which does not resemble the line feature with

<sup>53</sup>L.-H. Xu, Endres, and H. Müller, *CH<sub>3</sub>OH,  $v_t=0-2$* , 2016,

More information on the prediction and the origin is obtained in Appendix D *List of Molecular Databases*.

#### 4. Results and Discussion

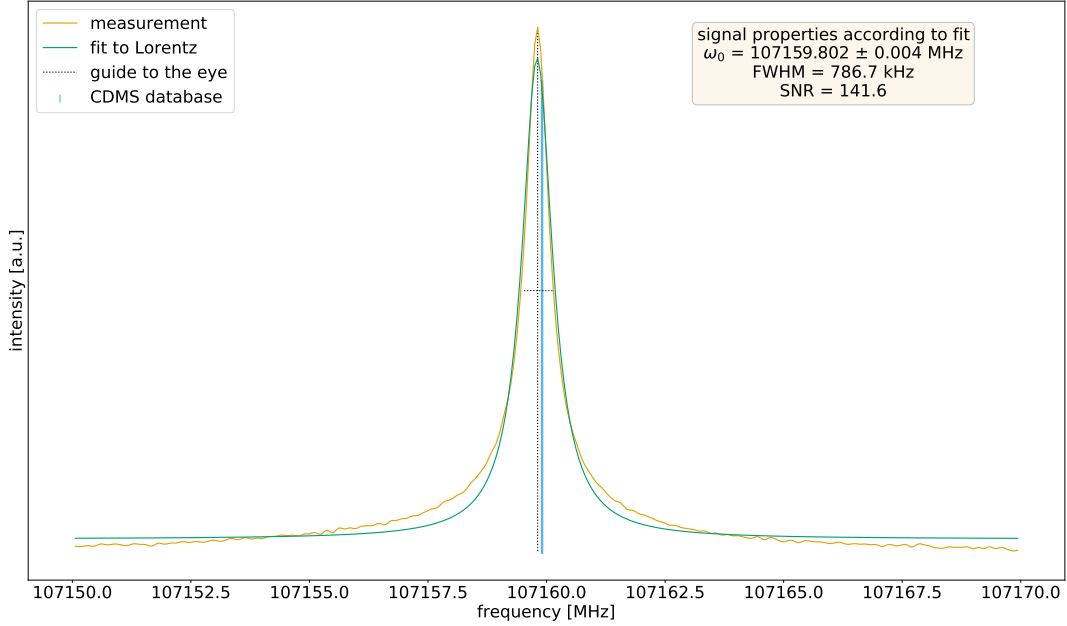


**Figure 4.1.3.:** Spectrum of methanol measured in a gas flow cell as shown as in figure 4.1.2, zoomed from 107.15 GHz to 107.17 GHz. The blue line represents the predicted line position according to the CDMS-database. A KAISER-BESSEL window with the parameter  $\beta = 2.23$  was used here in the data processing.

a LORENTZIAN shape. Instead, the line appears with a broader base. The fit therefore underestimates the peak height and eventually overestimates the line width. This is an additional effect to the natural broadening due to various effects such as finite lifetime, pressure and DOPPLER broadening as considered in section 2.2 *Line Shapes and Broadening*.

The fitted line position 107 159.802 MHz differs from the prediction (frequency of 107 159.906 MHz) by  $\Delta \approx 104$  kHz. This can in part be explained by measurement uncertainties (see section 4.3 *General Discussion*). The more likely explanation is a deviation due to uncertainties in the prediction, as it is a result of a fitting process. In this, molecular parameters are adjusted in an effort to resemble observations from multiple measurements. The analysis is complicated due to the properties of the  $\text{CH}_3$ -group as an internal rotor as described in section 2.1.13 *Internal rotation*. Therefore, deviations are to be expected.

### 4.1.2. Isotopologues of Acetonitrile

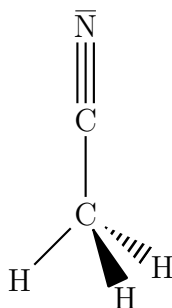


**Figure 4.1.4.:** Chemical structure of acetonitrile.

Acetonitrile consists of a methyl and a cyanide (CN) group and can be considered a prolate symmetric top that does not allow for internal rotation. The structure is shown in figure 4.1.4. In a laboratory environment it is a common organic solvent. With a dipole moment in the ground state of the main isotopologue of  $\mu_a = 3.922$  D,<sup>54</sup> line intensities are high, which makes it easily detectable. It has been identified early on in the ISM.<sup>55</sup>

In the frame of this work acetonitrile was investigated in gas flow experiments. This allowed to determine the spectrometers sensitivity for isotopologues in their natural abundance and the detectability of vibrationally excited states. The significant part of the spectrum with corresponding predictions is shown in figure 4.1.5. The intensity of the predictions of the isotopologues was scaled with their natural abundance as 1.11% for  $^{13}\text{C}$  and 0.37% for  $^{15}\text{N}$ .<sup>56</sup>

To see line features of the less abundant isotopologues the spectrum is zoomed at the regions around 107 - 107.3 GHz and 110.2 - 111.2 GHz in figure 4.1.6. The inset is yet another zoom at the region from 110.27 - 110.33 GHz showing line features of the vibrational ground state of the isotopologue  $\text{CH}_3^{13}\text{CN}$ . This and the region just above 107 GHz shows that even for a low abundance of 1.11% for  $^{13}\text{C}$  and 0.37% for  $^{15}\text{N}$  respectively the line features of the isotopologues can still be resolved. This allows for a more complete structure determination as the availability of rotational spectra of isotopomers facilitates the estimation of

<sup>54</sup>Gadhi et al., “Moment dipolaire de  $\text{CH}_3\text{CN}$ ”, 1995.

<sup>55</sup>Ulich and Conklin, “Detection of methyl cyanide in Comet Kohoutek”, 1974  
and Öberg et al., “The comet-like composition of a protoplanetary disk as revealed by complex cyanides”, 2015

<sup>56</sup>Rosman and Taylor, “Isotopic Compositions of the Elements 1997”, 1998.

#### 4. Results and Discussion

molecular parameters.<sup>57</sup>

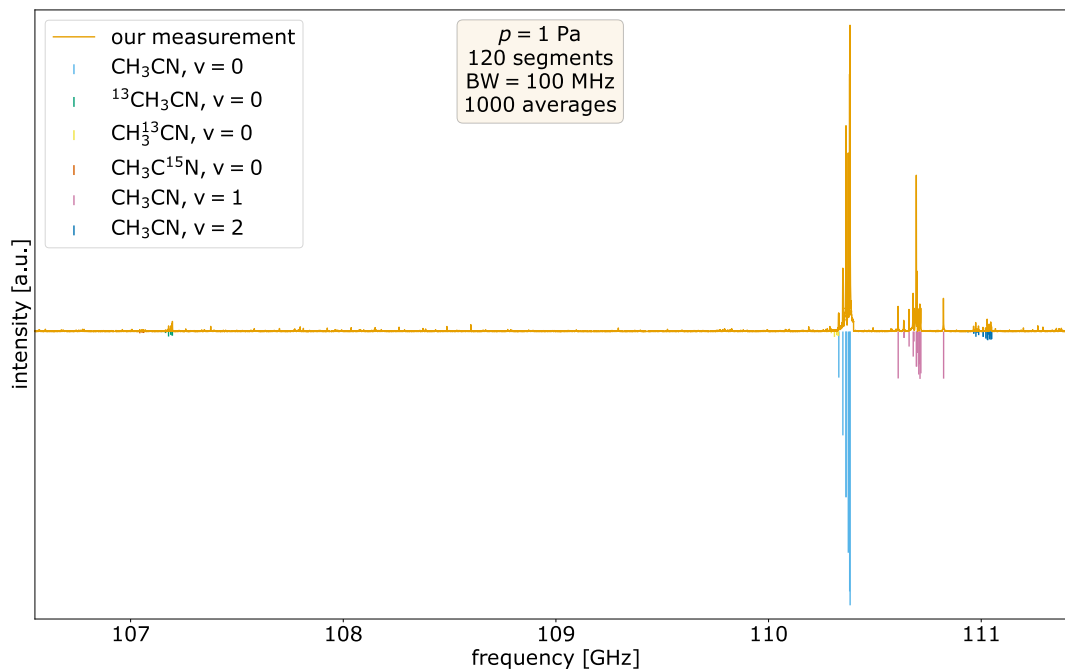


**Figure 4.1.5.:** Overview spectrum of the acetonitrile measurement. Conditions are given in the textbox. Predictions are taken from CDMS.<sup>58</sup> The intensity of the isotopologues was scaled with their natural abundance as described in the text.

The region around 111 GHz shows the vibrational ground, as well as the first and second excited state. The first vibrationally excited state ( $v = 1$ ) of the main isotopologue  $\text{CH}_3\text{CN}$  appears with a slightly higher intensity than expected in comparison to the vibrational ground state. This can be attributed to the instable intensity distribution across the spectrum. As devices show frequency-dependent losses, the measured intensity at two different frequencies cannot be assumed to be consistent. The intensity of a line feature is also strongly time dependent: The FID signal of transitions excited early in the chirp have decayed more in comparison to a transition excited towards the end of the chirp, when

<sup>57</sup>Shipman and Pate, “New Techniques in Microwave Spectroscopy”, 2011.

<sup>58</sup>H. S. P. Müller, L. R. Brown, et al., “Rotational spectroscopy as a tool to investigate interactions between vibrational polyads in symmetric top molecules: Low-lying states  $v_8 \leq 2$  of methyl cyanide,  $\text{CH}_3\text{CN}$ ”, 2015,

More information on the prediction and the origin is obtained in Appendix D *List of Molecular Databases*.

## 4.1. Gas Flow Experiments

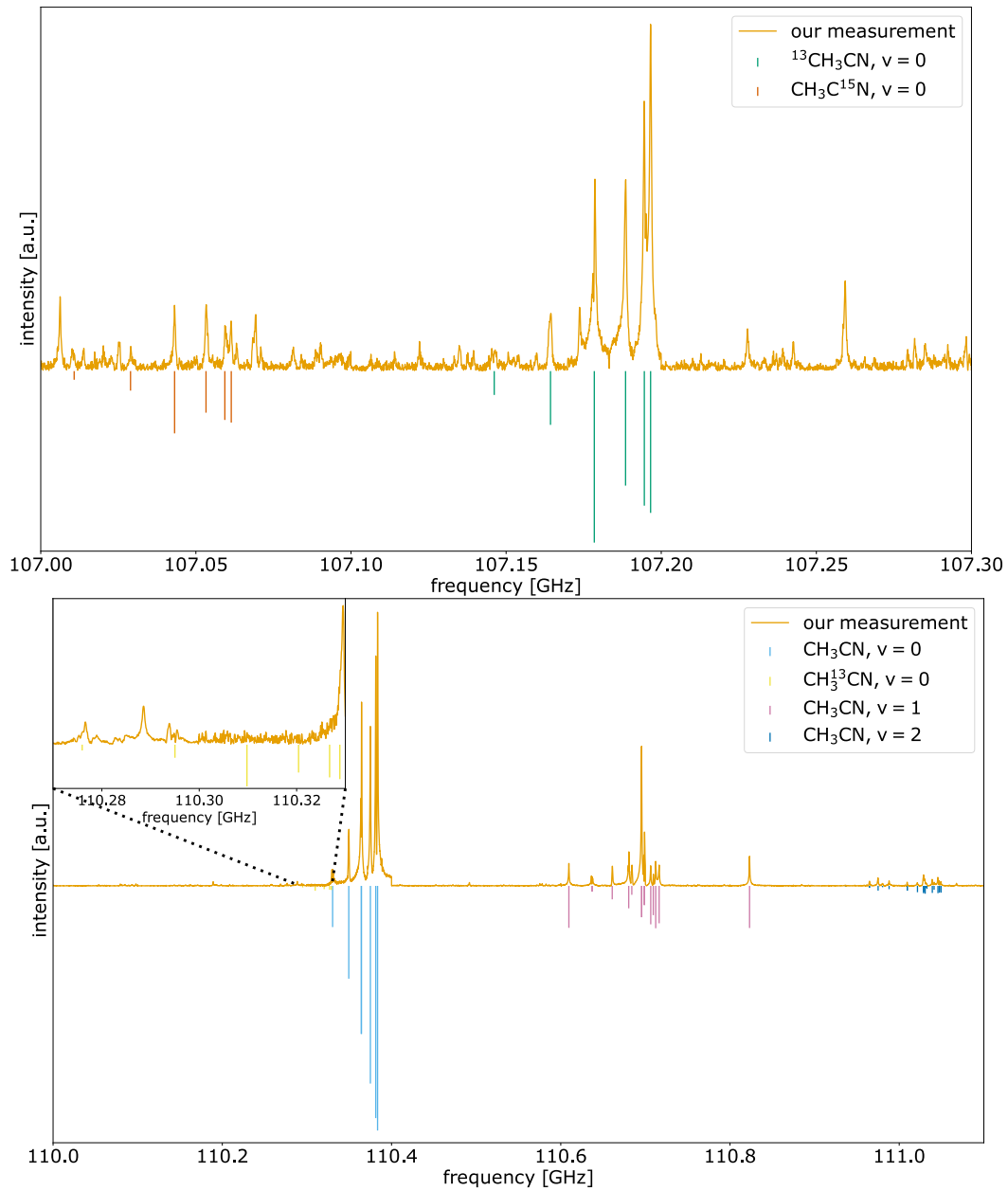


**Figure 4.1.6.:** Spectrum of acetonitrile zoomed at 107 - 107.3 GHz (top) and 110.0 - 111.1 GHz (bottom). Predictions originate from the CDMS database as in the description of figure 4.1.5.

the signal acquisition is finally started. These effects make analyses involving the intensity more complex.

#### 4. Results and Discussion

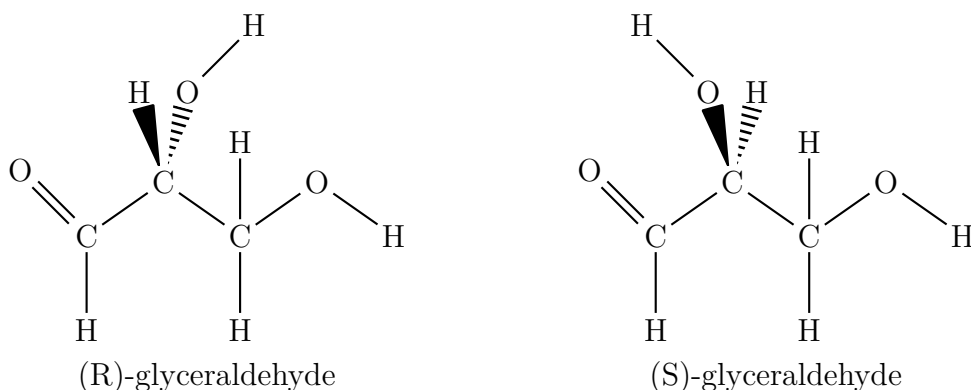


**Figure 4.1.7.:** Chemical structure of glyceraldehyde.

#### 4.1.3. Solid Samples

Glyceraldehyde is a simple sugar with 3 carbon atoms. A chiral centre can be identified at the central carbon. The structure is shown in figure 4.1.7. It is commonly found in the metabolism of earthbound living creatures.<sup>59</sup> Although clues of the presence of its precursors have been found in meteorites, Glyceraldehyde has not yet been identified in the ISM.<sup>60</sup>

A heatable crucible holder was introduced into the vacuum chamber to liquify and evaporate solid samples as described in section 3.1.5 *Vacuum Chamber*. Temperatures of about 510 K ( $\approx 240^\circ\text{C}$ ) are possible.

A granular powder of glyceraldehyde (GA) from SIGMA-ALDRICH (purity  $\geq 90\%$ )<sup>61</sup> was placed into the zirconia crucible<sup>62</sup> from ALMATH CRUCIBLES LTD and gradually heated up to 510 K ( $240^\circ\text{C}$ ). Above 410 K ( $140^\circ\text{C}$ ) grains of GA started to violently move, suggesting explosive evaporation processes at the grain surface, which accelerated at higher temperatures. Unfortunately, no line features were obtainable from the spectra taken during this process, that would allow an assignment to GA. This may indicate that disintegration processes instead of evaporation were the main cause of the sample loss.

<sup>59</sup>See for example Hagopian, Ramsey, and Weindruch, “Enzymes of glycerol and glyceraldehyde metabolism in mouse liver: effects of caloric restriction and age on activities”, 2008

<sup>60</sup>Layssac et al., “Detection of glyceraldehyde and glycerol in VUV processed interstellar ice analogues containing formaldehyde: a general formation route for sugars and polyols”, 2020.

<sup>61</sup>CAS-number: 56-82-6, EC-number: 200-290-0

<sup>62</sup>Low round zirconia crucible, product code: LR52Z

## 4.2. Measurements Using SuJeSTA

Experiments have been performed at the SUJESTA vacuum chamber as described in section 3.1.6 *Setup of SuJeSTA*. This allowed to investigate the spectrometers performance in supersonic jet applications and laser ablation experiments.

### 4.2.1. Jet Measurements

Supersonic jet measurements have been executed at the SUJESTA setup. The theory of jet expansion experiments is described in section 3.1.6.1 *Supersonic Jet Source*. Propylene oxide (PO) was chosen for these experiments because the spectrum shows a high amount of transitions in the observable spectral range. This allowed to observe a significant number of lines used for later analysis.

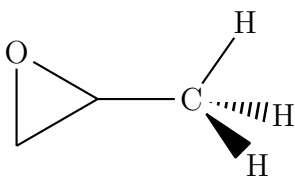


**Figure 4.2.1.:** Chemical structure of propylene oxide.

PO has a total of three carbon atoms, two of them bridged by an oxygen, called the epoxide group. The third carbon atom forms a methyl group, which is able to rotate internally in relation to the epoxide group. The structure is shown in figure 4.2.1. Propylene oxide is synthesised industrially<sup>63</sup> and has been detected in the ISM.<sup>64</sup>

The liquid PO was supplied in a container connected to a pressurised carrier gas supply of Argon. This allowed to create a background pressure in the nozzle system of 5 bar to achieve a significant cooling effect. Higher carrier gas pressures would make lower jet temperatures available, but this dilutes the sample molecules (PO), as the partial pressure remains unchanged, leading to a weaker signal.

Two different nozzle sizes have been used. The smaller orifice has a diameter of 1 mm, the larger one 3 mm. Their performance and their cooling effect are investigated in this section. A procedure to estimate temperatures of a molecular gas

<sup>63</sup>Kahlich, Wiechern, and Lindner, “Propylene Oxide”, 2000.

<sup>64</sup>McGuire et al., “Discovery of the interstellar chiral molecule propylene oxide (CH<sub>3</sub>CHCH<sub>2</sub>O)”, 2016.

#### 4. Results and Discussion

is to perform a BOLTZMANN plot. From equation (33) the number of molecules in a specific state  $m$  follows the proportionality<sup>65</sup>

$$N_m \propto g_m e^{-E_m/k_B T} \Leftrightarrow \ln\left(\frac{I}{g_m}\right) \propto -\frac{E_m}{k_B T} \quad (97)$$

with  $g_m$  as the degree of degeneracy and  $E_m$  the energy of the state. The intensity  $I$  is proportional to the number of molecules  $N_m$  in the lower state. The right hand side version of equation (97) is used when creating a BOLTZMANN plot:  $\ln\left(\frac{I}{g_m}\right)$  is plotted along the  $y$ -axis and  $E_m$  along the  $x$ -axis of a diagram. The slope of a fitted linear function then determines the temperature as it is proportional to  $1/T$ .<sup>66</sup>

Unfortunately, the intensity in chirped pulse experiments is not to scale as described previously in section 4.1.2 *Isotopologues of Acetonitrile*. To minimise the influence of this effect, lines have been manually selected to include only line features that

- are confidently assignable to a certain transition with known energy states
- appear together in one ‘group’, depending on when they are probed by the chirp.

For an up-chirp with a bandwidth of 100 MHz these groups were defined as the beginning (line appears in the first 30 MHz of the chirp), the middle (30–70 MHz) and at the end of the chirp (70–100 MHz). Lines within one group are considered to have comparable intensities, because they were excited on a similar timescale and therefore have decayed comparably long before detection. More groups with a narrower frequency spread would increase comparability, but also reduce the quantity of lines to be found in the region, making meaningful BOLTZMANN plots difficult.

The intensity of each line was estimated as the maximum of the specific line in the measured spectrum. The prediction used for the analysis is based on the parameters given by Mesko et al., “Millimeter and submillimeter spectrum of propylene oxide”, 2017. They were entered into PGOPHER to produce a linelist with predicted line positions. This approach allows to predict intensities in dependence of

<sup>65</sup>This expression is explicitly derived in Herzberg, *Molecular Spectra and Molecular Structure: I. Spectra of Diatomic Molecules*, 1950, p. 124

<sup>66</sup>Waßmuth, “Entwicklung einer THz-Multireflexionsoptik und hochauflösende Rotationspektroskopie von Eisenmonoxid”, 2021.

the temperature, which eases the assignment procedure. The energy of the lower state of a corresponding transition was then used for the analysis. The resulting BOLTZMANN plots are shown in figure 4.2.3. The lines from the measurement with both nozzles used for the consideration are plotted colour coded to indicate group assignment along with the prediction<sup>67</sup> in figure 4.2.2. The intensity of line features for the measurement with the large orifice is higher in comparison to the smaller one. Due to the larger orifice, more material can pass during the opening period, so more matter is present in the interaction volume leading to higher intensities. A list with all considered transitions shown in figure 4.2.2 can be found in table E.1 in Appendix E *Jet Experiments - Considered Lines*. The results of the BOLTZMANN plots and the respective fits are summarised in table 4.1.

**Table 4.1.:** Temperatures estimated from BOLTZMANN plots from supersonic jet measurements of acetonitrile. The analysis is performed with selected lines for three different groups depending on where the line is positioned in the chirp. Two different nozzle orifices have been used giving  $T_{small}$  (diameter 1 mm) and  $T_{large}$  (diameter 3 mm).

part of 100 MHz chirp considered	fit parameters	$T_{large}$
0 - 30 MHz	$f(x) = (-1.20 \pm 1.05) \cdot 10^{-21}x - (7.71 \pm 0.61)$	$T = 60.2^{+428.6}_{-28.1}$ K
30 - 70 MHz	$f(x) = (-1.58 \pm 0.42) \cdot 10^{-21}x - (7.20 \pm 0.24)$	$T = 45.9^{+16.6}_{-9.6}$ K
70 - 100 MHz	$f(x) = (-1.45 \pm 0.43) \cdot 10^{-21}x - (7.45 \pm 0.30)$	$T = 50.1^{+21.5}_{-11.6}$ K
whole chirp	$f(x) = (-1.49 \pm 0.28) \cdot 10^{-21}x - (7.39 \pm 0.17)$	$T = 48.7^{+11.1}_{-7.6}$ K
		$T_{small}$
0 - 30 MHz	$f(x) = (-1.88 \pm 0.74) \cdot 10^{-21}x - (7.72 \pm 0.43)$	$T = 38.6^{+25.2}_{-10.9}$ K
30 - 70 MHz	$f(x) = (-1.21 \pm 0.42) \cdot 10^{-21}x - (7.93 \pm 0.25)$	$T = 60.1^{+31.7}_{-15.4}$ K
70 - 100 MHz	$f(x) = (-1.54 \pm 0.43) \cdot 10^{-21}x - (7.67 \pm 0.29)$	$T = 46.9^{+18.1}_{-10.2}$ K
whole chirp	$f(x) = (-1.48 \pm 0.26) \cdot 10^{-21}x - (7.79 \pm 0.17)$	$T = 49.0^{+10.6}_{-7.4}$ K

The estimated temperatures differ only slightly between the groups of lines for each given orifice and are mostly covered by the asymmetric error intervals. A fit conducted across all frequency groups yields similar results. Both orifices only differ slightly, suggesting no significant difference in the cooling effect of the supersonic expansion jet. The large error can be attributed to the low number of reliably assignable lines, especially for the 0 – 30 MHz line group. Additionally, the inconsistent intensity distribution across different spectral regions introduces

<sup>67</sup>Mesko et al., “Millimeter and submillimeter spectrum of propylene oxide”, 2017.

#### 4. Results and Discussion

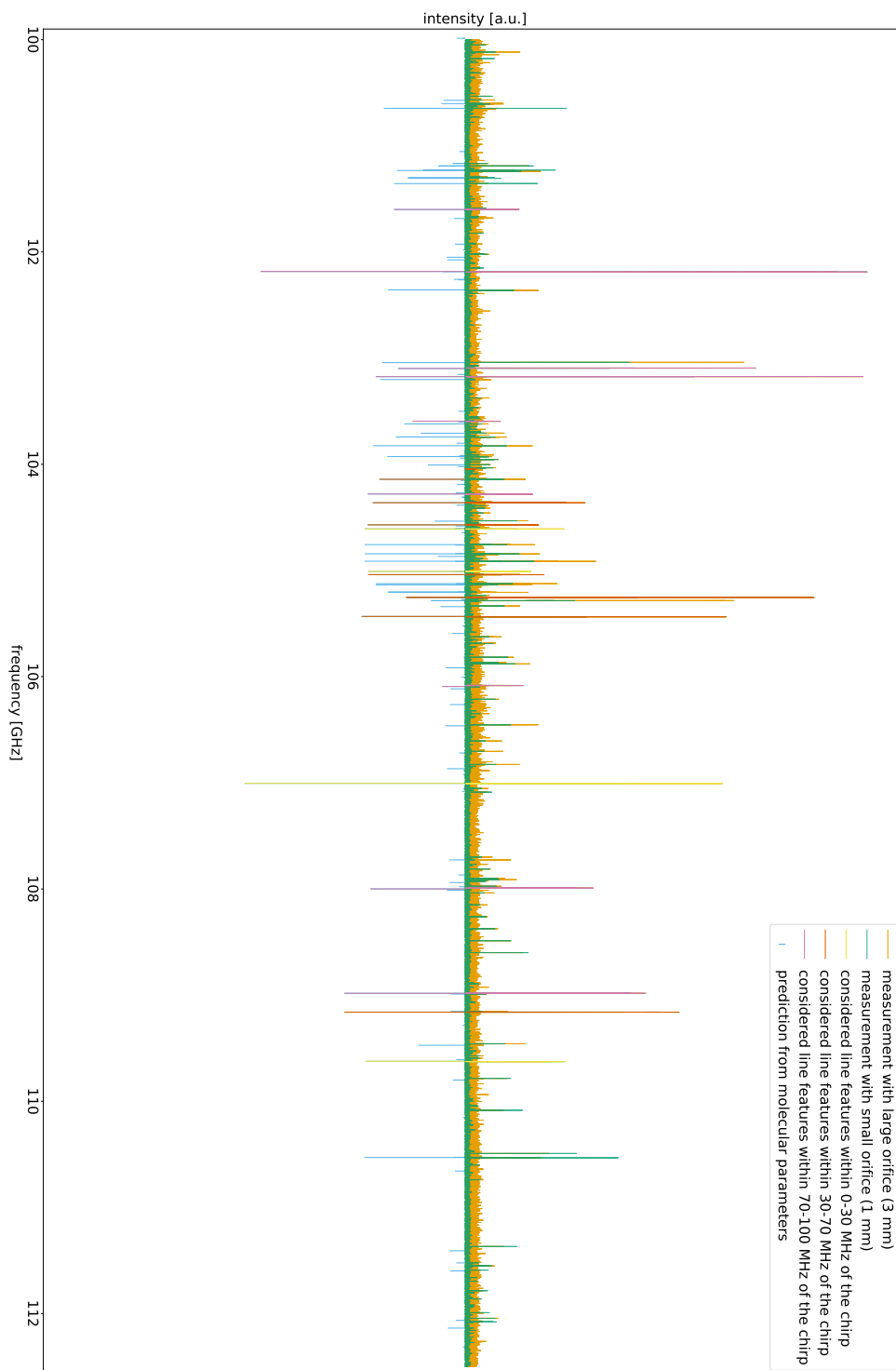


**Figure 4.2.2.:** Considered lines for the BOLTZMANN plots in figure 4.2.3. Details to the prediction can be found in Appendix D *List of Molecular Databases*.

## 4.2. Measurements Using SuJeSTA

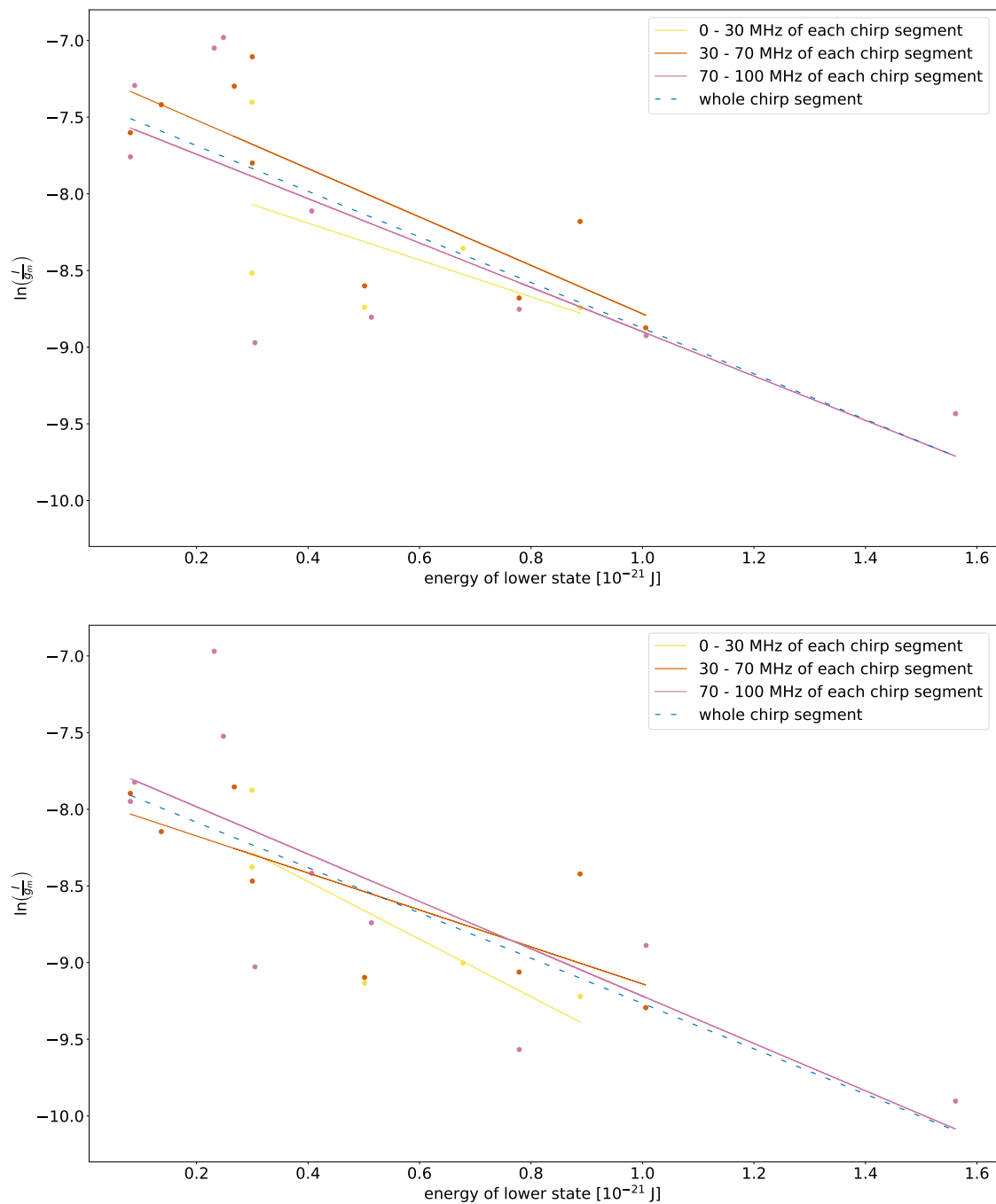


**Figure 4.2.3.:** BOLTZMANN plot for a selection of transitions of propylene oxide. Top figure shows the results for the use of a large nozzle orifice (diameter of 3 mm), bottom for a small orifice (diameter of 1 mm) respectively. The groups of transitions and their corresponding fit, including a general fit over all frequency groups, are colour coded as stated in the legend.

#### 4. Results and Discussion

deviations from theory which are reflected by large uncertainties. However, a fit across all frequency groups of the chirp surprisingly provides usable fit parameters as well. This is due to the logarithmic conversion of the intensities, which flattens intensity deviations.

The relative intensity could be corrected in future experiments. One option is to perform both, up- and down- chirps as already described in section 3.2.2.2 *Chirp Generation*. The option to perform down chirps has been implemented after the measurement presented here. Another way is to take the full spectrum with different initial offsets smaller than the bandwidth covered by the chirp. Both strategies allow to regroup the lines or average their intensities to minimise the effect of line intensity loss due to the chirp length. A different approach might use shorter pulses (e.g. 100 ns instead of 500 ns). This reduces the influence of the idle time but also significantly decreases the amount of energy introduced to the system and therefore might worsen the SNR. A theoretical approach to decrease the influence of the line position within the chirp by an extended data analysis is described by Fontanari et al., “Molecules probed with a slow chirped-pulse excitation: Analytical model of the free-induction-decay signal”, 2019.

Although, this only enhances the comparability of relative intensities. Absolute intensities are barely obtainable by CPFT spectrometers. Nevertheless, this experiment showed that a broadband spectrum taken with CPFTmmW technology in combination with supersonic jet expansion allows to estimate the cooling effect and the resulting temperature in the jet, despite the deficiencies of the multipass reflection cell discussed in section 4.3 *General Discussion*.

#### 4.2.2. Laser Ablation Measurements

The next step was the combination of the automatised spectrometer with laser ablation experiments as described in section 3.1.6.2 *Laser Ablation*. Two solid materials, bismuth tribromide ( $\text{BiBr}_3$ ) and titanium (Ti) have been probed with various gas mixtures, showing limited success. This is probably due to instable production conditions. The experiments are explained in the following.

#### 4.2.2.1. Bismuth Tribromide

Bismuth tribromide is a solid trihalide. Identification in the ISM is not yet reported. In this work  $\text{BiBr}_3$  has been used in laser ablation experiments, trying to create and investigate either  $\text{BiBr}_3$  or  $\text{BiBr}^{68}$  in the gas phase. The natural abundance of  $^{79}\text{Br}$  (50.7%) and  $^{81}\text{Br}$  (49.3%)<sup>69</sup> allows to investigate chiral species, when one Bromide is replaced by another substituent.

The light-yellow powder of bismuth tribromide with a purity of  $\geq 98\%$ <sup>70</sup> supplied by SIGMA-ALDRICH was compressed to create a solid sample rod. This was used as the target material for the laser ablation process. Upon laser interaction, bismuth bromide species  $\text{BiBr}_x$  are expected to be released from the solid framework. It is then cooled and transferred to the interaction volume by a carrier gas pulse of Argon. The measurement was performed with 2 bar of carrier gas pressure, resulting in an average 3.7 Pa chamber background pressure. The laser was used at a repetition frequency of 30 Hz at a power of 1250 V with a delay to the gas nozzle of 80  $\mu\text{s}$ . The AMC467 was used for this experiment as it covers a broader frequency range. 10 averages were taken for each segment.

The jet glowed visibly when the laser was adjusted properly, which correlated with the appearance of lines in the spectrum as depicted in figure 4.2.4. The prediction shows that the spectrum of  $\text{BiBr}_3$  is dense, supplying a large number of transitions even for a single segment of 100 MHz bandwidth. Unfortunately, the lines were neither stable nor reproducible as they appeared to change position and intensity between individual shots. An automatised acquisition of the spectrum was not achievable and only individual segments were evaluated. Averaging for longer intervals was not possible for the same reasons, hence the low SNR.

When the measurement was conducted for a few minutes, both the glow effect and line features vanished. After aborting the measurement, the sample rod appeared deformed and charred with a metallic glare. This implies that upon laser interaction mostly bromide species were evaporated, leaving behind a mixture enriched in bismuth. This explains the deterioration of both the signal and the optical excitation of the jet. It can also be interpreted as the origin for instabilities during the measurement. As the surface of the sample rod becomes

<sup>68</sup>Molecular parameters for the diatomic  $\text{BiBr}$ , measured and assigned lines can be found in Kuijpers and Dymanus, "Rotational spectrum of  $\text{BiBr}$ ", 1976

<sup>69</sup>Rosman and Taylor, "Isotopic Compositions of the Elements 1997", 1998.

<sup>70</sup>CAS-number: 7787-58-8, EC-number: 232-121-1

## 4. Results and Discussion

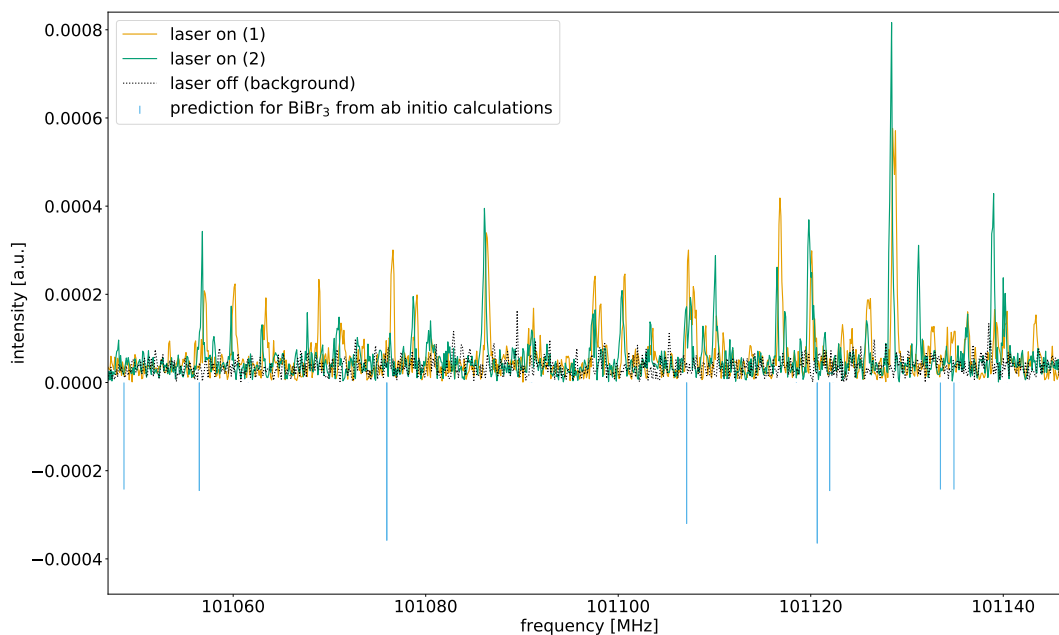


**Figure 4.2.4.:** Frequency domain spectrum for laser ablation experiments of bismuth tribromide. A HANNING window function was used and an FFT applied to the FID of two subsequent measurements indicated by (1) and (2), averaged over 10 shots each. The prediction is a line list export from PGOPHER based on ab initio calculations of  $\text{BiBr}_3$ .

increasingly metallic and deformed, the laser is reflected, and the carrier gas stream diverted into varying directions, destabilising molecule production and jet formation. DOPPLER shifts due to diverted jets may then attribute for positional jumps of individual lines.

Due to the aforementioned conditions, it was not possible to measure specific lines or even assign them to a certain transition or species. The lines measured might originate from bismuth bromide species, bromide molecules or radicals. The deficiencies regarding the SUJESTA setup for the used spectrometer are discussed in section 4.3 *General Discussion*.

### 4.2.2.2. Titanium Species

Due to the instability of the production with  $\text{BiBr}_x$ , titanium oxide species were chosen as the next investigation candidates, because they previously showed sta-

ble production conditions at the same setup in various experiments.<sup>71</sup>. A solid titanium rod was inserted to provide the source material. A gas mixture with  $\approx 2\%$   $\text{N}_2\text{O}$ ,  $\approx 7\%$   $\text{O}_2$  and  $\approx 91\%$  He as inert gas were used to create titanium oxide species such as TiO or  $\text{TiO}_2$  during laser ablation. The fraction of  $\text{N}_2\text{O}$  provided a sample molecule to be probed with non-optimised setup parameters. However, lines of the expected species were neither clearly identifiable nor distinctive from noise. The design of SUJESTA provides various drawbacks when being used with the provided spectrometer setup, which are discussed in section 4.3 *General Discussion*. Nevertheless, the detectability of jet- signals (see section 4.2.1 *Jet Measurements*) suggested that not only the detection method, but insufficient molecule production is the cause of the absence of lines. The 2% fraction of  $\text{N}_2\text{O}$  signal was detectable above the noise floor but molecule production in laser ablation is expected to have significantly lower yields. To optimise molecule production a liquid helium bolometer detector (QFI/2BI from QMC INSTRUMENTS LTD.) was used instead of the heterodyne mix detection arm. This setup is similar to previous experiments that have been performed at other frequencies with a step-scan method. Still, no molecular signal was obtained, despite the systematic variation of all relevant experimental parameters such as timing settings, laser powers, reaction channel lengths, nozzle sizes, nozzle trigger rates, various chirp parameters etc. The combination of suboptimal design properties of SUJESTA for the frequency domain around 100 GHz caused the inability to detect a molecular signal. Lacking this, optimising for molecule production became time consuming, so the experiment was abandoned.

## 4.3. General Discussion

The performance of a measurement depends on both, the specifications of the spectrometer itself and the properties of the interaction volume. For the latter, two setups have been used: a vacuum chamber, which provided reliable spectra of stable molecules, and SUJESTA, which yielded usable data more reluctantly.

---

<sup>71</sup>see for example Breier et al., “Mass-independent analysis of the stable isotopologues of gas-phase titanium monoxide – TiO”, 2019,  
Witsch et al., “The rotationally resolved infrared spectrum of TiO and its isotopologues”, 2021

#### 4. Results and Discussion

##### **Multipass Optics of SuJeSTA**

The multipass optics is originally designed for experiments at frequencies around or above 300 GHz. It is therefore not optimised for the spectrometer at hand operating in the range just above 100 GHz. The mirrors of the calibration optics and the inlet hole are too small for the used radiation. A lot of the incoming power is lost. Further losses are introduced with each reflection cycle due to the unfavourable specifications. Also, the multipass design might not be able to probe the jet efficiently with the extended beam widths at the used frequency range, when the reflections pass largely on or beyond the shock fronts. The additional reflections are then not beneficial for the measurement. These perturbations are strongly frequency dependent. Relative intensities between lines are not reliable and the sensitivity in certain frequency intervals is strongly reduced.

Additionally, excitation pulse back reflections from the mirror-setup force the spectroscopist to open the switch later to protect the receiver arm electronics. Unfortunately, during the added delay the FID decays rapidly, leading to a significant loss of intensity. SUJESTA and its multipass optics therefore have to be deemed impractical for the sensitive detection of transient molecules with the provided spectrometer.

##### **Sensitivity and Noise**

When focussing on the technical aspects of the CPFTmmW spectrometer, it is, as every measurement method, prone to a variety of uncertainties. Each device in the setup causes noise, that is usually amplified in the signal chain. It therefore contaminates the desired molecular signal and reduces the sensitivity. A more detailed analysis can be found in the PhD thesis of PASCAL STAHL<sup>72</sup>.

Having a stable timing and synchronisation is crucial for a successful measurement. Usually, the incoming FID-signal is averaged by the oscilloscope. Instabilities or phase jitter causes a deterioration of the signal, because contributions to the signal will be averaged out when the signal ‘jumps’ in time. Phase jitter therefore has to be avoided. A significant contribution to this is the trigger of the data acquisition on the first flank of the LO signal. This is not expected to always hit at the same position with each shot. Also, the reference clock is prone to drift. Both effects are small enough to allow for a satisfactory and practical

---

<sup>72</sup>Stahl, “PhD thesis: in preparation; Title pending”, 2022.

amount of averages (roughly a few thousand), but would eventually cause signal deterioration at longer timescales, which are desirable for an increase in sensitivity.

#### Frequency Uncertainty

The uncertainty of the FOURIER transformed signal is defined by its resolution. As described in section 3.2.1.4 *Fast Fourier Transform and Window Function*, zeropadding can be used to artificially increase the signal resolution. It is therefore not determined by the setup.

#### Limitations of the Provided Setup

In spectroscopy molecular parameters are adjusted to resemble reality with theoretical calculations. In order to get closer to the truth, a “fitting” procedure is performed: Line positions of certain transitions are predicted by theoretical considerations. With experimentally obtained spectra, empirically obtained line positions can be assigned to well-known transitions. The difference between theoretical prediction and measurement is then minimised by adjusting the molecular parameters, providing a better understanding of the molecule.

To reliably assign lines from an experimental spectrum, easily recognisable features, such as *P*- or *R*- branches, are helpful. For the spectroscopist to identify these features, the covered bandwidth has to be large enough to show distinctive parts of these branches. Also, a significant number of lines are needed in order to produce a stable, reproducible fit and to reliably improve the quality of the molecular parameter set. Both considerations benefit from a large bandwidth. The setup used in this work is limited to a bandwidth of 12.5 GHz for the HPAMC. This is insufficient for the reliable assignment of lines. Fitting of molecular parameters can be difficult due to the low number of molecular transitions in this region, depending on the probed molecule. This limits the significance especially when global predictions across multiple frequency regimes are desired. To improve the spectrometer and gain information of scientific value, further spectral regions need to be unlocked.

## 5. Conclusion and Outlook

This chapter summarises the achievements of this work. Furthermore, an outlook is given into possible future projects regarding the spectrometer.

### 5.1. Conclusion

An existing setup of a CPFTmmW spectrometer has been developed further with a specific focus on automatisation. Control and data processing has been automatised using LABVIEW™ to exploit the advantages the setup offers and to provide a user-friendly, ready-to-use software. The investigation of a variety of molecules in different setups of interaction volumes benefitted from the fast acquisition speed.

Gas flow experiments were used to collect overview spectra and to characterise the used setup.<sup>73</sup> In this work, line widths and SNR have been estimated from a spectrum of methanol (section 4.1.1 *Methanol Spectrum in Gas Flow Experiments and General Spectral Properties*). In the same setup acquisition of acetonitrile showed that isotopologues in their natural abundance and vibrationally excited states are detectable (see section 4.1.2 *Isotopologues of Acetonitrile*). A setup to allow evaporation of solid samples by heating of a crucible sample holder was established (see section 4.1.3 *Solid Samples*). As a first test, a sample powder of glyceraldehyde was used and vaporised in the process, but no signal of the species could be detected in the gas phase, indicating deterioration processes instead of evaporation.

The use of the vacuum chamber SUJESTA equipped with multipass optics, a pulsed nozzle setup and a laser ablation source allowed to perform more sophisticated experiments at astrophysically relevant conditions and to probe for

---

<sup>73</sup>Further information and more details can be found in Stahl, “PhD thesis: in preparation; Title pending”, 2022

transient molecules. Pulsed supersonic jet experiments have been carried out with propylene oxide (see section 4.2.1 *Jet Measurements*). Generally, intensity distributions in CPFTmmW spectroscopy are not consistent due to frequency-dependent losses of individual devices and the time-dependent decay of intensity of emission lines during the chirp. Albeit these circumstances, a careful selection of lines in different sections of individual chirp segments allowed to perform a BOLTZMANN plot to estimate temperatures in the jet. Significant differences in temperature when using nozzle orifices of different size were not detected.

Laser ablation jet experiments in combination with CPFTmmW spectroscopy are not yet common, but offer a lot of potential acquiring data of transient species. The presented setup promised to achieve this. Using bismuth tribromide as source material showed instable molecule production and jet conditions, that were difficult to optimise. A likely reason for this is the change of surface properties of the sample rod upon interaction with the laser, which leads to unequal plasma conditions and probably changes the chemical composition of the material. As a result, only narrow-bandwidth spectra were obtainable, showing only low-intensity and time fluctuating lines. Under these circumstances it was difficult to assign a carrier molecule to the observed transitions. Switching the source material to titanium and the carrier gas to an oxygen carrying mixture was expected to allow investigation of titanium oxide species. Despite widescale efforts in optimisation it was not possible to detect a signal. Possible reasons for this non-detection are interfering back reflections of the multipass optics in the SUJESTA setup, or insufficient production conditions for the ablation source. Nevertheless, first signals correlating laser ablation with spectral features promise that the combination of CPFTmmW with laser ablation sources is possible.

## 5.2. Outlook

The spectrometer and its accompanying software is now ready for use for a variety of future tasks. One option is to combine the laser ablation technique with CPFTmmW spectroscopy. For this a new vacuum chamber has to be designed with optics specified to the frequency range around 100 GHz. To house a multipass optical system adjusted to this, its dimensions have to be approximately a minimum of  $80 \times 80 \times 60 \text{ cm}^3$ . This also yields enough space to implement

## 5. Conclusion and Outlook

various molecular sources such as jet expansion nozzles, laser ablation or discharge sources. If intensity is a problem, even multiple nozzles may be installed as argued by BROWN et al.<sup>74</sup> Once the new chamber is set up, the detection and characterisation of a variety of molecules with transitions in this frequency regime is likely.

Another option is to improve the performance of the spectrometer and overcome its limitations. Exchanging the WR8.0 to a WR10.0 mixAMC in the receiver arm and adjustment of a few components may open up the frequency range down to 80 GHz, enabling to probe most of the W-band (75 - 110 GHz). This allows to investigate far more transitions and even molecules, that currently barely provide any transitions in the available frequency range.

The software provided in LABVIEW™ is extendable and new instrument parts can easily be implemented. The programming only needs to be changed when hardware alternations to the AWG or the oscilloscope are made. The spectrometer is ready-to-use for future applications.

Extending the frequency range and thus enabling to investigate molecules that are not yet within reach will largely benefit the work on molecular spectroscopy and, therefore, also astrochemical and -physical fields. The CPFTmmW technique is especially promising for the gas-phase structure determination of large molecules. Also, rotational spectroscopy of free radicals created with discharge sources is feasible and may provide information on electronic properties.<sup>75</sup>

---

<sup>74</sup>G. G. Brown et al., "A broadband Fourier transform microwave spectrometer based on chirped pulse excitation", 2008.

<sup>75</sup>Shipman and Pate, "New Techniques in Microwave Spectroscopy", 2011.

# Bibliography

- A. F. Harvey and M. Cerna. *The Fundamentals of FFT-Based Signal Analysis and Measurement in LabVIEW and LabWindows*. 1993. URL: <https://www.semanticscholar.org/paper/The-Fundamentals-of-FFT-Based-Signal-Analysis-and-Harvey-Cerna/9aaac129f06ae0079d803fb30829e2f594d95a3f> (visited on 08/20/2021).
- Barbara Elvers, ed. *Ullmann's Encyclopedia of Industrial Chemistry*. Weinheim, Germany: Wiley-VCH Verlag GmbH & Co. KGaA, 2000. ISBN: 3527306730.
- Bernath, Peter F. *Spectra of atoms and molecules*. 2nd edition. Oxford: Oxford Univ. Press, 2005. ISBN: 978-0-19-517759-6.
- Breier, Alexander A. "High-Resolution Microwave Spectroscopy of Radioactive Molecules: Mass-independent studies fo AlF, AlH, AlO, AlS, TiO and FeO". PhD Thesis. Kassel: Universität Kassel, 2019.
- Breier, Alexander A. et al. "Mass-independent analysis of the stable isotopologues of gas-phase titanium monoxide – TiO". In: *Journal of Molecular Spectroscopy* 355 (2019), pp. 46–58. ISSN: 00222852. DOI: [10.1016/j.jms.2018.11.006](https://doi.org/10.1016/j.jms.2018.11.006).
- Bronstein, I. N. et al. *Teubner-Taschenbuch der Mathematik*. Stuttgart, Leipzig, and Wiesbaden: Teubner, 2009. ISBN: 978-3-8351-0123-4.
- Brown, Gordon G. et al. "A broadband Fourier transform microwave spectrometer based on chirped pulse excitation". In: *The Review of scientific instruments* 79.5 (2008), p. 053103. ISSN: 0034-6748. DOI: [10.1063/1.2919120](https://doi.org/10.1063/1.2919120).
- Brünken, S. et al. "The Rotational Spectrum of TiO 2". In: *The Astrophysical Journal* 676.2 (2008), pp. 1367–1371. ISSN: 0004-637X. DOI: [10.1086/528934](https://doi.org/10.1086/528934).
- Cernicharo, J. et al. "Unveiling the Dust Nucleation Zone of IRC+10216 with ALMA". In: *The Astrophysical Journal* 778.2 (2013), p. L25. ISSN: 0004-637X. DOI: [10.1088/2041-8205/778/2/L25](https://doi.org/10.1088/2041-8205/778/2/L25).
- Colombo, Anthony P. "Chirped-pulse millimeter-wave spectroscopy, dynamics, and manipulation of Rydberg-Rydberg Transitions". Thesis (Ph. D.) Cam-

## Bibliography

- bridge (Massachusetts): Massachusetts Institute of Technology, 2013. URL: <https://dspace.mit.edu/handle/1721.1/82169> (visited on 03/11/2021).
- Endres, Christian P., Stephan Schlemmer, Peter Schilke, et al. “The Cologne Database for Molecular Spectroscopy, CDMS, in the Virtual Atomic and Molecular Data Centre, VAMDC”. In: *Journal of Molecular Spectroscopy* 327 (2016), pp. 95–104. ISSN: 00222852. DOI: [10.1016/j.jms.2016.03.005](https://doi.org/10.1016/j.jms.2016.03.005).
- Endres, Christian P., Stephan Schlemmer, Jürgen Stutzki, et al. *Cologne Database for Molecular Spectroscopy (CDMS)*. URL: <https://cdms.astro.uni-koeln.de/classic> (visited on 08/20/2021).
- Eravant, ed. *SAR-2507-08-S2: Data Sheet*. URL: <https://sftp.eravant.com/content/datasheets/SAR-2507-08-S2.pdf> (visited on 08/09/2021).
- ed. *SKD-7531143530-1010-R1-M: Data Sheet*. URL: <https://sftp.eravant.com/content/datasheets/SKD-7531143530-1010-R1-M.pdf> (visited on 08/09/2021).
- Fischer, Hermann O. L. and Carl Taube. “Über Acetonieren mit Aceton und Zinkchlorid”. In: *Berichte der deutschen chemischen Gesellschaft (A and B Series)* 60.2 (1927), pp. 485–490. ISSN: 03659488. DOI: [10.1002/cber.19270600235](https://doi.org/10.1002/cber.19270600235).
- Fontanari, D. et al. “Molecules probed with a slow chirped-pulse excitation: Analytical model of the free-induction-decay signal”. In: *Physical Review A* 100.4 (2019). ISSN: 2469-9926. DOI: [10.1103/PhysRevA.100.043407](https://doi.org/10.1103/PhysRevA.100.043407).
- Fowler, Alfred and Hugh Longbourne Callendar. “The spectra of Antarian stars in relation to the fluted spectrum of titanium”. In: *Proceedings of the Royal Society of London* 73.488-496 (1904), pp. 219–225. ISSN: 0370-1662. DOI: [10.1098/rspl.1904.0034](https://doi.org/10.1098/rspl.1904.0034).
- Gadhi, J. et al. “Moment dipolaire de CH<sub>3</sub>CN”. In: *Journal de Chimie Physique* 92 (1995), pp. 1984–1992. ISSN: 0021-7689. DOI: [10.1051/jcp/1995921984](https://doi.org/10.1051/jcp/1995921984).
- Gambogi, Joseph. “Titanium and titanium dioxide”. In: *Mineral Commodity Summaries*. 2021, pp. 174–175.
- Grabow, Jens-Uwe. “Fourier Transform Microwave Spectroscopy Measurement and Instrumentation”. In: *Handbook of high-resolution spectroscopy*. Ed. by Martin Quack and Frédéric Merkt. Chichester: Wiley, 2011, pp. 723–799. ISBN: 9780470749593.
- Hachenberg, O. and Bernd Vowinkel. *Technische Grundlagen der Radioastronomie*. Mannheim: Bibliographisches Institut, 1982. ISBN: 3411016450.

- Hagopian, Kevork, Jon J. Ramsey, and Richard Weindruch. “Enzymes of glycerol and glyceraldehyde metabolism in mouse liver: effects of caloric restriction and age on activities”. In: *Bioscience reports* 28.2 (2008), pp. 107–115. ISSN: 0144-8463. DOI: [10.1042/BSR20080015](https://doi.org/10.1042/BSR20080015).
- Herbst, Eric et al. “A new analysis and additional measurements of the millimeter and submillimeter spectrum of methanol”. In: *Journal of Molecular Spectroscopy* 108.1 (1984), pp. 42–57. ISSN: 00222852. DOI: [10.1016/0022-2852\(84\)90285-6](https://doi.org/10.1016/0022-2852(84)90285-6).
- Herzberg, Gerhard. *Molecular Spectra and Molecular Structure: I. Spectra of Diatomic Molecules*. 2. Vol. 1. New York: van Nostrand Reinhold Company, 1950.
- Heuvel, J.E.M. and A. Dymanus. “Hyperfine structure of CH<sub>3</sub>OH”. In: *Journal of Molecular Spectroscopy* 45.2 (1973), pp. 282–292. ISSN: 00222852. DOI: [10.1016/0022-2852\(73\)90159-8](https://doi.org/10.1016/0022-2852(73)90159-8).
- Huber+Suhner AG, ed. *SUCOFORM 141: Formable microwave cable: Data Sheet*. URL: <https://ecatalog.hubersuhner.com/media/documents/datasheet/en/pdf/22511925> (visited on 08/08/2021).
- Jacob, Daniel J. “Global budget of methanol: Constraints from atmospheric observations”. In: *Journal of Geophysical Research* 110.D8 (2005). ISSN: 0148-0227. DOI: [10.1029/2004JD005172](https://doi.org/10.1029/2004JD005172).
- Kahlich, Dietmar, Uwe Wiechern, and Jörg Lindner. “Propylene Oxide”. In: *Ullmann’s Encyclopedia of Industrial Chemistry*. Ed. by Barbara Elvers. Weinheim, Germany: Wiley-VCH Verlag GmbH & Co. KGaA, 2000. ISBN: 3527306730. DOI: [10.1002/14356007.a22\\_239](https://doi.org/10.1002/14356007.a22_239).
- Keysight Technologies, ed. *M8190A Arbitrary Waveform Generator: 12 GSa/s Arbitrary Waveform Generator: Data Sheet*. 2021. URL: <https://www.keysight.com/de/de/assets/7018-02903/data-sheets/5990-7516.pdf> (visited on 07/19/2021).
- Kuijpers, P. and A. Dymanus. “Rotational spectrum of BiBr”. In: *Chemical Physics Letters* 39.2 (1976), pp. 217–220. ISSN: 00092614. DOI: [10.1016/0009-2614\(76\)80058-9](https://doi.org/10.1016/0009-2614(76)80058-9).
- Laysac, Y. et al. “Detection of glyceraldehyde and glycerol in VUV processed interstellar ice analogues containing formaldehyde: a general formation route for sugars and polyols”. In: *Monthly Notices of the Royal Astronomical Society* 496.4 (2020), pp. 5292–5307. ISSN: 0035-8711. DOI: [10.1093/mnras/staa1875](https://doi.org/10.1093/mnras/staa1875).

## Bibliography

- Lovas, F. J. et al. “The microwave spectrum of the C3 sugars: glyceraldehyde and 1,3-dihydroxy-2-propanone and the dehydration product 2-hydroxy-2-propen-1-al”. In: *Journal of Molecular Spectroscopy* 222.2 (2003), pp. 263–272. ISSN: 00222852. DOI: [10.1016/j.jms.2003.08.007](https://doi.org/10.1016/j.jms.2003.08.007).
- Lutter, Volker. “Infrarot-Laserspektroskopie an Silizium- und Germanium- Kohlenstoffverbindungen”. Dissertation. Kassel, 2015.
- McGuire, Brett A. et al. “Discovery of the interstellar chiral molecule propylene oxide (CH<sub>3</sub>CHCH<sub>2</sub>O)”. In: *Science (New York, N.Y.)* 352.6292 (2016), pp. 1449–1452. DOI: [10.1126/science.aae0328](https://doi.org/10.1126/science.aae0328).
- Merrill, Paul W., Armin J. Deutsch, and Philip C. Keenan. “Absorption Spectra of M-Type Mira Variables”. In: *The Astrophysical Journal* 136 (1962), p. 21. ISSN: 0004-637X. DOI: [10.1086/147348](https://doi.org/10.1086/147348).
- Mesko, A. J. et al. “Millimeter and submillimeter spectrum of propylene oxide”. In: *Journal of Molecular Spectroscopy* 335 (2017), pp. 49–53. ISSN: 00222852. DOI: [10.1016/j.jms.2017.02.003](https://doi.org/10.1016/j.jms.2017.02.003).
- Mineral Commodity Summaries*. 2021. DOI: [10.3133/mcs2021](https://doi.org/10.3133/mcs2021).
- Mini-Circuits, ed. *VHF-3500+: Data Sheet*. URL: <https://www.minicircuits.com/pdfs/VHF-3500+.pdf> (visited on 07/19/2021).
- ed. *VHF-7150+: Data Sheet*. URL: <https://www.minicircuits.com/pdfs/VHF-7150+.pdf> (visited on 08/08/2021).
- ed. *ZDPLX-2150-S+: Data Sheet*. URL: <https://www.minicircuits.com/pdfs/ZDPLX-2150-S+.pdf> (visited on 08/09/2021).
- ed. *ZX60-123LN-S+ Coaxial Low Noise Amplifier: Data Sheet*. URL: <https://www.minicircuits.com/pdfs/ZX60-123LN-S+.pdf> (visited on 08/08/2021).
- ed. *ZX75BP-1350-S+: Data Sheet*. URL: <https://www.minicircuits.com/pdfs/ZX75BP-1350-S+.pdf> (visited on 08/09/2021).
- ed. *ZX90-2-24+: Data Sheet*. URL: <https://www.minicircuits.com/pdfs/ZX90-2-24+.pdf> (visited on 08/08/2021).
- ed. *ZX90-2-36-S+: Data Sheet*. URL: <https://www.minicircuits.com/pdfs/ZX90-2-36-S+.pdf> (visited on 07/19/2021).
- ed. *ZX90-2-50-S+: Data Sheet*. URL: <https://www.minicircuits.com/pdfs/ZX90-2-50-S+.pdf> (visited on 08/08/2021).
- Müller, H. S. P. <sup>13</sup>CH<sub>3</sub>CN, *v=0*. 2009. URL: <https://cdms.astro.uni-koeln.de/cgi-bin/cdmsinfo?file=e042508.cat> (visited on 08/27/2021).

- $CH_3^{13}CN$ ,  $v=0$ . 2009. URL: <https://cdms.astro.uni-koeln.de/cgi-bin/cdmsinfo?file=e042509.cat> (visited on 08/27/2021).
  - $CH_3C^{15}N$ ,  $v=0$ . 2009. URL: <https://cdms.astro.uni-koeln.de/cgi-bin/cdmsinfo?file=e042510.cat> (visited on 08/27/2021).
  - *Glyceraldehyde - CHOCHOHCH<sub>2</sub>OH*. 2014. URL: <https://cdms.astro.uni-koeln.de/cgi-bin/cdmsinfo?file=e090501.cat> (visited on 08/10/2021).
  - $CH_3CN$ ,  $v=0$ . 2015. URL: <https://cdms.astro.uni-koeln.de/cgi-bin/cdmsinfo?file=e041505.cat> (visited on 08/10/2021).
  - $CH_3CN$ ,  $v=1$ . 2015. URL: <https://cdms.astro.uni-koeln.de/cgi-bin/cdmsinfo?file=e041509.cat> (visited on 08/10/2021).
  - $CH_3CN$ ,  $v=2$ . 2015. URL: <https://cdms.astro.uni-koeln.de/cgi-bin/cdmsinfo?file=e041510.cat> (visited on 08/10/2021).
- Müller, H. S. P., Linda R. Brown, et al. “Rotational spectroscopy as a tool to investigate interactions between vibrational polyads in symmetric top molecules: Low-lying states  $v_8 \leq 2$  of methyl cyanide,  $CH_3CN$ ”. In: *Journal of Molecular Spectroscopy* 312 (2015), pp. 22–37. ISSN: 00222852. DOI: [10.1016/j.jms.2015.02.009](https://doi.org/10.1016/j.jms.2015.02.009).
- Müller, H. S. P., B. J. Drouin, and J. C. Pearson. “Rotational spectra of isotopic species of methyl cyanide,  $CH_3CN$ , in their ground vibrational states up to terahertz frequencies”. In: *Astronomy & Astrophysics* 506.3 (2009), pp. 1487–1499. ISSN: 0004-6361. DOI: [10.1051/0004-6361/200912932](https://doi.org/10.1051/0004-6361/200912932).
- Mütterlein, Bernward. *Handbuch für die Programmierung mit LabVIEW: mit Studentenversion LabVIEW 8.6*. Heidelberg: Spektrum Akad. Verl., 2011. ISBN: 978-3-8274-2337-5.
- NASA - Jet Propulsion Laboratory (JPL) - California Institute of Technology, ed. *JPL - Molecular Database*. URL: <https://spec.jpl.nasa.gov/> (visited on 07/20/2021).
- National Instruments Corp., ed. *Erfassen von Analogsignalen: Bandbreite, Nyquist-Abtasttheorem und Alias-Effekt*. 2019. URL: <https://www.ni.com/de-de/innovations/white-papers/06/acquiring-an-analog-signal--bandwidth--nyquist-sampling-theorem-.html#section--2010261171> (visited on 07/19/2021).

## Bibliography

- Nijhuis, T. Alexander et al. “The Production of Propene Oxide: Catalytic Processes and Recent Developments”. In: *Industrial & Engineering Chemistry Research* 45.10 (2006), pp. 3447–3459. ISSN: 0888-5885. DOI: [10.1021/ie0513090](https://doi.org/10.1021/ie0513090). NIST. *Standard Reference Database*. 2019. URL: <https://physics.nist.gov/cuu/Constants/index.html> (visited on 02/16/2021).
- Nummelin, A. et al. “A Three-Position Spectral Line Survey of Sagittarius B2 between 218 and 263 GHz. II. Data Analysis”. In: *The Astrophysical Journal Supplement Series* 128.1 (2000), pp. 213–243. ISSN: 0067-0049. DOI: [10.1086/313376](https://doi.org/10.1086/313376).
- Nyquist, H. “Certain topics in telegraph transmission theory”. In: *Proceedings of the IEEE* 90.2 (2002), pp. 280–305. ISSN: 00189219. DOI: [10.1109/5.989875](https://doi.org/10.1109/5.989875).
- Öberg, Karin I. et al. “The comet-like composition of a protoplanetary disk as revealed by complex cyanides”. In: *Nature* 520.7546 (2015), pp. 198–201. DOI: [10.1038/nature14276](https://doi.org/10.1038/nature14276).
- Oerlikon Leybold Vacuum GmbH, ed. *PT Turbomolecular Pump Systems 30 - 400 l · s<sup>-1</sup>: 178.01.02*. 2010. URL: [https://www.idealvac.com/files/literature/10\\_Oerlikon\\_Leybold\\_Vacuum\\_Catalog\\_2010\\_PT\\_CS\\_Turbo\\_Pump\\_Systems.pdf](https://www.idealvac.com/files/literature/10_Oerlikon_Leybold_Vacuum_Catalog_2010_PT_CS_Turbo_Pump_Systems.pdf) (visited on 08/31/2021).
- ed. *High Vacuum Pumps: Excerpt from the Oerlikon Leybold Vacuum Full Line Catalog 2015/2016: 240.00.02*. 2015. URL: [https://www.leyboldproducts.com/media/pdf/c5/88/98/CP\\_040\\_TURBOVAC\\_MAG\\_EN.pdf](https://www.leyboldproducts.com/media/pdf/c5/88/98/CP_040_TURBOVAC_MAG_EN.pdf) (visited on 08/09/2021).
- Park, G. Barratt and Robert W. Field. “Perspective: The first ten years of broadband chirped pulse Fourier transform microwave spectroscopy”. In: *The Journal of chemical physics* 144.20 (2016), p. 200901. DOI: [10.1063/1.4952762](https://doi.org/10.1063/1.4952762).
- Pasternack Enterprises, ed. *PE15A1007: Technical Data Sheet*. URL: <https://www.pasternack.com/images/ProductPDF/PE15A1007.pdf> (visited on 08/09/2021).
- Pfeiffer Vacuum AG, ed. *EVN116: Datenblatt*. URL: <https://www.pfeiffer-vacuum.com/productPdfs/PFI32031.de.pdf> (visited on 08/09/2021).
- Pickett, H. M. et al. “Submillimeter, millimeter, and microwave spectral line catalog”. In: *Journal of Quantitative Spectroscopy and Radiative Transfer* 60.5 (1998), pp. 883–890. ISSN: 00224073. DOI: [10.1016/S0022-4073\(98\)00091-0](https://doi.org/10.1016/S0022-4073(98)00091-0).

- Quack, Martin and Frédéric Merkt, eds. *Handbook of high-resolution spectroscopy*. Chichester: Wiley, 2011. ISBN: 9780470749593. DOI: [10.1002/9780470749593](https://doi.org/10.1002/9780470749593).
- Quantum Composers, Inc., ed. *9520 Series Digital Delay Pulse Generators: Data Sheet*. URL: [https://drive.google.com/open?id=0B2\\_5vhSneaPVRnBmeWYtUjMwbVE](https://drive.google.com/open?id=0B2_5vhSneaPVRnBmeWYtUjMwbVE) (visited on 08/08/2021).
- Rosman, K. J. R. and P. D. P. Taylor. “Isotopic Compositions of the Elements 1997”. In: *Journal of Physical and Chemical Reference Data* 27.6 (1998), pp. 1275–1287. ISSN: 0047-2689. DOI: [10.1063/1.556031](https://doi.org/10.1063/1.556031).
- RPG Radiometer Physics GmbH, ed. *W-LNA 75-110 20 3: Data Sheet*. URL: [https://www.radiometer-physics.de/download/datasheets/mmwave-and-terahertz-products/amplifiers/RPG\\_LowNoiseAmplifiers\\_W-LNA-75-110-20-3\\_ProductDataSheet.pdf](https://www.radiometer-physics.de/download/datasheets/mmwave-and-terahertz-products/amplifiers/RPG_LowNoiseAmplifiers_W-LNA-75-110-20-3_ProductDataSheet.pdf) (visited on 08/09/2021).
- Scoles, Giacinto et al., eds. *Atomic and Molecular Beam Methods*. New York: Oxford University Press, 1992. ISBN: 0195042808.
- Shannon, C. E. “Communication in the Presence of Noise”. In: *Proceedings of the IRE* 37.1 (1949), pp. 10–21. ISSN: 0096-8390. DOI: [10.1109/JRPROC.1949.232969](https://doi.org/10.1109/JRPROC.1949.232969).
- Shipman, Steven T. and Brooks H. Pate. “New Techniques in Microwave Spectroscopy”. In: *Handbook of high-resolution spectroscopy*. Ed. by Martin Quack and Frédéric Merkt. Chichester: Wiley, 2011, pp. 801–827. ISBN: 9780470749593.
- Stahl, Pascal. “Aufbau eines Chirped-Pulse Mikrowellenspektrometers mit Überschalldüsenstrahl”. Master Thesis. Kassel: Universität Kassel, 2017.
- “PhD thesis: in preparation; Title pending”. PhD Thesis. Kassel: Universität Kassel, 2022.
- Stahl, Pascal, Benjamin E. Arenas, et al. “Deciphering the rotational spectrum of the first excited torsional state of propylene oxide”. In: *Journal of Molecular Spectroscopy* 378 (2021), p. 111445. ISSN: 00222852. DOI: [10.1016/j.jms.2021.111445](https://doi.org/10.1016/j.jms.2021.111445).
- Stahl, Pascal, Denis Kargin, et al. “The Millimeter-Wave Spectrum of Doubly Deuterated Propylene Oxide CH<sub>3</sub>CHCD<sub>2</sub>O”. In: *Journal of Molecular Spectroscopy* 380 (2021). ISSN: 00222852. DOI: [10.1016/j.jms.2021.111498](https://doi.org/10.1016/j.jms.2021.111498).
- Tektronix, ed. *6 Series B MSO: Mixed Signal Oscilloscope: Datasheet*. URL: <https://download.tek.com/datasheet/MS06B-Datasheet-EN-US-48W-61716-04.pdf> (visited on 08/09/2021).

## Bibliography

- Tkachenko, Nikolai V., ed. *Optical spectroscopy: Methods and instrumentations*. 1st ed. Amsterdam and Boston: Elsevier, 2006. ISBN: 9780444521262.
- Townes, Charles H. and Arthur L. Schawlow. *Microwave spectroscopy*. unabridged, corrected republication. Dover books on physics. New York, NY: Dover, 2012. ISBN: 978-0-486-61798-5.
- Ulich, B. L. and E. K. Conklin. “Detection of methyl cyanide in Comet Kohoutek”. In: *Nature* 248.5444 (1974), pp. 121–122. DOI: [10.1038/248121a0](https://doi.org/10.1038/248121a0).
- Virginia Diodes, Inc., ed. *AMC467 WR10M-AMC: User Guide*.  
– ed. *AMC672 105 GHz: User Guide*.  
– ed. *WR8.0AMC-I Specifications: Data Sheet*. URL: <https://www.vadiodes.com/en/wr8-0amc-i> (visited on 08/09/2021).
- Walsh, Catherine and Richard Hook. *First Detection of Methyl Alcohol in a Planet-forming Disc*. 2016. URL: <https://www.eso.org/public/news/eso1619/> (visited on 03/04/2021).
- Waßmuth, Björn. “Hochauflösende Rotationsspektroskopie an metallhaltigen zweiatomigen Molekülen”. Master Thesis. Kassel, 2017.  
– “Entwicklung einer THz-Multireflexionsoptik und hochauflösende Rotationsspektroskopie von Eisenmonoxid”. PhD Thesis. Kassel: Universität Kassel, 2021.
- Wenzel Associates, Inc., ed. *Premium 10 MHz-SC Streamline Crystal Oscillator: Data sheet*. URL: <http://www.wenzel.com/wp-content/parts/501-04609.pdf> (visited on 08/08/2021).
- Western, Colin. *PGOPHER: version 10.1*. 2018. DOI: [10.5523/bris.3mqfb4glgkr8a2rev7f73t300c](https://doi.org/10.5523/bris.3mqfb4glgkr8a2rev7f73t300c). URL: <http://pgopher.chm.bris.ac.uk/> (visited on 09/02/2021).
- Witsch, Daniel et al. “The rotationally resolved infrared spectrum of TiO and its isotopologues”. In: *Journal of Molecular Spectroscopy* 377 (2021), p. 111439. ISSN: 00222852. DOI: [10.1016/j.jms.2021.111439](https://doi.org/10.1016/j.jms.2021.111439).
- Xu, Li-Hong et al. “Torsion–rotation global analysis of the first three torsional states ( $v_t=0, 1, 2$ ) and terahertz database for methanol”. In: *Journal of Molecular Spectroscopy* 251.1-2 (2008), pp. 305–313. ISSN: 00222852. DOI: [10.1016/j.jms.2008.03.017](https://doi.org/10.1016/j.jms.2008.03.017).

- Xu, L.-H., Christian P. Endres, and H.S.P. Müller. *CH<sub>3</sub>OH,  $v_t=0-2$* . 2016. URL: <https://cdms.astro.uni-koeln.de/cgi-bin/cdmsinfo?file=e032504.cat> (visited on 08/10/2021).
- Zasowski, G. et al. “SPITZER infrared spectrograph observations of Class I/II objects in Taurus: Composition and thermal history of the circumstellar ices”. In: *The Astrophysical Journal* 694.1 (2009), pp. 459–478. ISSN: 0004-637X. DOI: [10.1088/0004-637X/694/1/459](https://doi.org/10.1088/0004-637X/694/1/459).
- Ziurys, Lucy M. “Millimeter and Submillimeter Wave Spectroscopy and Astrophysical Applications”. In: *Handbook of high-resolution spectroscopy*. Ed. by Martin Quack and Frédéric Merkt. Chichester: Wiley, 2011, pp. 939–963. ISBN: 9780470749593.

# List of Figures

2.1.1.	Energy diagram showing the rotational transitions of a linear molecule. . . . .	10
2.1.2.	Spectrum predicted for a hypothetical molecule. . . . .	12
2.1.3.	Energy diagram showing the rotational transitions of prolate and oblate symmetric top molecules. . . . .	20
2.1.4.	Correlation diagram for labelling asymmetric top energy levels. . . . .	21
2.2.1.	Convolution of homogenous LORENTZIAN lineshapes of different velocity components in a gas with inhomogeneous GAUSSIAN line-shape to a VOIGT profile due to DOPPLER broadening. . . . .	25
3.1.1.	Schematic setup of the spectrometer. . . . .	28
3.1.2.	Continuum free-jet expansion and labels of the typically characteristic zones. . . . .	35
3.2.1.	Schematic function of the LABVIEW™ program. . . . .	38
3.2.2.	Frontpanel of the automatised LABVIEW™ program used to take broadband spectra. . . . .	39
3.2.3.	Visualisation of chirped pulses. . . . .	46
4.1.1.	Chemical structure of methanol. . . . .	52
4.1.2.	Overview spectrum of methanol measured in a gas flow cell with a prediction from the CDMS-database. . . . .	53
4.1.3.	Spectrum of methanol measured in a gas flow cell from 107.15 GHz to 107.17 GHz. . . . .	54
4.1.4.	Chemical structure of acetonitrile. . . . .	55
4.1.5.	Overview spectrum of the acetonitrile measurement. . . . .	56
4.1.6.	Spectrum of acetonitrile zoomed at 107 - 107.3 GHz and 110.0 - 111.1 GHz. . . . .	57
4.1.7.	Chemical structure of glyceraldehyde. . . . .	58

4.2.1.	Chemical structure of propylene oxide. . . . .	59
4.2.2.	Considered lines for the Boltzmann plots in the analysis of the temperature of PO in the jet spectrum. . . . .	62
4.2.3.	BOLTZMANN plot for a selection of transitions of propylene oxide.	63
4.2.4.	Frequency domain spectrum for laser ablation experiments of bis-muth tribromide. . . . .	66
C.0.1.	Back panel of the LabView™ program with a colour legend to assign each part of the program to its function. . . . .	89

## List of Tables

2.1.	Selection rules for <i>a</i> , <i>b</i> and <i>c</i> type asymmetric tops. . . . .	22
4.1.	Temperatures estimated from BOLTZMANN plots performed with selected lines from supersonic jet measurements of acetonitrile. . .	61
B.1.	List of setup components. . . . .	86
D.1.	List of molecular databases. . . . .	90
E.1.	Considered lines for the BOLTZMANN plots. . . . .	92

# Appendix A. Used software and programs

Scientific work requires handling of a significant amount of data and information. This becomes manageable with the help of the appropriate software. The use of very helpful tools shall be outlined here.

## A.1. LabView

*LabView*<sup>TM</sup> (**L**aboratory **V**irtual **I**nstrumentation **E**ngineering **W**orkbench)<sup>76</sup> is a graphical programming interface provided by *National Instruments*. It was used to centralise communication with independently operating devices of the measurement set-up and therefore automatise the measurement process (see section 3.2 *LabView Programming* for further information). This includes setting various parameters to prepare and initialise the measurement, but also to retrieve measured data and save them for later analysis.

## A.2. Python

*Python* is an open-source, community developed programming language, which is in frame of this work mainly used for data analysis. The program package *ANACONDA* along with its development environments *Spyder* and *jupyter notebook* proved to be especially helpful. All plots in this work were created using python's libraries *matplotlib*, *pandas*, *scipy*, *numpy* and *math*.

---

<sup>76</sup>Mütterlein, *Handbuch für die Programmierung mit LabVIEW: mit Studentenversion LabVIEW 8.6*, 2011, p. VI.

## A.3. PGopher

PGOPHER is a general program for simulation, analysis and fitting of rotational, vibrational and electronic spectra provided by DR. COLIN WESTERN.<sup>77</sup> In the frame of this work the program was used for the generation of predictions from molecular parameters and the comparison of these with experimental spectra.

---

<sup>77</sup>Western, *PGOPHER: version 10.1*, 2018.

# Appendix B. Setup Components

**Table B.1.:** List of setup components.

Manufacturer	Component	Function	Comment	Specifications source
KEYSIGHT TECHNOLOGIES, INC.	M8190A	AWG	12 GS/s, Dual-channel AWG, 12 bit, 2 GB memory, 5 GHz analog bandwidth, AC amplifier	Keysight Technologies, <i>M8190A Arbitrary Waveform Generator: 12 GSa/s Arbitrary Waveform Generator: Data Sheet</i> , 2021
MINI CIRCUITS, INC.	ZX90-2-36-S+	Frequency Multiplier	(2x; input: 1700 - 3600 MHz), 11 dB typ. conversion loss	Mini-Circuits, <i>ZX90-2-36-S+: Data Sheet</i>
MINI CIRCUITS, INC.	VHF-3500+	High-Pass Filter	3900 - 3600 MHz, < 2 dB insertion loss	Mini-Circuits, <i>VHF-3500+: Data Sheet</i>
QUANTUM COMPOSERS, INC.	9520 DIGITAL DELAY PULSE GENERATOR	Trigger Box	option TZ50 (50 $\Omega$ compatible, high current), 250 ps resolution, > 50 ps jitter	Quantum Composers, Inc., <i>9520 Series Digital Delay Pulse Generators: Data Sheet</i>
WENZEL ASSOCIATES, INC.	STREAMLINE 501-04609A	Reference Clock	10 MHz reference signal, 13 $\pm$ 2dBm output power	Wenzel Associates, Inc., <i>Premium 10 MHz-SC Streamline Crystal Oscillator: Data sheet</i>
MINI CIRCUITS, INC.	ZX60-123LN-S+	Low Noise Amplifier	input range 0.5 - 12 GHz, 17 dB gain	Mini-Circuits, <i>ZX60-123LN-S+ Coaxial Low Noise Amplifier: Data Sheet</i>
NATIONAL INSTRUMENTS CORP.	SMA 100 SMA-SMA COAXIAL CABLE	Signal transmission	50 $\Omega$ , 0.381 m	
MINI CIRCUITS, INC.	ZX90-2-50-S+	Frequency Multiplier	2x; input: 3500 - 5000 MHz, 12.5 dB typ. conversion loss	Mini-Circuits, <i>ZX90-2-50-S+: Data Sheet</i>
MINI CIRCUITS, INC.	VHF-7150+	High-Pass Filter	7900 - 11 000 MHz, < 2 dB insertion loss	Mini-Circuits, <i>VHF-7150+: Data Sheet</i>
HUBER + SUHNER AG	SUCOFORM 141 SMA-SMA COAXIAL CABLE	Signal transmission	50 $\Omega$ , 1 m	Huber+Suhner AG, <i>SUCOFORM 141: Formable microwave cable: Data Sheet</i>

Manufacturer	Component	Function	Comment	Specifications source
MINI CIRCUITS, INC.	ZX90-2-24- S+	Frequency Multiplier	2x; input: 5000 - 10 000 MHz, 12 dB typ. conversion loss	Mini-Circuits, <i>ZX90-2-24+:</i> <i>Data Sheet</i>
QUINSTAR TECHNOLOGY, INC.	QLJ- 06183014	Low Noise Amplifier	input range 6 - 18 GHz, 14 dB gain	
VIRGINIA DIODES, INC.	AMC672	High Power Radiation Source	input range: 8.3 - 9.3 GHz, output range: 100 - 112.5 GHz, multiplication factor = 12, used with a 10.0WR horn antenna	Virginia Diodes, Inc., <i>AMC672</i> <i>105 GHz: User Guide</i>
VIRGINIA DIODES, INC.	AMC467	Radiation Source	input range: 12.5 - 18.3 GHz, output range: 75 - 110 GHz, multiplication factor = 6, used with a 10.0WR horn antenna	Virginia Diodes, Inc., <i>WR8.0AMC-I Specifications:</i> <i>Data Sheet</i>
MECHANICAL WORKSHOP OF THE UNIVERSITY OF KASSEL	PTFE LENSES	Focussing of Radiation	150 mm diameter, 150 mm focal length	
MECHANICAL WORKSHOP OF THE UNIVERSITY OF KASSEL	PTFE WINDOWS	Seal of Interaction Volume		
PFEIFFER VACUUM AG	VACUUM CHAMBER	Interaction Volume	ISO-K 160; stainless steel; 1.6 m	
OERLIKON LEYBOLD VACUUM GMBH	TURBOVAC 360V	Turbo- molecular Pump	ISO-K 160 inlet	successor model described in Oerlikon Leybold Vacuum GmbH, <i>High Vacuum Pumps:</i> <i>Excerpt from the Oerlikon</i> <i>Leybold Vacuum Full Line</i> <i>Catalog 2015/2016: 240.00.02,</i> <i>2015, p. 354+</i>
OERLIKON LEYBOLD VACUUM GMBH	TRIVAC D 2,5 E	Rotary Vane Backing Pump		Oerlikon Leybold Vacuum GmbH, <i>PT Turbomolecular</i> <i>Pump Systems 30 - 400 l · s<sup>-1</sup>:</i> <i>178.01.02, 2010</i>
ERAVANT, INC.	SAR-2507- 08-S2	WR-08 Waveguide Rectangular Horn Antenna	90 - 140 GHz	Eravant, <i>SAR-2507-08-S2:</i> <i>Data Sheet</i>
ERAVANT, INC.	SKD- 7531143530- 1010-R1-M	W-Band Reflective SPDT Pin Diode Switch	75 - 110 GHz, 100 ns switching speed	Eravant, <i>SKD-7531143530-1010-R1-M:</i> <i>Data Sheet</i>

## Appendix B. Setup Components

Manufacturer	Component	Function	Comment	Specifications source
RPG RADIOMETER PHYSICS GMBH	W-LNA 75-110 20 3	Low Noise Amplifier	19 dB gain	RPG Radiometer Physics GmbH, <i>W-LNA 75-110 20 3: Data Sheet</i>
VIRGINIA DIODES, INC.	WR8.0 MixAMC-I	Integrated Mixer (MixAMC)	RF frequency band 90 - 140 GHz; LO frequency input 7.5 - 11.67 GHz	Virginia Diodes, Inc., <i>WR8.0AMC-I Specifications: Data Sheet</i>
MINI CIRCUITS, INC.	ZX75BP- 1350-S+	Bandpass Filter	1300 - 1400 MHz	Mini-Circuits, <i>ZX75BP-1350-S+: Data Sheet</i>
PASTERNAK ENTERPRISES, INC.	PE15A1007	Low Noise Amplifier	32 dB gain, frequency range 9 kHz - 3 GHz	Pasternack Enterprises, <i>PE15A1007: Technical Data Sheet</i>
MINI CIRCUITS, INC.	ZDPLX- 2150-S+	Coaxial Diplexer	DC - 10 MHz / 50 - 2150 MHz; 0.5 dB / 0.9 dB typ. insertion loss	Mini-Circuits, <i>VHF-7150+: Data Sheet</i>
TEKTRONIX, INC.	MSO64	Mixed Signal Oscilloscope	25 Gsa/s, bandwidth: 6 GHz	Tektronix, <i>6 Series B MSO: Mixed Signal Oscilloscope: Datasheet</i>
PFEIFFER VACUUM AG	EVN116	Needle Valve		Pfeiffer Vacuum AG, <i>EVN116: Datenblatt</i>

# Appendix C. LabView Backpanel

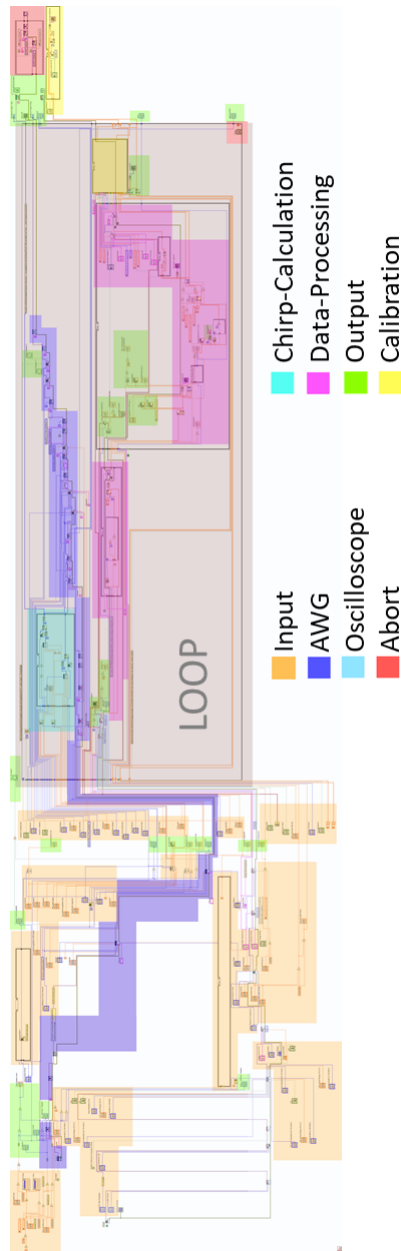


**Figure C.0.1.1:** Back panel of the LabView™ program with a colour legend to assign each part of the program to its function.

# Appendix D. List of Molecular Databases

Table D.1 holds information on where predictions for the investigated molecules originate from. The column *CDMS* refers to an entry to the bibliography, which includes a link to the respective molecule in the CDMS database. There extensive information on the considered data is presented. The paper describing the fit itself is cited in column *Based On*.

**Table D.1.:** List of molecular databases.

Molecule	CDMS	Based On
Methanol (CH <sub>3</sub> OH) as found in 4.1.1	L.-H. Xu, Endres, and H. Müller, <i>CH<sub>3</sub>OH, v<sub>t</sub>=0-2</i> , 2016	fit described in Li-Hong Xu et al., “Torsion–rotation global analysis of the first three torsional states ( <i>v<sub>t</sub></i> =0, 1, 2) and terahertz database for methanol”, 2008
Acetonitrile main isotopologue (CH <sub>3</sub> CN, <i>v</i> =0, 1, 2)	H. S. P. Müller, <i>CH<sub>3</sub>CN, v=0</i> , 2015, H. S. P. Müller, <i>CH<sub>3</sub>CN, v=1</i> , 2015, H. S. P. Müller, <i>CH<sub>3</sub>CN, v=2</i> , 2015	fit described in H. S. P. Müller, L. R. Brown, et al., “Rotational spectroscopy as a tool to investigate interactions between vibrational polyads in symmetric top molecules: Low-lying states <i>v<sub>8</sub></i> ≤ 2 of methyl cyanide, CH <sub>3</sub> CN”, 2015

Molecule	CDMS	Based On
Acetonitrile isotopologues ( $^{13}\text{CH}_3\text{CN}$ , $\text{CH}_3^{13}\text{CN}$ , $\text{CH}_3\text{C}^{15}\text{N}$ , each $v=0$ )	H. S. P. Müller, $^{13}\text{CH}_3\text{CN}$ , $v=0$ , 2009, H. S. P. Müller, $\text{CH}_3^{13}\text{CN}$ , $v=0$ , 2009, H. S. P. Müller, $\text{CH}_3\text{C}^{15}\text{N}$ , $v=0$ , 2009	fit described in H. S. P. Müller, Drouin, and Pearson, “Rotational spectra of isotopic species of methyl cyanide, $\text{CH}_3\text{CN}$ , in their ground vibrational states up to terahertz frequencies”, 2009

The prediction for propylene oxide was created with PGOPHER by exporting a linelist after adjusting the molecular parameters according to Mesko et al., “Millimeter and submillimeter spectrum of propylene oxide”, 2017.

## Appendix E. Jet Experiments - Considered Lines

The transitions of propylene oxide considered in the BOLTZMANN plot in section 4.2.1 *Jet Measurements* are summarized in table E.1. The prediction for this linelist was created with PGOPHER by exporting a linelist after adjusting the molecular parameters according to Mesko et al., “Millimeter and submillimeter spectrum of propylene oxide”, 2017.

Appendix E. Jet Experiments - Considered Lines

Table E.1.: List of considered lines for the BOLTZMANN plots in figure 4.2.2.

line group	$f_{meas}$ [MHz]	$I_{small}$ [a.u.]	$I_{large}$ [a.u.]	$f_{pred}$ [MHz]	$I_{pred}$ [a.u.]	$J'$	$J''$	$J'''$	$E_{upper}$	$E_{lower}$	transition label	vib'	$J'$	$K'_a$	$K'_c$	vib''	$J''$	$K''_a$	$K''_c$	
0 - 30 MHz	103827	0.000099	0.000160	103824.8139	0.00001916	13	11	13	9	1444606.0	1340781.2	v=0	13	5	8	-	v=0	13	4	9
0 - 30 MHz	104610	0.000123	0.000235	104608.3279	0.00007060	11	11	11	9	1127725.8	1023117.4	v=0	11	5	6	-	v=0	11	4	7
0 - 30 MHz	105009.5	0.000108	0.000160	105008.8673	0.00018960	9	11	9	861774.4	756765.5	rQ4.5(9)	v=0	9	5	4	-	v=0	9	4	5
0 - 30 MHz	107006	0.000380	0.000610	107005.6782	0.00138630	9	1	8	558913.9	451908.2	pR1.8(8)	v=0	9	0	9	-	v=0	8	1	8
0 - 30 MHz	109626	0.000230	0.000200	109623.4377	0.00062900	9	2	8	561531.7	451908.2	qR1.8(8)	v=0	9	1	9	-	v=0	8	1	8
30 - 70 MHz	103039.5	0.000388	0.000677	103041.857	0.00063040	8	5	7	507078.9	404037.0	qR2.5(7)	v=0	8	2	6	-	v=0	7	2	5
30 - 70 MHz	104043	0.000092	0.000140	104141.5551	0.00000903	14	10	14	1622145.5	1518004.0	rQ4.11(14)	v=0	14	5	10	-	v=0	14	4	11
30 - 70 MHz	104362.5	0.000220	0.000280	104361.8674	0.00001926	13	10	13	1444583.2	1340721.3	rQ4.10(13)	v=0	13	5	9	-	v=0	13	4	10
30 - 70 MHz	104571	0.000116	0.000170	104570.5966	0.00003829	12	10	12	1279780.5	1176209.9	rQ4.9(12)	v=0	12	5	8	-	v=0	12	4	9
30 - 70 MHz	105040	0.000112	0.000184	105039.2789	0.00018970	9	10	9	861773.8	756734.6	rQ4.6(9)	v=0	9	5	5	-	v=0	9	4	6
30 - 70 MHz	105253	0.000210	0.000820	105252.9444	0.00036980	6	11	6	558077.7	452824.8	rQ4.2(6)	v=0	6	5	1	-	v=0	6	4	2
30 - 70 MHz	105254.75	0.000290	0.000410	105254.0319	0.00036980	6	10	6	558077.7	452823.7	rQ4.3(6)	v=0	6	5	2	-	v=0	6	4	3
30 - 70 MHz	105436	0.000372	0.000600	105432.9897	0.00167300	6	4	5	311870.2	206437.2	rR1.4(5)	v=0	6	2	5	-	v=0	5	1	4
30 - 70 MHz	109160.5	0.000260	0.000500	109160.4755	0.00267970	4	7	3	231789.1	122628.6	rR2.2(3)	v=0	4	3	1	-	v=0	3	2	2
70 - 100 MHz	101189	0.000160	0.000150	101189.5034	0.00004882	8	13	7	876475.0	775285.5	qR6.1(7)	v=0	8	6	2	-	v=0	7	6	1
70 - 100 MHz	101599	0.000120	0.000127	101600.1251	0.000043700	8	7	7	561477.9	459877.8	qR3.4(7)	v=0	8	3	5	-	v=0	7	3	4
70 - 100 MHz	102189	0.000940	0.000868	102183.6251	0.00192090	8	2	7	451908.2	349724.6	rR0.7(7)	v=0	8	1	8	-	v=0	7	0	7
70 - 100 MHz	103094	0.000400	0.000680	103097.5651	0.00143340	5	5	4	237396.5	134298.9	rR1.4(4)	v=0	5	2	3	-	v=0	4	1	4
70 - 100 MHz	103174	0.000540	0.000930	103174.3326	0.00075990	8	3	7	477777.1	374602.8	qR1.6(7)	v=0	8	1	7	-	v=0	7	1	6
70 - 100 MHz	103594.5	0.000070	0.000080	103593.9357	0.00000222	18	10	18	2460298.6	2356704.7	rQ4.15(18)	v=0	18	5	14	-	v=0	18	4	15
70 - 100 MHz	104281.5	0.000138	0.000158	104279.8021	0.00003818	12	11	12	1279780.7	1176510.9	rQ4.8(12)	v=0	12	5	7	-	v=0	12	4	8
70 - 100 MHz	106083.5	0.000138	0.000133	106092.7637	0.00000239	15	6	14	1625084.8	1518992.1	pR4.10(14)	v=0	15	3	13	-	v=0	14	4	10
70 - 100 MHz	107392.25	0.000221	0.000300	107399.7946	0.00031910	10	3	9	721767.3	613767.5	pR2.8(9)	v=0	10	1	9	-	v=0	9	2	8
70 - 100 MHz	108983	0.000353	0.000427	108982.8409	0.00267930	4	6	3	231782.1	122799.2	rR2.1(3)	v=0	4	3	2	-	v=0	3	2	1

# Units and Constants

Prefactors.

Name	Symbol	Value
Tera	T	$10^{12}$
Giga	G	$10^9$
Mega	M	$10^6$
kilo	k	$10^3$
dezi	d	$10^{-1}$
centi	c	$10^{-2}$
milli	m	$10^{-3}$
micro	$\mu$	$10^{-6}$
nano	n	$10^{-9}$
pico	p	$10^{-12}$

Units.

Quantity	Symbol	Unit	Dimension
Frequency	Hz	hertz	$s^{-1}$
Length	m	meter	
Mass	kg	kilogram	
Time	s	second	
Parts per million	ppm		$10^{-6}$
Temperature	K	Kelvin	
Pressure	p	bar <i>or</i> Pascal	

Constants.<sup>78</sup>

Constant	Symbol	Value (Uncertainty)	Dimension
Speed of light	$c$	299 792 458(0)	$\text{m s}^{-1}$
BOLTZMANN constant	$k_B$	$1.380\,649(0) \cdot 10^{-23}$	J K
PLANCK constant	$h$	$6.626\,070\,15(0) \cdot 10^{-34}$	J s
reduced PLANCK constant	$\hbar \left( = \frac{h}{2\pi} \right)$	$1.054\,571\,817(0) \cdot 10^{-34}$	J s

## Abbreviations

Abbreviations.

Abbreviation	Meaning
(HP)AMC	(High Power) Amplifier Multiplier Chain
a.k.a.	also known as
AWG	Arbitrary Waveform Generator
BW	Bandwidth
CDMS	Cologne Database for Molecular Spectroscopy
CP	Chirped Pulse
DAC	digital-to-analog-converter
e.g.	exempli gratia (Latin: for example)
EM	electro-magnetic
etc.	et cetera (Latin: and so forth)
(F)FT	(Fast) FOURIER Transform
FID	Free Induction Decay
FWHM	Full Width at Half Maximum
GA	Glyceraldehyde
i.e.	id est (Latin: this means)

<sup>78</sup>Data taken from NIST, *Standard Reference Database*, 2019

Abbreviations.

---

<b>Abbreviation</b>	<b>Meaning</b>
IF	Intermediate Frequency
ISM	Interstellar Medium
JPL	Jet Propulsion Laboratory
LO	Local Oscillator
MMW	Millimeter Wave
MW	Micro Wave
p. [pp.]	Page[s]
PC	Personal Computer
PO	Propylene Oxide
RF	Radio Frequency
SC	Sample Count
SNR	Signal to Noise Ratio
SR	Sample Rate

---